UNIVERSITY OF INSUBRIA

Ph.D. Program in Experimental and Translational Medicine

XXXII Cycle

Parkinson's disease and mitochondrial dysfunctions: exploring the effect of *PARK2* mutations in human skin fibroblasts

Tutor: Prof. Mauro Fasano

Coordinator: Prof. Daniela Negrini

Ph.D. thesis of:
ILARIA COLUGNAT

Index

2-DE, two-dimensional electrophoresis; BCA, Bicinchoninic Acid Protein Assay; BNIP3, Bcl2/adenovirus E1B 19 kDa protein-interacting protein 3; CCCP, carbonyl cyanide m-chlorophenyl hydrazine; COMT, Catechol-O-methyl transferase; CS, citrate synthase; CV%, coefficient of variation; DA, dopamine; DAPI, 4',6-diamidino-2-phenylindole; DAT, dopamine transporter; DIA, data-independent acquisition; DMEM, Dulbecco's modified Eagle's medium; DMSO, dimethyl sulfoxide; DRP1, dynamin-related protein 1; FA, formic acid; FBS, Fetal Bovine Serum; FDR, false discovery rate; Fis1, Mitochondrial fission 1 protein; GSEA, gene set enrichment analysis; HDMS$_E$, High Definition MS$_E$; HSPs, heat shock proteins; HUPO, Human Proteome Organization; IMM, inner mitochondrial membrane; IMS, intermembrane space; iPSCs, induced pluripotent stem cells; LC, liquid chromatography; LB, Lewy bodies; L-DOPA, L-3,4-dihydroxyphenylalanine; LRRK2, leucine-rich repeat serine/threonine-protein kinase 2; MAO-B, monoamine oxidase B; MFN1, mitofusin 1; MFN2, mitofusin 2; MPP, mitochondrial processing peptidase; MS, mass spectrometry; MS/MS, tandem mass spectrometry; mt-HPP, Mitochondrial Human Proteome Project; mtDNA, mitochondrial DNA; MTS, mitochondrial targeting signal domain; NRF1, nuclear respiratory factors 1; NRF2, nuclear respiratory factors 2; nUPLC, nano-Ultra Performance Liquid Chromatography; OMM, outer mitochondrial membrane; OPA, optic atrophy 1; PARIS, Parkin interacting substrate; PARK2, autosomal recessive juvenile Parkinson's disease-2; Parkin, E3 ubiquitin ligase parkin; PARL, presenilin-associated-rhomboid-like; PBS, Phosphate Buffered Saline; PD, Parkinson's disease; PINK1, PTEN-induced putative kinase 1; PVDF, polyvinylidene difluoride; ROS, reactive oxygen species; SILAC, stable isotope labelling with amino acids in cell culture; SNpc, Substantia nigra pars compacta; TBST, tris-buffered saline with 0.05% TWEEN; Tfam, mitochondrial transcription factor A; TH, tyrosine hydroxylase; TIM, translocase of the inner membrane; TOM, translocase of the outer membrane; tRNA, transfer RNAs; UPS, Ubiquitin-Proteasome System; VDAC1, voltage-dependent anion channel 1; VDACs, voltage-dependent anion channels; α-syn, α-synuclein; $\Psi\Delta_m$, Mitochondrial Membrane Potential.

Abstract

Parkinson's disease (PD) is a complex and multifactorial neurodegenerative disease whose etiology has not been totally clarified yet. Strong evidences suggest that a complex interplay between environmental and genetic factors are involved in PD pathogenesis, underlining its multifactorial nature. Although the cause of PD is not completely understood, strong evidences suggest that the impairment of the ubiquitin-proteasome system, the increased oxidative stress, the dysregulation of protein trafficking and the mitochondrial damage are hallmarks of PD. In this intricate scenario, many of the molecular pathways implicated in PD etiology converge on mitochondria, resulting in their dysfunction.

Mutations in *PARK2* gene are the most frequent cause of familial forms of PD. This gene encodes Parkin, an E3 ubiquitin ligase involved in several cellular mechanisms, such as mitophagy. Parkin loss-of-function is responsible for the cellular accumulation of damaged mitochondria, which in turn determines an increment of reactive oxygen species levels, lower ATP production, and apoptosis activation. Although PARK2 is a familiar and rare form of PD, it offers a unique opportunity to study how the impairment in the Parkin functionality can cause the improper disposal of dysfunctional mitochondria.

Given the importance of mitochondrial dysfunctions and mitophagy impairment in PD pathogenesis, *PARK2*-mutated primary skin fibroblasts were used as a cellular model to explore the effects of *PARK2* mutations both on the mitochondrial function and morphology and on the total and mitochondrial proteome. Indeed, it is already been demonstrated that skin fibroblasts from PARK2 patients can be used to investigate the mitochondrial impairment that characterized these subjects. Therefore, fibroblasts are an easily accessible peripheral source of proliferating cells, which can mirror at the periphery what it is happening at the central level.

The first part of this thesis investigates the impact of Parkin impairment on mitochondrial function and network in primary skin fibroblasts of five PARK2 patients and five control subjects. We unveiled that the mitochondrial membrane potential was reduced in PARK2 patients, without inducing PINK1 accumulation, even when triggered with the ionophore CCCP. The analysis of the mitochondrial network morphology did not reveal any significant alterations between PARK2 patients and control subjects. Thus, our results suggested that the network morphology was not influenced by the mitochondrial depolarization and by the lack of Parkin, revealing a possible impairment of fission and, more in general, of mitochondrial dynamics.

The second part of this project is focused on the characterization of the mitochondrial and the total proteome alterations that characterize patients carrying *PARK2* mutations. Because of the multifactorial nature of PD, the use of a global approach, such as proteomics, may give a more comprehensive view about its etiopathogenesis. Mitochondrial-enriched and whole cell fractions

were analyzed by quantitative shotgun proteomics analysis in order to identify proteins specifically altered by Parkin loss-of-function. Eventually, a systems biology approach was used to identify the molecular pathways altered by mutations in *PARK2* gene.

In conclusion, the present work highlighted new molecular factors and pathways altered by *PARK2* mutations, which will unravel possible biochemical pathways altered in the sporadic form of the disease.

1. Introduction

1.1. Parkinson's disease

Parkinson's disease (PD) is the second most common neurodegenerative disorder after Alzheimer's disease (Bose et al., 2016). This pathology was first described in 1817 by James Parkinson in the "Essay on the shaking palsy". Approximately 50 years later, the neurologist Jean Martin Charcot honored James Parkinson's work by renaming the disorder as "Parkinson's disease" (Charcot, 1879).

PD affects 1% of the individuals above 60 years (Deng et al., 2018). The disease is lightly more frequent in men than in women with an annual incidence estimated to be 15 per 100 000 people worldwide with an age at onset from 65 to 70 years. Nevertheless, 5% of cases are characterized by an onset before 40 years of age (Tysnes and Storstein, 2017).

PD affects several regions of the brain, but the most important pathological hallmark of PD is the progressive degenerations of dopaminergic neurons of the substantia nigra pars compacta (SNpc), a basal ganglia structure located in the midbrain that controls balance and movement (Samii et al., 2004). The soma of nigrostriatal neurons is located in the SNpc and they project to the basal ganglia and synapse in the striatum. The loss of these neurons impaired the signaling to the basal ganglia leading to a decreased output to the cortex and brainstem. Since dopaminergic neurons normally contain a considerable amount of neuromelanin, the loss of these neurons produces the classic neuropathological finding of SNpc depigmentation (Dauer et al., 2003).

Another pathological feature of PD is the presence of intracellular protein inclusion called Lewy bodies (LB) that are mostly composed by the α-synuclein (α-syn) protein (Lewy, 1912; Shults, 2006; Spillantini et al., 1998), which accumulation precedes the loss of neuromelanin in the SNpc (Fasano et al., 2003).

The neurodegenerative process leads to the onset of three cardinal symptoms: tremor, rigidity and bradykinesia. Despite PD is classified as movement disorder, some affected individuals developed a wide range of non-motor symptoms, such as depression, sleep disturbances, gait dysfunction and cognitive impairment (Gallagher et al., 2010).

At the onset of motor symptoms, 60% of SNpc dopaminergic neurons have already been loss. Due to the onset of clinical motor signs at a very late stage of neurodegeneration, the only possible treatment is symptomatic and aims at restoring dopamine (DA) levels in the striatum by administration of L-3,4-dihydroxyphenylalanine (L-DOPA). L-DOPA is a DA precursor (metabolized to DA in the brain) that it is able to pass the blood-brain barrier. Catechol-O-methyl transferase (COMT) and monoamine oxidase B (MAO-B) inhibitors may be administered in association with L-DOPA in order to inhibit DA inactivation. These treatments only have the function to compensate the reduced levels of DA, though they do not prevent the

neurodegeneration of dopaminergic neurons. For this reason, a protective treatment that increases the survival of neurons is necessary. In order to develop such treatments, it is important to identify the molecular mechanisms involved in early stages of the disease.

1.1.1. Etiology of Parkinson's disease

PD is a multifactorial disease with both genetic and environmental factors involved in the pathogenesis (Shapira and Jenner, 2011). The cause of PD is not completely understood, but over the last 20 years knowledge regarding the pathophysiological basis of PD has been increased with the massive contributions from the genetic studies. Genetic predisposition is one of the major contributions underlying PD pathology (Gasser, 2009). Moreover, exposition to environmental toxins (*e.g.*, paraquat, rotenone, 1-methyl-4-phenyl-1,2,3,6-tetrahydropyridine (MPTP)) can be a risk factor for PD (Subramaniam and Chesselet, 2013).

1.1.1.1. Genetic forms of Parkinson's disease

Although 5-10% of PD patients suffer from a monogenic form of the disease, the majority of PD cases are sporadic with unknown etiology probably caused by a complex interplay between genetic susceptibility and environmental factors (Deng et al., 2018). For this reason, the investigation of cellular functions of the genes linked to rare monogenic forms of PD provides a better understanding of the molecular pathogenesis of sporadic PD. Indeed, many mechanisms underlying neurodegeneration in familial PD are the same discovered in the sporadic form of the disease (Corti et al., 2011).

Over the last 15 years, the list of PD-linked mutations grew rapidly, and several loci have been associated with PD. Till now, 26 loci involved in PD have been identified (Lill, 2016). The most relevant ones will be discussed below.

SNCA (PARK1/PARK4)

SNCA gene encodes for α-syn, a small 140 aa protein, natively unfolded, expressed in brain with smaller amounts found in heart, muscles and other tissues. *SNCA* was the first gene identified to be genetically linked to PD. This gene was mapped on the long arm of chromosome 4 in 1996 (Polymeropoulos et al., 1997). Missense mutations, duplications or triplications of *SNCA* gene have been associated with the onset of autosomal dominant forms of PD indicating that an increase of α-syn expression can be toxic for neurons. In the brain, α-syn is localized in the presynaptic terminals where it seems to play a fundamental role in DA metabolism (Stefanis, 2012) and in the maintaining of synaptic functions by the interaction with the Rab families highlighting the

important role of α-syn in vesicular trafficking (Gitler et al., 2008). Mutated α-syn has the tendency to form β-sheet-rich oligomers, which aggregates and form mature fibrils. In PD brain, α-syn accumulates and aggregates in the LB (Lee and Trojanowski, 2006). Aggregation of α-syn can cause cellular damage by the disruption of lysosomal and proteasomal functions (Xilouri et al., 2016).

Parkin (*PARK2*)

PARK2 gene encodes for the protein Parkin, an E3 ubiquitin ligase. Mutations in this gene has been linked to autosomal recessive juvenile Parkinson's disease-2 (PARK2) (Shimura et al., 2000). This form of juvenile PD is characterized by an early onset typically between childhood and 40 years of age, a slow disease progression and the absence of LB (Sun et al., 2006). Several mutations have been identified including point mutations and exon rearrangements including both duplications and deletions. Most of the point mutations cause alteration in the cellular localization or in the protein solubility, while insertions and deletions result in Parkin loss-of-function (Sun et al., 2006). Parkin catalyzes the binding between ubiquitin and proteins that have to be degraded via the proteasome. Moreover, Parkin was also described as a fundamental regulator of mitochondrial dynamics by tagging dysfunctional mitochondria and sending them to autophagic degradation. For this reason, mutations in this gene can lead to mitochondrial dysfunctions and accumulation of organelle and substrates that may have a toxic effect on the neurons (Geisler et al., 2010).

PINK1 (*PARK6*)

PARK6 gene encodes for PTEN-induced putative kinase 1 (PINK1), a 581 aa serine/threonine kinase, which acts upstream to Parkin in the regulation of the mitophagy process (Narendra et al., 2010). The convergence of *PARK6* and *PARK2* genes in the mitophagy pathway highlight the importance of these two proteins in the regulation of impaired mitochondria disposal. Mutations in this gene were found both in familial and in sporadic cases of PD (Valente et al., 2004). Clinically, PD patients affected by PINK1 mutations display atypical features such as dystonia, cognitive and psychiatric problems. Most of the mutations reside in the kinase domain of PINK1, thus causing a loss-of-function of the protein (Sim et al., 2006). Moreover, PINK1 deficiency leads to a lower complex I activity and increased sensitivity to apoptotic stress (Morais et al., 2009).

DJ-1 (*PARK7*)

PARK7 encodes for DJ-1 protein. Mutations in this gene induced a form of PD with an onset between 20 and 30 years of age. DJ-1 localizes in the cytosol, as well as in the mitochondria, and can protect dopaminergic neurons against oxidative stress acting as antioxidant, thus limiting the neuronal cell damage (Bonifati et al., 2003). It has been demonstrated that Parkin, PINK1 and DJ1 are implicated together in several pathways, such as oxidative injury, Ubiquitin-Proteasome System (UPS) dysfunction and mitochondrial dysfunction, which are involved in PD pathogenesis (Wilhelmus et al., 2012).

LRRK2 (*PARK8*)

PARK8 gene encodes for leucine-rich repeat serine/threonine-protein kinase 2 (LRRK2), a large multidomain protein with GTP-regulated serine/threonine kinase activity (Martin et al., 2014). Mutations in this gene are associated with autosomal dominantly inherited PD of late onset (Di Fonzo et al., 2005) and not only account for rare familial forms of PD but also have been identified in sporadic cases (Lesage and Brice, 2009). Most of LRRK2 mutations are located in the GTPase and kinase domain and for several of them an increased kinase activity was reported (Cookson, 2010). LRRK2 is largely localized in the cytoplasm but can be also associated with the outer mitochondrial membrane (OMM), indicating its potential role in the maintenance of mitochondrial functions. Indeed, this protein is involved in the translocation of the dynamin-related protein 1 (Drp1) from cytosol to mitochondria and the inhibition of LRRK2 activity causes mitochondrial fission and an increased production of reactive oxygen species (ROS) (Saez-Atienzar et al., 2014). Moreover, mutations in this gene determine the formation of a more elongated and interconnected mitochondrial network and an impairment of mitochondrial functions, such as lower ATP production and lower mitochondrial membrane potential (Mortiboys et al., 2010).

GBA

GBA gene encodes for β-glucocerebrosidase, a lysosomal enzyme involved in glycolipid metabolism. GBA is the most common risk factor known for PD (Sidransky et al., 2009). Homozygous GBA mutations result in Gaucher disease, an autosomal-recessive lysosomal storage disorder. The proportion of PD patients that carry heterozygous GBA mutations is estimated to be between 5 and 10% (Beavan and Schapira, 2013). The observation of accumulated dysfunctional mitochondria in both diseases highlight the importance of the appropriate turnover of these organelles (Osellame and Duchen, 2014) and suggest that lysosome and mitochondria are strictly interconnected.

RAB39B

This gene encodes for the protein RAB39B, a small GTPase involved in the regulation of vesicular trafficking between membrane compartments (Wilson et al., 2014). Mutations in this gene are associated with X-linked cognitive disability and early-onset PD. A postmortem study revealed the presence of LB and an extensive dopaminergic neuronal loss in the SNpc (Wilson et al., 2014). More recently, Lesage and colleagues identified a single French man with a novel nonsense mutation in the RAB39B gene. This patient had early disease onset (39 years) and typical Parkinsonism without family history of PD (Lesage et al., 2015).

1.1.1.2. Environmental factors and Parkinson's disease

The first and most important environmental factor correlated to PD is the ageing process. Aging is characterized by irreversible cell damage, increased predisposition to neurodegenerative diseases and reduced activity of the cellular repair machinery (Hindle et al., 2010).

It has been demonstrated that environmental toxin exposures are involved in PD pathogenesis. Nowadays, there has been increasing interest in pesticide exposure, such as rotenone and paraquat. Indeed, people exposed to these toxins show an increased risk in developing PD (Tanner et al., 2011; Nandipati and Litvan, 2016).

Rotenone is a lipophilic molecule that crosses the blood-brain barrier and biological membranes without using a specific receptor or transporter. In neuronal cells, rotenone inhibits complex I activity in the respiratory chain causing ROS generation and lower ATP production (Sherer et al., 2002). Moreover, rotenone causes proteolytic stress due to the inhibition of the proteasome activity (Chou et al., 2010).

Paraquat is a compound that accumulates in mitochondria, where it converts free radicals to superoxide and other ROS thus increasing cellular oxidative stress (Yumino et al., 2002). Paraquat is not able to passively cross the blood-brain-barrier but enters the brain through the neutral amino acid transporter (Shimizu et al., 2001).

Eventually, in the late 1970s it was discovered in heroin users that the compound MPTP, a by-product in the synthesis of a meperidine analog, is able to induce an irreversible form of Parkinsonism (Langston et al., 1983) by inhibiting complex I functionality (Antony et al., 2013). MPTP is a lipophilic toxin able to cross the blood-brain-barrier. Once MPTP enters the glial cells, it is metabolized to MPP^+ by the monoamine oxidase enzyme. MPP^+ accumulates in dopaminergic neurons through the dopamine transporter (DAT) and localizes in mitochondria (Ramsay et al., 1986). The inhibition of the activity of the complex I of the electron transport chain leads to lower

ATP production, increased ROS generation and neuronal cell death (Johnson and Bobrovskaya, 2015).

All these toxins are commonly used to generate *in vitro* and *in vivo* models in order to recapitulate the sporadic PD pathology.

1.1.1.3. Oxidative stress and Parkinson's disease

Under physiological conditions, ROS are continuously produced, and their potentially damaging role is neutralized by antioxidant systems that work in synergy to maintain a correct balance. When this balance is shifted in favor of ROS production, oxidative stress occurs (Lotharius and Brundin, 2002). Oxidants and superoxide radicals are produced as by-products of oxidative phosphorylation, making mitochondria the main site of ROS generation within the cell.

Oxidative stress affects mainly dopaminergic neurons in the SNpc, suggesting that DA itself may be a source of oxidative stress (Alberio et al., 2010). Indeed, altered dopamine homeostasis seems to be a key factor in the early steps of PD pathogenesis (Alberio et al., 2012; Herrera et al., 2017). DA is synthetized from tyrosine first by tyrosine hydroxylase (TH) and further by aromatic amino acid decarboxylase. DA is taken up by the vesicular monoamine transporter-2 that stores it into synaptic vesicles, where the low pH stabilizes the molecule. When not properly handled, DA accumulates in the cytoplasm and goes through auto oxidation at neutral pH conditions. This process causes the formation of quinone and semi-quinone species (Berg et al., 2006) together with hydrogen peroxide. Hydrogen peroxide can be reduced to cytotoxic hydroxyl radicals in a reaction catalyzed by iron, which is more present in SNpc than in other brain regions due to the iron-neuromelanin system (Fasano et al., 2006).

DA quinones can modify several PD-related proteins, such as α-syn, Parkin and DJ1. Moreover, these species cause inactivation of DAT and the TH enzyme, as well as mitochondrial dysfunction (Lee et al., 2003) and dysfunction in complex I activity (Alberio et al., 2010). Moreover, DA quinones can be oxidized to aminochrome, which is able to induce and stabilize the formation of neurotoxic protofibrils of α-syn (Conway et al., 2001), to cause dysfunction of proteasome system (Zhou and Lim, 2009) and to prevent the fusion of autophagy vacuoles with lysosomes (Paris et al., 2010).

Alpha-syn plays an important role in dopamine homeostasis. Indeed, mutated or modified α-syn has an increased tendency to form protofibrils. Protofibrils can influence membranes and vesicles permeability by forming pores, ending in the leakage of DA into the cytoplasm, which in turn leads to cell death (Lotharius and Brundin, 2002). The interplay between altered homeostasis of DA and α-syn aggregation into protofibrils is at the basis of the oxidative stress (Alberio et al.,

2012). This condition can be enhanced by the mitochondrial impairment caused by ROS generated from changes in DA metabolism, so that the main consequences are dysfunction in mitochondria respiration (Berman and Hastings, 1999). Toxins like MPP^+ or rotenone have remarkable affinity for DAT, and they can be taken up into dopaminergic cells causing damage by inhibiting complex I with the consequent activation of the apoptotic pathway (Alberio et al., 2012).

1.2. Mitochondria

1.2.1. Structure and function

Mitochondria are 0.5-1 μm double membranes-enclosed cytoplasmic organelles. The structure of mitochondria consists in four components: the OMM, the intermembrane space (IMS), the inner mitochondrial membrane (IMM) and the mitochondrial matrix. The IMM is highly folded, forming tubular or lamellar structures called cristae, where the complexes of the respiratory chains are embedded. The OMM displays porins or voltage-dependent anion channels (VDACs) that allow molecules smaller than 6 kDa to passively diffuse across, as well as the translocase of the outer membrane (TOM) that allows specific proteins with a particular N-terminal signal peptide to enter into the mitochondrion (Chipuk et al., 2006; Naghdi and Hajnóczky, 2016). The IMS is an aqueous compartment that coordinates the mitochondrial activity with other cellular processes (*e.g.*, exchange of proteins and lipids between the matrix and the cytosol, the regulation of the signaling pathways or the control of mitochondrial morphogenesis) (Herrmann and Riemer, 2010).

The IMM presents hundreds of proteins involved in ATP synthesis, together with proteins responsible of the transport across the membrane, such as the translocase of the inner membrane (TIM) (Frey et al., 2000). The mitochondrial matrix contains enzymes involved in the pyruvate oxidation, fatty acid oxidation and citric acid cycle as well as several proteases such as Lon, a serine protease responsible of the degradation of denatured and oxidized proteins. Furthermore, mitochondrial matrix contains mitochondrial ribosomes, transfer RNAs (tRNA) and different copies of mitochondrial DNA (Schapira, 2008).

Mitochondria are very dynamic organelles involved in cellular homeostasis with the main function to provide energy in form of ATP to the cell. Neurons highly depend on ATP and are quite susceptible to stressors (Golpich et al., 2017), thus underlying the fundamental role of mitochondrial dysfunctions in the pathogenesis of neurodegenerative diseases. Moreover, mitochondria are involved in the biosynthesis of several macromolecules (*e.g.*, nucleotides, lipids, heme, and iron-sulfur clusters) and in controlling the apoptotic cell death. Regarding this last process, a key factor is the cytochrome c. This protein is normally segregated in mitochondria

cristae. In response to cellular stress, cytochrome c is released in the cytosol where it activates proteolytic enzymes called caspases, a key factor in activating the apoptotic process. Mitochondria also have an important role in maintaining the intracellular Ca^{2+} homeostasis (Vakifahmetoglu-Norberg et al., 2017).

As mitochondria are essential for a plethora of cellular processes, regulation and maintenance of mitochondrial function is very important for the cell.

1.2.2. Mitochondrial proteome

Mitochondria have their own genetic system that is a mixture of several bacterial-like features, such as compact circular DNA genome (mtDNA) and eukaryotic-derived proteins. The human mitochondrial proteome is a circular molecule constituted by 16569 base pairs (Anderson et al., 1981). The mtDNA contains 37 genes, among these genes 13 encode proteins that are core constitutes of the mitochondrial respiratory complex I-IV, 22 encode for tRNAs and 2 encode for the mitochondrial ribosomes (rRNA 12S and 16S), essential for mitochondria own translational apparatus. The majority of mitochondrial proteins are encoded by nuclear genes that are synthesized in the cytosol and imported into the appropriate mitochondrial compartment through multimeric translocation machines (*e.g.*, TOM and TIM) (Boengler et al., 2011; Kang et al., 2017). Nowadays, by combining proteomics, genomics and bioinformatics, it is known that the estimated number of strictly mitochondrial proteins in human cells is 1158-1626 (Monti et al., 2018). The mitochondrial proteome is plastic, varying in response to cellular and tissue-specific requirements. The complexity is increased by the presence of specific cytosolic proteins, the interactors, that contribute to mitochondrial functionality, dynamics and metabolism. Therefore, the number of these proteins that do not belong to the strictly concept of the mitochondrial proteome is 3395. For this reason, the mitochondrial proteome is dynamic, and the quality and quantity of those interactors determine the functional mitochondrial proteome (Figure 1) (Monti et al., 2018).

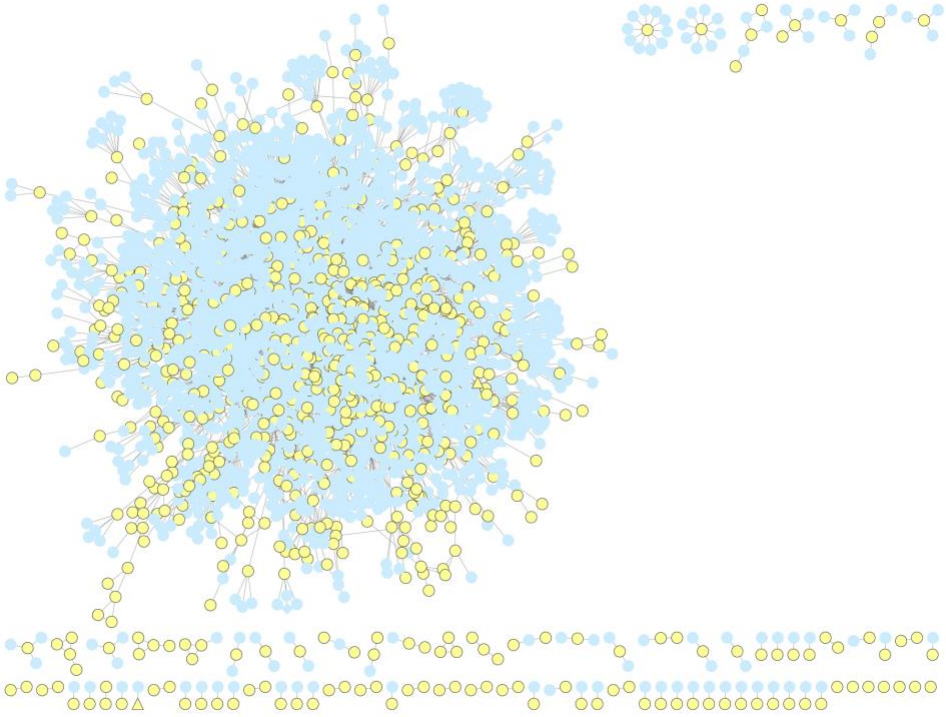

Figure 1. The functional mitochondrial human proteome network. Yellow nodes represent mitochondrial proteins (encoded by the mitochondrial genome or translocated to the mitochondrion, if indicated as mitochondrial in the sublocation or GO Cellular Component sections of the neXtProt database). Blue nodes represent gold interactors of the mitochondrial proteins, as obtained by querying the protein interaction sections of the neXtProt database. Image adapted from Monti et al., 2018.

Several human diseases are associated with mutations in the mitochondrial proteins or in proteins that, interacting with mitochondria, regulate mitochondrial homeostasis (Su et al., 2018). Thus, the number of studies of the mitochondrial proteome associated with a specific pathological condition is increased. The functional mitochondrial human proteome network takes into consideration all mitochondrial proteins and their first interactors and can be used to map proteins derived from proteomics studies on mitochondrial alterations in a specific disease (*e.g.*, PD) highlighting the mitochondrial molecular factors and pathways involved in the disease (Fasano et al., 2016).

The Mitochondrial Human Proteome Project (mt-HPP) is an international project promoted by the Human Proteome Organization (HUPO) that aims at understanding the function of the mitochondrial proteome focusing on proteins that act at the mitochondrial level, considering both those encoded by mtDNA and the nuclear encoded proteins.

1.2.3. Mitochondrial network

The term network describes an extended arrangement of individual elements connected by edges, essential in the conduction and the distribution of data and materials among all the component and over a large area. It characterizes a complex system designed to function in a specific manner (Benard and Rossignol, 2008). Modifications in the mitochondrial network are observed during a variety of conditions like cell division, apoptosis, oxidative stress and metabolic dysfunction. These modifications are responsible for the alteration in the mitochondrial mobility and in the balance of the fusion and fission processes (Hoppins, 2014).

Mitochondria adopt several morphologies depending on the cell types (Kuznetsov et al., 2009). Overall, the various morphologies adopted by mitochondria depend on the cellular type and on different cell energy requirements. In neurons, mitochondria are enriched in areas of high-energy demand (*e.g.*, presynaptic termini). In muscle cells, mitochondria have a uniform intermyofibrillar conformation. Eventually, in fibroblasts, mitochondria form an extensive reticular network.

1.2.4. Mitochondrial dynamics

The idea of mitochondria as solitary and static organelles has evolved. Nowadays, mitochondria are considered as a dynamic population. Mitochondria exist in the cell in two interconverting forms, as isolated particles and as extended filaments, connected together with intermitochondrial junctions, organizing a plastic and dynamic network (Skulachev, 2001) that continuously changes to meet the needs of metabolic stimuli. The entire mitochondria population is in a constant flux, driven by fusion and fission processes. These processes are fundamental to maintain mitochondrial shape and functionality, giving rise to different morphologies of the network (Chen and Chan, 2009). Indeed, the balance between fusion and fission determines the average size and degree of connectivity of the mitochondrial network. Constant network remodeling establishes a mechanism for quality control of the mitochondrial population and provides an additional protection against mitochondrial damage.

Neurons are cells with a high metabolic rate and energy demand. Thus, they are strictly dependent on mitochondrial functions and on their dynamic properties (Chen and Chan, 2009). For this reason, derangements in fusion and fission processes can have a role in the insurgence of neurodegenerative disease (Zeviani and Di Donato, 2004).

1.2.4.1. Mitochondrial fusion

Mitochondrial fusion allows the exchange of components between mitochondria, thus enabling the maintenance of their functional state (Chen and Chan, 2006) and also have a protective role

against apoptosis (Chen and Chan, 2006). The fusion process is made possible by three different proteins (*i.e.*, mitofusin 1 (MFN1), mitofusin 2 (MFN2) and optic atrophy 1 (OPA1)) (Figure 2).
MFN1 and MFN2 are integral OMM proteins with GTPase activity that are responsible for the fusion of the OMMs (Chen et al., 2003; Dimmer and Scorrano, 2006). Both MFN1 and MFN2 share relevant functional domains and connect adjacent membranes through coiled-coil dimers, that can be homotypic (MFN1-MFN1) or heterotypic (MFN1-MFN2). The turnover of MFN1 and MFN2 depends on the recruitment of chaperon proteins such as p97, which mediate retrotranslocation of mitofusins and promote their proteasomal degradation (Tanaka et al., 2010). MFN2 has also a crucial role in tethering mitochondria and endoplasmic reticulum during calcium exchange between organelles (de Brito and Scorrano, 2008). MFN2 plays a fundamental role in mitochondrial motility by connecting mitochondria to the Miro/Milton transport complex (Misko et al., 2010). Because of the higher GTPase activity of MFN1 protein, mitochondria that own only MFN1 protein show a better tethering efficiency than mitochondria with only MFN2 protein (Ishihara et al., 2004). MFN1 is thus able to partially rescue the defects caused by MFN2 mutations (Detmer and Chan, 2007).
Deletion of either MFN1 or MFN2 results in mitochondrial fragmentation and poor mitochondrial function, although low levels of mitochondrial fusion remains. However, mitochondrial fusion is completely abolished when they are both deleted (Perier and Vila, 2012).
OPA1 is a 120 kDa proteins belonging to the family of dynamin related GTPases (Chan, 2006), requiring the presence of MFN1 for its activity (Cipolat et al., 2004). As mitofusins, OPA1 creates complexes that tether membranes and promote inner membrane fusion (Hoppins et al., 2007). Expression of OPA1 is highly regulated at the transcriptional level with eight possible isoforms available through alternative splicing (Song et al., 2009). OPA1 is imported in the IMS, where it is processed by several proteases, such as the presenilin-associated-rhomboid-like (PARL) and HTRA2 in the intermembrane space, and OMA1 in the IMM, thus leading the formation of both long (L-OPA1) and short (S-OPA1) protein forms. The L-OPA1 isoforms have an N-terminal domain anchored to the IMM, while the S-OPA1 isoforms are targeted to the IMM through association with L-OPA1 (Cipolat et al., 2006). Under physiological conditions, proteolytic cleavage of L-OPA1 results in the balanced accumulation of long and short OPA1 forms (Song et al., 2009) in order to preserve the mitochondrial network morphology. However, mitochondria depolarization induces the activation of OMA1 protease that determine the complete shift of L-OPA1 into S-OPA1 (Song et al., 2009). Stress-induced OPA1 processing leads to the inhibition of membrane fusion, thus causing mitochondrial fragmentation (Twig et al., 2008). OPA1 is also involved in the protection against apoptotic cell death and in the maintaining of cristae structure

and junctions, thus preventing the release of cytochrome c from mitochondria (Ramonet et al., 2013; Zhang and Chan, 2007).

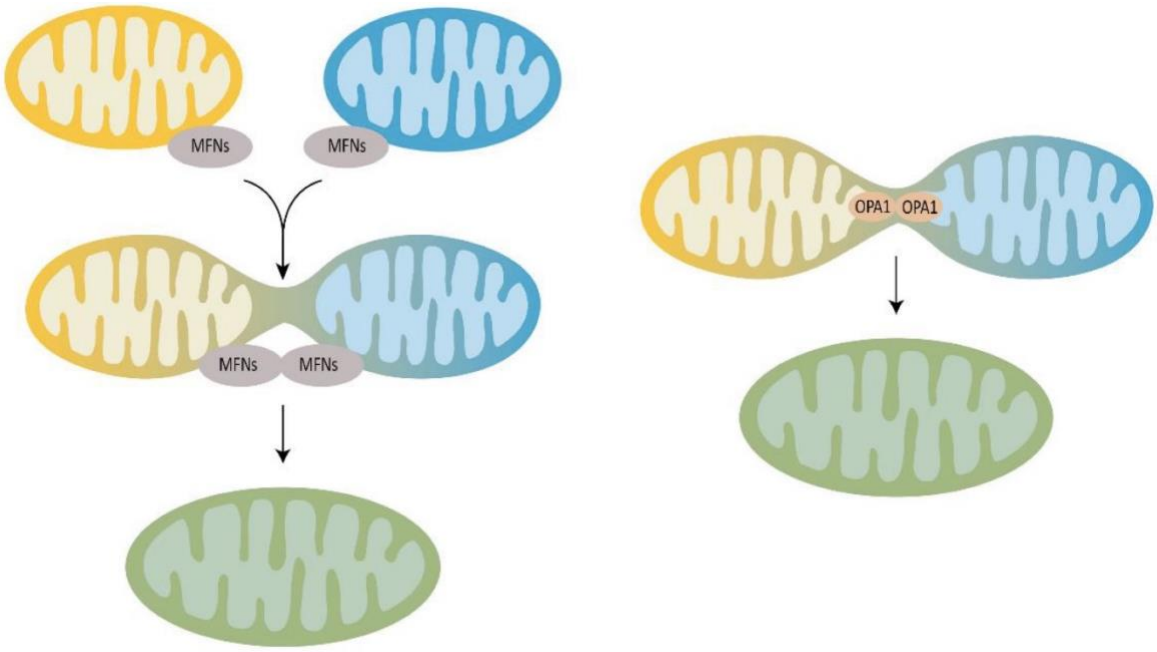

Figure 2. Mitochondrial fusion process. Both MFN1 and MFN2 proteins are responsible for the fusion of the OMMs (left), while OPA1 plays a key role in the fusion of the IMMs (right).

1.2.4.2. Mitochondrial fission

Mitochondrial fission is important to allow the proper cellular distribution of mitochondria and to ensure the degradation of damage mitochondria through the mitophagy process (Otera and Mihara, 2011). Fission process is mediated by Drp1. Drp1 is a cytosolic GTPase recruited to mitochondria that forms distinct mitochondrial foci consistent with fission sites (Smirnova et al., 2011). Drp1 polymerized around mitochondria and acts by forming a ring around the membrane and by the GTP hydrolysis it tightens and causes mitochondrial separation (Santos and Cardoso, 2012) (Figure 3).

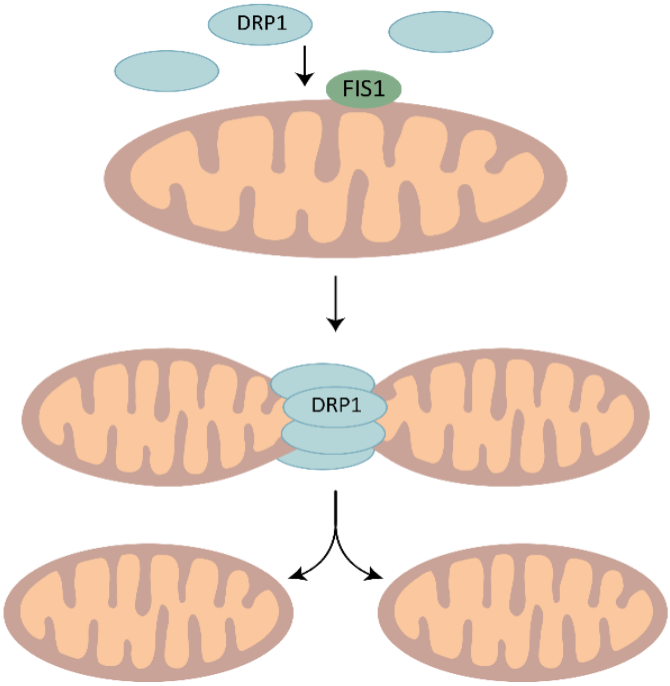

Figure 3. Mitochondrial fission process. Fis1 is a mitochondrial membrane receptor involved in the recruitment of Drp1 protein. Once Drp1 localized and oligomerized on the OMM, it constricts mitochondria by the hydrolysis of GTP molecules.

The recruitment of Drp1 to mitochondria is mediated by several post-translational modification, such as sumoylation, ubiquination, phosphorylation and S-nitrosylation (Otera and Mihara, 2011). For example, β-Amyloid protein stimulates the nitric oxide production to cause S-nitrosylation of Drp1 leading to an enhanced GTPase activity that results in excessive mitochondrial fission in neurons. This process leads to a synaptic loss and neuronal damage (Otera and Mihara, 2011). Drp1 recruitment on the OMM is allowed by the action of specific mitochondrial receptors (Parone et al., 2008). The most characterized receptor is the Mitochondrial fission 1 protein (Fis1), an integral membrane protein located on the OMM (Mozdy et al., 2000), important for the translocation of Drp1 from the cytosol to the mitochondria. The N-terminus of Fis1 faces the cytosol whereas the C-terminus is exposed to the IMS (Mozdy et al., 2000). Other mitochondrial membrane proteins interact with Drp1 causing the fission process, such as the mitochondrial fission factor that can recruit Drp1 independently of Fis1 and its overexpression determines mitochondrial fragmentation (Otera et al., 2010). In addition, MiD49 and MiD51 are involved in the fission process by recruiting Drp1 on the OMM (Palmer et al., 2011).

1.2.5. Mitochondrial quality control

Mitochondria play a key role in energy homeostasis. This process necessarily causes the production of ROS as a by-product (Tatsuta, 2009). For this reason, these organelles require lifetime control and constant renewal. The life cycle of mitochondria includes both the division of pre-existing organelles (mitochondrial biogenesis) and the degradation of older and dysfunctional organelles (mitophagy). In this complex scenario, mtDNA replication and mitophagy, as well as fusion and fission processes, must be coordinated in order to maintain a healthy cellular mitochondrial pool and bioenergetic function. Through fission and fusion processes mitochondria repair damage components by segregating or exchanging materials (van der Bliek et al., 2013). Several damages of mitochondria impair fusion and result in fragmentation of mitochondria, which are then removed by the mitophagic process. Thus, an impairment in these pathways cause mitochondrial dysfunction that underlies PD pathogenesis.

Moreover, mitochondria have their own proteolytic system fundamental to degrade misfolded or unfolded proteins inside mitochondrial compartments (Koppen and Langer, 2007). In addition, the proteasome system is involved in the elimination of damage outer mitochondrial proteins and proteins that fail to be imported (Palikaras and Tavernarakis, 2014).

1.2.5.1. Mitochondrial biogenesis

Mitochondrial biogenesis is a growing and division process of pre-existing mitochondria and occurs not only by variations in number of mitochondria, but also in size and mass. Mitochondria have their own genome and can auto replicate. Correct mitochondrial biogenesis requires the synthesis of 1 000-1 500 proteins and can be influenced by environmental stress such as oxidative stress. As described above, mtDNA is a circular DNA molecule that has its own translational and transcriptional system. Mitochondrial mtDNA polymerase γ is responsible for the mtDNA replication. The transcription of mtDNA is performed by the mitochondrial RNA polymerase (Scarpulla, 2008). Several factors regulating mitochondrial biogenesis have been described. For example, PGC-1α is a co-transcriptional regulation factor that induces mitochondrial biogenesis by activating the nuclear respiratory factors 1 and 2 (NRF1 and NRF2). NFR1 and NFR2 bind several promoters of genes involved in mtDNA transcription (Virbasius and Scarpulla, 1994). The activation of NRF1 and NFR2 by PGC-1α promotes the expression of several transcriptional factors such as the mitochondrial transcription factor A (Tfam). Tfam is then able to activate transcription and replication of mtDNA (Gleyzer et al., 2005). Another co-transcriptional regulation factor is PGC-1β that has similar molecular structure and functions of PGC-1α. Given its fundamental role in the mitochondrial biogenesis, PGC-1α is regulated on both the

transcriptional and post-translational levels. CREB, after the activation by protein kinase A, regulates directly the expression of PGC-1α (Herzig et al., 2001). On the other hand, AMP-activated protein kinase is responsible for the post translational modification of PGC-1α. Indeed, the phosphorylation of PGC-1α can promote the mitochondrial biogenesis activation. Another activator of PGC-1α is c-GMP, which is activated following an increase of nitric oxide cellular levels (Nisoli et al., 2004).

Strong evidences suggest that the impairment of mitochondrial biogenesis process is strictly connected to the development of neurodegenerative diseases, such as PD. For example, α-syn can regulate the PGC-1α leading to a reduction of the mitochondrial biogenesis (Ryan et al., 2013). Moreover, Parkin has several functions in maintaining healthy mitochondria by regulating their biogenesis. Under physiological levels, Parkin mediates the degradation of Parkin interacting substrate (PARIS), a repressor of PGC-1α activity (Shin et al., 2011). Mutations in *PARK2* gene can cause a loss-of-function of Parkin protein that allows PARIS to accumulate and repress mitochondrial biogenesis (Stevens et al., 2015).

1.2.5.2. Mitophagy

Because of the essential role of mitochondria for the cell, it is important to keep them in a functional state and to remove the dysfunctional ones. The accumulation of damaged mitochondria is highly risk for the cell due to ROS production, which are harmful for the cell wellbeing (Pickles et al., 2018). Mitochondria can be degraded by autophagy either in a non-selective manner or through a process that selectively targets damaged mitochondria, termed “mitophagy”.

Mitophagy is a physiological mechanism that acts as a quality control checkpoint for mitochondrial turnover and it is strictly connected to fusion and fission processes since it allows to get rid of damage mitochondria that cannot be rescue.

The most characterized mitophagy mechanism is the PINK1/Parkin pathway. PINK1 is a serine/threonine kinase with three insertional loops within its catalytic domain and an N-terminal mitochondrial targeting signal domain (MTS). Under basal conditions, when the mitochondrial membrane is well polarized, the precursor of PINK1, previously synthesized in the cytosol, is imported into the OMM via TOM complex. The full-length PINK1 (64 kDa) is translocated into the IMM through the TIM complex in a membrane potential-dependent manner. PINK1 is processed by the mitochondrial processing peptidase (MPP) that cleaves the MTS sequence, resulting in a 60 kDa PINK1 form. This form spans the IMM and is cleaved by PARL, which gives rise to the 52 kDa mature form. The mature form of PINK1 has a very short half-life and it is rapidly removed and degraded through the proteasome. In this way, endogenous PINK1 levels are

kept very low in polarized mitochondria, in order to prevent mitophagy in healthy mitochondria (Eiyama and Okamoto, 2015; Ashrafi and Schwarz, 2013; Matsuda et al., 2010) (Figure 4).

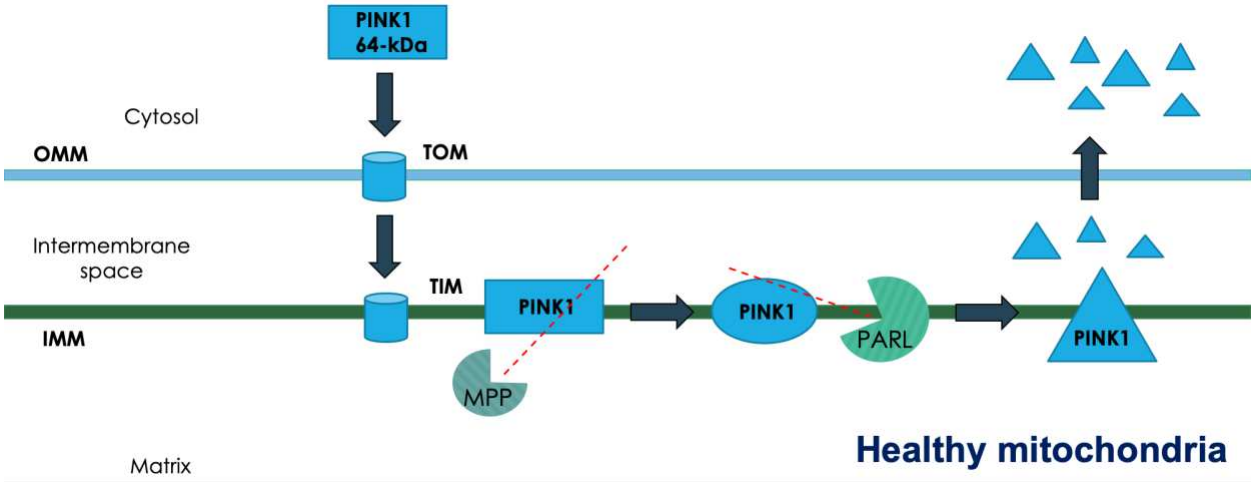

Figure 4. PINK1 degradation in healthy mitochondria. Under physiological conditions, the PINK1 precursor (64 kDa) is imported into the OMM via TOM and further transferred into IMM through TIM complex in a membrane potential-dependent manner. Here, 64 kDa PINK1 is processed by MPP that removes the MTS sequence. This form of PINK1 is then cleaved by PARL, giving rise to the 52 kDa mature form and subsequently degraded by mitochondrial peptidases and by the proteasome.

When mitochondria are damaged and lose their membrane potential, PINK1 processing is inhibited and its long form accumulates on the OMM (Narendra et al., 2010). PINK1 kinase domain is exposed to the cytosol and accessible to substrates, such as Parkin (Jin et al., 2010; Narendra et al., 2010). Parkin is a cytosolic E3 ubiquitin ligase, highly abundant in the substantia nigra. Once Parkin is recruited, PINK1 promotes its activity by phosphorylation (Kondapalli et al., 2012). Activated Parkin ubiquitinates different OMM proteins (*e.g.*, VDACs and MFNs), facilitating the recruitment of some adaptor proteins that work together to construct the autophagosome structure (Fimia et al., 2007). In this way, the ubiquitination of MIRO, MFN1 and MFN2 serve to immobilize the mitochondrion and to prevent it from rejoining the mitochondrial network through fusion (Gegg et al., 2011; Chen et al., 2013).

Several autophagy receptors are recruited to damaged mitochondria in order to bind the ubiquitin-tagged OMM proteins such as neighbor of BRCA1 or sequestrome-1 (p62/SQSTM1). p62/SQSTM1 is involved in the mitochondrial clustering during mitophagy and it is required for mitochondrial disposal (Geisler et al., 2010) (Figure 5). Furthermore, Parkin is able to bind AMBRA1, an autophagy-promoting protein that determines the local formation of autophagosomes, thus causing the PINK1/Parkin-mediated mitophagy (Van Humbeeck et al., 2011). The autophagosomes, with its cargo, fuses with a lysosome, forming the acid

autophagolysosome. The cargo is degraded by lysosomal hydrolases, liberating amino acids and fatty acids that are exported to the cytosol via lysosomal permeases.

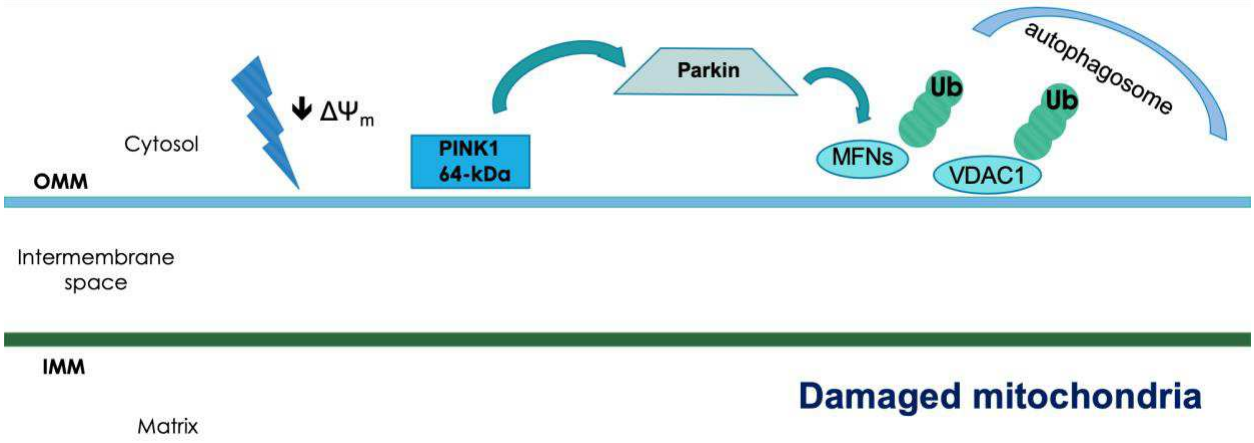

Figure 5. PINK1/Parkin mitophagy pathway. When mitochondria are depolarized, PINK1 accumulates onto the OMM, thus recruiting Parkin. Parkin catalyzes the covalent attachment of ubiquitin moieties onto specific mitochondrial proteins. This process leads to the selective engulfment of damaged organelles by the autophagosome.

Mitophagy can also occur independently of Parkin. Several autophagy receptor proteins localize on mitochondria and interact with LC3 to recruit autophagosomes to damaged mitochondria, including Parkin-independent mediators such as Bcl2/adenovirus E1B 19 kDa protein-interacting protein 3 (BNIP3), NIX and Fun14 Domain containing 1. BNIP3 and NIX activate autophagy by determining the dissociation of the Bcl-2-Beclin-1 complexes (Bellot et al., 2009). BNIP3 can also recruit Drp1 and Parkin to the mitochondria to promote fission and mitophagy (Lee et al., 2011).

1.2.5.3. Intraorganellar quality control system

The first line of defense operates within mitochondria. Several chaperones and proteases act in the mitochondrial quality control system by promoting the folding of newly imported proteins, by protecting mitochondrial proteins against heat stress and by degrading irreversibly damage polypeptides.

The mitochondrial chaperones, such as the heat shock proteins (HSPs) (*e.g.*, HSP60 and HSP70) and HtrA2/OMI are essential due to the continuous import of the vast majority of mitochondrial proteins and to the predisposition to oxidation of misfolded proteins (Vande Walle et al., 2008).

Mitochondrial proteases recognize misfolded proteins and degrade them into peptides. Peptides are further exported from mitochondria or degraded to amino acids by the action of oligopeptidases (Rugarli and Langer, 2012). Two ATP-dependent mitochondrial proteases are contained in the mitochondrial matrix. The first one is Lon, a serine protease that degrades denatured and oxidized

proteins. The second one is Clp, which is involved in the degradation of damage proteins in the mitochondrial matrix (Hamon et al., 2015).

The quality control of the IMM is mediated by two membrane-embedded metalloprotease complexes, the AAA protease. The i-AAA protease faces towards intermembrane space, while the m-AAA protease exposes the catalytic domain to the matrix side of the inner membrane. These two complexes play a fundamental role because of the high number of proteins that can be targeted for oxidative and nitrosative stress, even considering the presence of respiratory chain complexes in the IMM (Hamon et al., 2015; Koppen and Langer, 2007).

1.2.6. Mitochondrial dysfunctions and Parkinson's disease

Mitochondrial dysfunction plays a crucial role in the degeneration of dopaminergic neurons in PD pathogenesis. Several genes linked to PD encode proteins that take part to processes involving mitochondria, thus being fundamental for mitochondrial homeostasis. For this reason, mutations in these genes can compromised the function of these proteins leading to an impaired mitochondrial function, a modified mitochondrial morphology and an increase of ROS production. Parkin and PINK1 act in a common way to modulate the mitochondrial shape (Poole et al., 2008). Mutations in PINK1 and Parkin genes can cause an impairment in mitochondria functionality. More precisely, mutations in *PARK2* gene, correlated to early onset familial PD, are associated with mitophagy impairment (Lee et al., 2010), while mutations in *PARK6* gene result in the alterations of mitochondrial morphology and function, together with a reduced activity of complex I (Song et al., 2013). The overexpression of PINK1 acts in a pro-fission manner, determining the formation of a more fragmented mitochondrial network. On the other hand, knockdown of PINK1 leads to the formation of a more interconnected mitochondrial network (Yu et al., 2011). Furthermore, Zanellati and colleagues demonstrated that the loss-of-function of Parkin protein cause the appearance of a "chain-like" network (Zanellati et al., 2015). The impairment of PINK1/Parkin mitophagy pathway could lead to the accumulation of dysfunctional mitochondria that may contribute to dopaminergic cell death due to increased production of ROS and the enhanced release of mitochondrial apoptogenic factors (Fernández-Moriano et al., 2015).

Mutations in *PARK8* gene cause mitochondrial fragmentation and a reduction in the ATP production and in the mitochondrial membrane potential (Li et al., 2014).

Mutations in *SNCA* gene lead to an accumulation of α-syn in dopaminergic neurons that can be responsible for mitochondrial fragmentation and for a reduction in the complex I activity (Martin et al., 2006).

1.3. Human skin fibroblasts as cellular model of Parkinson's disease

Tissues and cell lines derived from patients represent a good source for studying phenotypes related to the disease of interest (Vangipuram et al., 2013). Human skin fibroblasts are an easily accessible source of proliferating cells that share the same genetic complexity of neurons (Auburger et al., 2012; Connolly, 1998). In particular, these cells mirror the polygenic risk factor and reflect the cumulative cell damage that occurs in patients, together with the chronological and biological aging (Auburger et al., 2012). Skin fibroblasts can be easily obtained from 2 mm punch skin biopsies performed by dermatologists, without excessive surgical complications. Since it is not a routine procedure, a written consent and ethical commission approval is mandatory (Auburger et al., 2012). Moreover, fibroblasts are available from a large number of cell banks with known genetic defects and can be efficiently propagated by simple cell culture procedures (Connolly, 1998).

Several studies carried out on fibroblasts obtained from skin biopsies from PD patients showed that these cells reported some deficit associated with PD pathogenesis that are typical of neuronal tissue (Kilpatrick et al., 2016; Lippolis et al., 2015). Indeed, human fibroblasts from PD patients showed relevant expression levels of PINK1 and Parkin genes and since both genes take part to the pathogenesis of PD, patient skin fibroblasts are a suitable model for PD (Auburger et al., 2012). For example, skin fibroblasts from *PARK6* patients reported a strong respiratory deficit, altered mitochondria morphology and an increase of oxidative stress (Grünewald et al., 2009; Klinkenberg et al., 2010). Zanellati and colleagues demonstrated that fibroblasts from PARK2 patients could be used to study the mitochondrial impairment that characterizes these patients. In particular, these cells showed alteration in mitochondrial bioenergetics, such as an increased oxygen consumption rate with a reduction in ATP levels, a lower complex I activity and a lower membrane potential (Zanellati et al., 2015). The uncoupling between oxygen use and ATP synthesis was reflected by the loss of mitochondrial membrane potential, as previously reported (Mortiboys et al., 2008; Grünewald et al., 2010). Moreover, Zanellati and coworkers reported an accumulation of damaged mitochondria (Zanellati et al., 2015). Since Parkin and PINK1 are involved in mitophagy regulation, Parkin may control mitochondrial dynamics (Buhlman et al., 2014).

Accordingly, fibroblasts can be used as primary cells model for neurodegenerative disorders, where the tissue primary affected is not available (Devine et al., 2011). The main disadvantage in the use of these cells is that they not fully represent the tissue directly affected by the disease. Nevertheless, the advent of induced pluripotent stem cells (iPSCs) technology gives a way to generate patient-specific cellular models of diseases (Beevers et al., 2013). Indeed, it is possible to transform skin fibroblasts into dopaminergic neurons (Takahashi et al., 2007).

1.4. Proteomics

PD is a complex and multifactorial disorder characterized by a not completely understood etiology. Therefore, it is clear the difficulties to obtain an exhausting view of the mechanisms underlying PD pathogenesis. In this framework, the identification of the molecular pathways involved in the pathology could facilitate the understanding of the disease processes. The research in this field has recently focused on the use of omics approaches such as transcriptomics, proteomics and metabolomics (Caudle et al., 2010).

Proteomics is an unbiased and global approach that studies structure and function of proteins by a variety of methods. The term proteome was first coined by Wilkins in 1994 to identify the entire set of PROTEin coded by a genOME (Wilkins et al., 1997). Proteomics aimed at investigating the complete set of proteins present in a cell, organ or organisms highlighting what is happening in the system under determined conditions. The definition of proteome is strictly connected to the time factor. Indeed, all the protein complexes that regulate biological processes undergo different variations, in the alterations in the proteins expression, in their abundance, in their cellular or tissue localization, in their post-translational modifications that are dependent on temporal and spatial factors such as the physiological or pathological status of the cell (Villoslada et al., 2009). Nowadays, the proteome assumes a more functional meaning (Monti et al., 2019). The list of proteins thus generated can be integrated with data mining methods, thus revealing proteins involved in specific biological pathways that were hidden by the complexity of data themselves (Alberio et al., 2010; Alberio and Fasano, 2011). Moreover, proteomics allows generating new hypotheses that should be further verified by targeted study (Monti et al., 2019).

Proteomics can be performed through two distinct approaches: gel-based proteomics, based on the separation of proteins by two-dimensional electrophoresis (2-DE) followed by mass spectrometry (MS) protein identification, and gel-free proteomics, where proteins are digested into peptides and then separated by liquid chromatography (LC). The latter includes various isotopic labeling strategies for quantitative proteomics analysis as well as label-free quantitative approaches. The quantitation of proteomes is difficult and presents some issues. Gel-based technique are top-down approaches that directly analyze proteins. The extrapolation of protein abundance is complicated by the presence of multiple proteoforms (Jorrin-Novo et al., 2018). Thus, changes wrongly attributed to protein amounts may be due to post-translational modifications. On the other hand, gel-free technique are bottom-up approaches and analyze peptides. The extrapolation of protein abundance from peptides is not trivial, since the information on both identity and amount of each protein is obtained by the peptide-to-protein mapping.

1.4.1. Gel-based proteomics

Gel-based proteomics requires as a first step the separation of proteins by a simple SDS-PAGE or 2-DE. 2-DE is the most common technique that allows the separation of proteins, first by their isoelectric point (1st dimension) and second by their molecular weight (2nd dimension). By isoelectric focusing, proteins migrate through a gel-strip embedded with immobilized pH gradients. Migration ends when each protein reaches the point where the net charge is neutral. Proteins are then separated in the second dimension according to their molecular mass using a common SDS-PAGE. Proteins can be visualized by staining the gel with specific chemical stains (*e.g.*, Coomassie blue) or fluorescent protein dyes (*e.g.*, SYPRO stains and ruthenium-based dyes) in order to detect differences in protein staining intensities among samples (Pienaar et al., 2008). Separation in these two dimensions allows the resolutions of multiple isoforms and variants of the same proteins, such as post-translational modifications. Moreover, 2-DE is able to resolve thousands of spots simultaneously and represents the only technique that can be routinely applied for parallel quantitative profiling of large sets of complex protein mixtures such as whole cell lysates (Albrecht et al., 2010). Nevertheless, there are intrinsic weaknesses in 2-DE because less represented proteins are lost, thus limiting the global characteristic of the proteomic approach. Furthermore, proteins of extreme hydrophobicity or extreme basic or acid are not considered in the majority of published studies (Albrecht et al., 2010).

1.4.2. Gel-free proteomics

Gel-based proteomics is a well-established technique, but it suffers from difficulties in quantitative reproducibility and limitations in analyzing certain classes of proteins. In recent years, alternative approaches to 2-DE have been developed to overcome the limits of gel-based technique (Abdallah, 2012). The advance represented by this approach made it possible to avoid some of the limitations of gel-based proteomics, including the requirement of large amounts of starting material, a limited dynamic range, low-throughput analysis, difficulties in the identification of acidic, basic, hydrophobic, very small or very large proteins and biases due to the presence of abundant proteins (Walther and Mann, 2010).

The term “shotgun proteomics” was coined by the Yates Lab and refers to the application of bottom-up proteomics analysis to protein mixtures, thereby indirectly measuring proteins by analyzing the peptides generated from proteolysis of intact proteins using proteolytic enzymes (*e.g.*, trypsin). The peptide mixtures are separated by LC, which is coupled to tandem mass spectrometry (MS/MS) for further analysis (McDonald and Yates, 2002). In shotgun proteomics,

peptides are identified using different approaches, namely *de novo* sequencing and database searching (Zhang et al., 2012).

De novo sequencing obtains the peptide sequence directly from each MS/MS input spectrum using a proper algorithm. The *de novo* sequence tags are then used to reveal matches in the protein sequence database, generating a protein shortlist. All the peptides generated by an *in-silico* digestion of this list are compared with initial MS/MS spectra and a precise scoring function is used to highlight the best peptide for each spectrum. The identified peptides are then used to infer the proteins (Zhang et al., 2012).

In database sequencing, a sequence database is queried in order to find out the best peptide fitting with the peaks in the MS/MS spectrum. Peptides are thus identified by comparing tandem mass spectra of fragmented peptides with deposited theoretical tandem mass spectra available in protein databases. If the protein of interest is present in the sequence database, the aim is to retrieve that precise entry, whereas, if it is not present, the aim is to find out entries with the closest homology (Zhang et al., 2012).

1.4.2.1. Quantitative Mass Spectrometry

Although shotgun proteomics can mine deeper into the proteome, several problems arise with the quantification if samples are too complex.

Nowadays, two different approaches are used to quantify the proteome: the differential isotopic labelling and the label-free quantification. These two techniques have different advantages, isotope-labelling methods measure protein abundance with higher accuracy, whereas label-free approaches have a greater dynamic range and achieve higher levels of proteome coverage.

1.4.2.2. Differential isotope labelling

This approach is built on the theory of stable isotope dilution (Ong and Mann, 2005), where the relative signal intensity obtained in a mass spectrometer of two analytes that are chemically identical, but have different stable isotope composition, represents the relative abundance of the two analytes in the sample. Protein abundance can be analyzed in a LC-MS/MS based on observable mass shifts caused by differential isotope labeling (Ong and Mann, 2005). The isotope labelling can be applied either *in vitro* by labeling of isolated proteins and peptides, or *in vivo* by the incorporation of isotope-labeled amino acids through metabolic labeling, which is also called stable isotope labelling with amino acids in cell culture (SILAC).

The main advantage of this strategy is that the differentially treated samples can be mixed at the level of intact cells. However, the cost of this approach in *in vivo* models is often inadequate with the amount of the information provided (Bantscheff et al., 2007).

1.4.2.3. Label-free quantification

Label-free quantitative MS methods are based either on spectral counting or on peptide precursor ion intensities that are obtained using the first analyzer of a tandem mass spectrometer (Colinge et al., 2005). This method is based on the assumption that the rate at which a peptide precursor ion is selected for fragmentation in a mass spectrometer is correlated to its abundance. For relative protein quantification, the spectral counts are then averaged to the protein abundance index. Label-free quantification is based on the accurate mass and time tag approach (Strittmatter et al., 2003) and builds on the alignments of high-mass accuracy spectra that are obtained from the analysis of two different sample conditions by separate LC-MS/MS experiments. Peptides are identified across different LC runs based on their specific retention time coordinates and precise mass to charge (m/z) values, which allows the quantification of all peptides detected from a biological sample that are within the sensitivity range of a MS analyzer, independent of MS/MS acquisition (Bantscheff et al., 2007).

Label-free quantification has many advantages: there is no limit on the number of samples that can be compared, and it can be applied to any kind of sample that cannot be directly metabolically labeled including many clinical samples.

2. Aim of the project

PD is a multifactorial disorder in which both genetic and environmental factors are involved in the disease onset and progression. Although the cause of PD is not completely understood, strong evidences suggest that the impairment of the ubiquitin-proteasome system, the increased oxidative stress, the dysregulation of protein trafficking and the mitochondrial damage are hallmarks of PD. In particular, mitochondrial dysfunction and mitophagy impairment seem to be clearly involved in PD pathogenesis (Schapira and Jenner, 2011). In this context, a better insight into the molecular mechanisms driving this pathological landscape is necessary.

To this purpose, *PARK2*-mutated primary skin fibroblasts were used as a cellular model to explore the effects of *PARK2* mutations both on the mitochondrial function and morphology and on the total and mitochondrial proteome. PARK2 patients carry genetic mutations that lead to the loss-of-function of Parkin protein, which is essential for the elimination of damaged mitochondria. Although PARK2 is a familiar and rare form of PD, it offers a unique opportunity to study how the impairment in the Parkin functionality can cause the improper disposal of dysfunctional mitochondria. The accumulation of these organelles determines an increment of ROS levels, lower ATP production, and apoptosis activation. Moreover, it is already been demonstrated that skin fibroblasts from PARK2 patients can be used to investigate the mitochondrial impairment that characterized these subject (Zanellati et al., 2015). Therefore, fibroblasts are an easily accessible peripheral source of proliferating cells, which can mirror at the periphery what is happening at the central level.

The first part of this thesis investigates the impact of Parkin impairment on mitochondrial function and network in primary skin fibroblasts of five PARK2 patients and five control subjects. In particular, mitochondrial network alterations were investigated from a morphological point of view. Furthermore, we focused on mitochondrial alterations and we related molecular outcomes with information on the mitochondrial membrane potential. As a reference model of mitophagy induction, treatment with the IMM uncoupler carbonyl cyanide m-chlorophenyl hydrazone (CCCP) was used as a positive control.

The second part of this project is focused on the characterization of the mitochondrial and the total proteome alterations that characterize patients carrying *PARK2* mutations. Because of the multifactorial nature of PD, the use of a global approach, such as proteomics, may give a more comprehensive view about its etiopathogenesis. Mitochondrial-enriched and whole cell fractions were analyzed by quantitative shotgun proteomics analysis in order to identify proteins specifically altered by Parkin loss-of-function. Eventually, a systems biology approach was used to identify the molecular pathways altered by mutations in *PARK2* gene.

3. Materials and methods

3.1. Cell cultures and treatments

Human primary skin fibroblast cell lines from five PARK2 patients (2 males, 3 females; mean age 45± 20) and five age-matched control subjects (2 males, 3 females; mean age 38 ± 13) were obtained from the "Cell line and DNA Bank of Genetic Movement Disorders and Mitochondrial Diseases" of the Telethon Network of Genetic Biobanks. Personal and clinical data and genetic characterization were collected from each subject after specific informed consent (Table 1).

Subject [a]	**Gender** [b]	**Age at onset (years)**	**Age at skin biopsy (years)**	***PARK2* mutation**
P1	F	61	74	Del_1/p.R275W
P2	M	17	45	Del_3-4-5/p.R33X
P3	F	14	18	Dup_2/Del_3-4-5
P4	M	40	52	p.Q34Rfs*X5 homo
P5	F	22	35	p.Thr240Met/Del3
C1	F	Control	27	CTRL
C2	F	Control	27	CTRL
C3	M	Control	33	CTRL
C4	M	Control	54	CTRL
C5	F	Control	51	CTRL

Table 1. Summary of personal and clinical data and genetic characterization of subjects involved in the study. [a] P: PARK2 PD patients; C: control subjects. [b] F: Female; M: Male.

Fibroblasts were cultured in 5% humified atmosphere at 37°C in high-glucose Dulbecco's modified Eagle's medium (DMEM) (Euroclone) supplemented with 15% Fetal Bovine Serum (FBS) (Euroclone), 1% of Penicillin-Streptomycin (Euroclone) and 1% of L-glutamine (Euroclone). Cells were seeded at the density of 5×10^5 per T25 flask and expanded up-to a maximum of 13 passages. Every two days the medium was changed until fibroblasts reached 80% of confluence. Cells were detached using Accutase (Euroclone) and collected after centrifugation for 10 minutes, 500×g, 25°C.

Cells were seeded at a density of 5×10^5 per T75 flask and cultured for 24 hours at 37°C before assay. Fibroblasts were exposed to CCCP at a concentration of 60 μM or an equal volume of vehicle, the dimethyl sulfoxide (DMSO) (Sigma-Aldrich). Treatment lasted for 24 hours.

3.2. Total pellet preparation and mitochondrial enrichment

Fibroblasts were detached with Accutase and centrifuged for 10 minutes, 500×g, 4°C. Cellular pellet was washed Phosphate Buffered Saline (PBS), collected in Eppendorf tube and centrifuged for 10 minutes, 1 200×g, RT. The resulting whole cell pellet was collected and stored at -80°C for following total proteome analysis.

Mitochondria were isolated from 1.5×10^7 fibroblast cells using the Mitochondria Isolation Kit (Sigma-Aldrich), a commercial kit based on surfactants. Fibroblasts were detached and centrifuged as described above. After centrifugation, the pellet was washed twice in ice cold PBS, cellular pellet was resuspended in 1 ml of Lysis buffer and incubated on ice for 10 minutes. Two volume of Extraction buffer were added, and the lysate was centrifuged for 10 minutes, 600×g, 4°C. The supernatant was removed whereas the pellet was subjected to a second lysis as already described. The supernatant was centrifuged for 10 minutes, 11 000×g, 4°C to obtain the mitochondrial-enriched fraction. The mitochondrial pellet was stored at -80°C for further mitochondrial proteome analysis. The efficiency of the mitochondrial enrichment was evaluated by Western blot, by the quantification of the nuclear marker histone H3 and citrate synthase (CS) and voltage-dependent anion channel 1 (VDAC1), two mitochondrial markers.

3.3. Western blot analysis

Cells were lysed in RIPA buffer (50 mM Tris-HCl pH 7.6, 150 mM NaCl, 1% sodium deoxycholate, 1% NP-40, 0.1% SDS, 1x protease inhibitor cocktail (Sigma-Aldrich)), sonicated on ice (0.5 cycles, 10 pulses, amplitude 100% and 0.5 cycles, 10 pulses, amplitude 80%). Lysates were centrifuged for 30 minutes, 15 000×g at 4°C in order to collect the supernatant in new Eppendorf tubes. Protein content evaluation was performed using the Bicinchoninic Acid Protein Assay (BCA) (Thermo Fisher Scientific). Equal amounts of proteins were incubated in Laemmli loading buffer (Tris HCl 0.5 M pH 6.8, 10% SDS, glycerol, H_2O and bromophenol blue) and denaturated at 95°C for 5 minutes. Proteins were separated by electrophoresis in 16% or 8% SDS-gels and transferred to polyvinylidene difluoride (PVDF) membranes (Millipore) at 1.0 mA/cm_2, 2 hours (TE77pwr, Hoefer). PVDF membranes were saturated for 2 hours in tris-buffered saline with 0.05% TWEEN (TBST) with 5% milk powder and then incubated with primary antibodies overnight at 4°C: Parkin (#2132, 1:500; Cell Signaling), PINK1 (#6946, 1:500; Cell Signaling), β-actin (ab8226, 1:10000; Abcam), CS (AMAb91006, 1:1000; Sigma-Aldrich), histone H3 (H0164, 1:2500; Sigma-Aldrich), VDAC1 (ab15895, 1:1000; Abcam). Membranes were then incubated with peroxidase-conjugated secondary antibodies for 1.5 hours at RT goat anti-rabbit

IgG antibody (#AP132P, 1:1500; Millipore Corporation) and goat anti-mouse IgG antibody (#12349, 1:2000; Millipore Corporation) in 5% milk-TBST. Signals were revealed by chemiluminescence using Enhanced chemiluminescence substrate (Millipore Corporation). Images were acquired using a 16 bit acquisition system (G:BOX Chemi XT4 Syngene) and analyzed using the software ImageJ (National Institute of Health, Bethesda, MD). Beta-actin contents were established as loading controls. Statistical analysis was performed by two-tailed, unpaired Student's t-test and by two-way ANOVA. $p < 0.05$ was considered significant.

3.4. Mitochondrial Membrane Potential ($\Psi\Delta_m$) quantification

Fibroblast cells were seeded in 12-well plates at 8×10^3 cells per well and cultured for 24 hours at 37°C. Medium was removed and replaced with fresh DMEM with 100 nM Mitotracker Red CMXRos (Life Technologies). After 30 minutes of incubation at 37°C, the medium was removed, and cells were washed with PBS and fixed with 4% paraformaldehyde for 15 minutes. Nuclei were stained with 300 nM 4',6-diamidino-2-phenylindole (DAPI) for 5 minutes (Life Technologies). Images were acquired through a cooled CCD camera (Sensicam; PCO, Kelheim, Germany) and a 40× objective on an Olympus IX81 microscope (Olympus, Tokyo, Japan) and analyzed using Image J software. Seven fields of view randomly taken from three independent experiments were evaluated for each subject. Mitotracker signal intensity was evaluated measuring the integrated density values. The corrected intensity was normalized with respect to the number of cells, as defined by nuclear staining with DAPI. Statistical analysis was performed using two-tailed, unpaired Student's t-test.

3.5. Immunofluorescence stain

For the analysis of mitochondrial network morphology, fibroblasts were seeded onto 18 mm glass coverslips at a density of 5×10^3 per well in a 12-well plate. Cells were cultured under routine conditions for 24 hours. For the colocalization and quantification analysis, fibroblasts were seeded at a density of 5×10^3 or 15×10^3 per well and cultured under routine conditions for 24 hours or treated with 60 μM CCCP or an equal volume of DMSO. Treatments lasted for 24 hours. After removing culture medium, cells were washed with fresh PBS, fixed with 4% paraformaldehyde for 15 minutes, permeabilized with Triton X-100 solution (Triton X-100 0.2% in PBS) for 5 minutes and blocked with 5% FBS in PBS for 1 hour at RT. Coverslips were incubated ON at 4°C with primary antibodies: ATP Synthase β (A9728, 1:400; Sigma-Aldrich) and RAB7A (HPA006964, 1:200; Sigma-Aldrich) in 5% FBS diluted in PBS. Cells were incubated with secondary antibodies: Alexa Fluor 488 anti-rabbi and 647 anti-mouse secondary antibody

(A21236, 1:1000; Thermo Fisher Scientific) in 5% FBS in PBS and counter-stained with 300 nM DAPI for 3 minutes. Coverslips were mounted with ProLong Gold Antifade mountant (Thermo Fisher Scientific). Images were acquired using laser-scanning confocal microscope (Leica TCS SP5) through a 63×/1.40 NA oil-immersion objective (HCX PL APO lambda blue). Z-stacks with 0.2 μm step size were acquired with sequential excitation at 1024×1024 pixels resolution and 1.5× magnification, 2 frames average. Image processing and analysis were performed using ImageJ software.

3.5.1. Mitochondrial network morphology analysis

3.5.1.1. Image processing

Mitochondrial network morphology analysis was performed using the "Analyze Particles" function of ImageJ software as previously described (Bondi et al., 2016). For the analysis, z-stacks of fibroblast cells labeled with ATP Synthase β antibody were used. Seven fields of view were randomly captured and analyzed for each coverslip.

The "Analyze Particles" tool allow the application of several filters and algorithms in order to identify mitochondrial objects from the background and to obtain several spatial and shape descriptors. First of all, a spatial calibration was performed, according to the magnification used during image acquisition. The filter "unsharp mask" was applied to all z-stack slices in order to sharpen edges of the elements without increasing noise. An automatic thresholding procedure, the Huang algorithm, was applied to generate a binary image. Images were processed to improve the mask's representation of the data. The final masks were stored in order to measure the mitochondrial network parameters.

3.5.1.2. Morphology analysis

Several spatial and shape-descriptor parameters were evaluated using the "Analyze Particles" function.

- Area: the area of the particle calculated as the sum of the area of each individual pixel and expressed in calibrated square units (μm^2).
- Perimeter: the total length of the object boundary.
- Major and minor axis: the length of the primary and the secondary axis of the best fitting ellipse for each particle.
- Angle: angle between the primary axis and a line parallel to the x-axis of the image.
- Aspect ratio: ratio between major and minor axis of the best fitting ellipse.

- Circularity: the degree to which an object is similar to a circle, based on the smoothness of its perimeter.
- Roundness: the shape of particles compared to a perfect circle built on the major axis of the particle.
- Solidity: the total concavity of a particle defined as the area of the particle divided by the area of the convex hull of the particle.

3.5.1.3. Mitochondrial network properties analysis

Images were converted to binary. Binary z-stacks were skeletonized in order to remove pixels from the edges of objects until they were reduced to single-pixel-wide shapes. The "Analyze Skeleton" plug-in was used to analyze the mitochondrial skeleton counting and measuring branches, as previously described (Valente et al., 2017).
- Number of branches: number of segments that connect endpoints to junctions or junctions to another junction.
- Number of junctions: number of pixels of an object having more than 2 neighbours.
- Average branch length: average of segment lengths of an object.
- Maximum branch length: maximum length of an object.

3.5.1.4. Statistical analysis of network morphology and properties

The distribution density of all spatial and shape parameters was calculated for each field of view. The distance between the empirical distribution density of each sample and the distribution density of all controls (*i.e.*, particles from five fields of view from each control subject) was obtained by the Kolmogorov-Smirnov test. Significant distances were analyzed by the non-parametric Wilcoxon test followed by the post-hoc Dunn's test for multiple comparisons. All steps and the results of the statistical analysis were obtained using the R environment for statistical computing (http://www.r- project.org/).
The output tables generated by the analysis of the network properties were compared using the univariate non-parametric Wilcoxon test. The boxplots of PARK2 patients and control subjects were generated using the statistics programming language R.

3.5.2. Immunofluorescence quantification and co-localization analysis

In order to quantify the amount of Rab7A localized at the mitochondrial level after CCCP treatment, mitochondrial surface was measured on the z-projection of ATP Synthase β. The analysis was done using the ImageJ software by setting an automated thresholding process (the

IsoData function). Mitochondrial area was selected and transposed on Rab7A corresponding z-projection. Signals of Rab7A antibodies inside the selected areas were quantified and normalized with respect to mitochondrial area values.

The co-localization analysis between Rab7A and ATP Synthase β signals after CCCP treatment was performed among four most representative z-stacks with the JaCoP plugin (Bolte and Cordelières, 2006), after transformation into 8-bit format. The degree of co-localization between the two signals was evaluated by the Manders' Overlap Coefficient, corresponding to the fraction of Rab7A signal overlapping to ATP Synthase β (Manders et al., 1992). Statistical analysis was performed by two-way ANOVA. $p < 0.05$ was considered significant.

3.6. Mass spectrometry analysis

Whole cell pellets and mitochondrial-enriched fractions obtained from human primary skin fibroblasts of PARK2 patients and control subjects were lysed in 0.1% RapiGest SF Surfactant (Waters) diluted in 50 mM $(NH_4)_2CO_3$, pH 8.0, according to the manufacturer instructions. Protein quantification was evaluated using the Bradford assay (Bio-Rad Protein Assay Dye Reagent Concentrate). Samples were reduced with 10 mM TCEP for 30 minutes at 55°C and alkylated with 20 mM IAA for 30 minutes at RT in dark conditions. Tryptic digestion was performed overnight at 37°C using a final protease:protein ratio of 1:50 (w/w) of sequence-grade trypsin (Promega). Reaction was stopped by acidification with 0.5% formic acid (FA) at 37°C for 30 minutes. Samples were dried in a vacuum centrifuge for 30 minutes, 16 200×g at 60°C to get rid of the acid-labile surfactant RapiGest SF.

Samples were diluted with an aqueous solution of 0.1% FA, 3% CH_3CN. Each digested sample (0.25 µg) was loaded on a 5 µm Symmetry C18 trapping column 180 µm × 20 mm (Waters). Peptides were separated by a 120 minutes reverse phase gradient at 300 nl/minute (linear gradient, 2-40% ACN over 90 minutes) using an HSS T3 C18 1.8 µm, 75 µm × 150 mm nanoscale LC column (Waters) maintained at 40 °C on a nanoACQUITY UPLC System (Waters). Separated peptides were analyzed in a shotgun experiment on a Synapt G2-Si Mass spectrometer (Waters), directly coupled to the chromatographic system. Data have been acquired in High Definition MS^E ($HDMS^E$), a data-independent acquisition (DIA) protocol where ion mobility separation has been integrated into LC-MS^E workflow (Distler et al., 2016).

Continuum LC-MS data from three replicate experiments for each sample were processed for qualitative and quantitative analysis using the ProteinLynx Global Server v. 3.0.3. software (PLGS, Waters). Qualitative identification of proteins was obtained by searching in human database neXtProt (release 2017_08_01) (http://www.nextprot.org). The search parameters

included: automatic tolerance for precursor ions and for product ions, minimum one fragment ion matched per peptide, minimum three fragment ions matched per proteins, minimum of one peptide matched per protein, two missed cleavages, carbamidomethylation of cysteines as fixed modification and oxidation of methionines as variable modifications and false discovery rate (FDR) of the identification algorithm ≤ 1%.

Tables including quantifications for all identified proteins were generated for mitochondrial and whole cell fractions. Label free quantitative analysis was obtained by using the protein expression analysis mode integrated in PLGS software, applying an automatic normalization. Filtered tables for mitochondrial and whole cell fractions were generated to include proteins found at least in two out of three technical replicates and to exclude proteins showing less than 30% change (corresponding to a ratio of ± 0.38 in $\log_2$ scale) and those showing no statistical significance according to the PLGS software. Multiple isoforms were reduced to non-redundant UniProt IDs and median values for ratio and variance were calculated. P value was then calculated from sample size, variance and ratio using the BSDA library. Procedures were written using the statistics programming language R.

3.7. Systems biology analysis

The interactions among all significantly altered proteins in PARK2 patients were analyzed by STRING (http://string-db.org/) (Szklarczyk et al., 2017). Several parameters were set for the analysis as follows. Meaning of network edges: evidence; active interaction sources: databases, experiments and co-expression; minimum required score: high confidence (0.700). The enriched networks were exported as a .txt file, edited and visualized by Cytoscape (http://cytoscape.org/). The analysis of the mitochondrial proteome was carried out by identifying the strictly mitochondrial proteins using the information recovered by the neXtProt (https://www.nextprot.org) and Gene Ontology Consortium (http://geneontology.org) databases. To provide a more robust definition of the mitochondrial proteins, only the gold annotations were considered. We used the functional mitochondrial human proteome network (Monti et al., 2018) to visualize the interactions between the strictly mitochondrial proteins and the mitochondrial associated proteins. To investigate the whole-cell proteome alterations, the network was divided in sub-clusters by the ClusterMaker app and the GLay algorithm (Su et al., 2010). The over-representation analysis of nodes of the network was performed using the BiNGO app (Maere et al., 2005).

Eventually, a gene set enrichment analysis (GSEA) was performed both for the whole cell and the mitochondrial fractions to identify classes of proteins that were over-represented. We used the

input list generated by including all observed proteins in PARK2 patients and control subjects. Proteins that were detected only in either control subjects or in PARK2 patients (unique) were excluded. The analysis was conducted using the ReactomePA package that provides functions for pathway analysis based on Reactome pathways database (Yu and He, 2016). The $\log_2$ (P/C ratio) was used as a metrics for ranking the gene list. Gene IDs were obtained using UniProt.ws, a collection of functions for retrieving, processing and repackaging the UniProt web services (Carlson and Ortutay, 2019), and the Rentrez library that provides an R interface to the NCBI (Winter et al., 2017). The parameters used for the GSEA were number of permutations: 10000 and p values cut off: 0.5. Benjamini-Hochberg adjustment for multiple comparisons was employed to adjust p values. All data analysis was written using the R environment for statistical computing.

4. Results

4.1. Effect of *PARK2* mutations on Parkin protein levels

To examine the possible effect of *PARK2* mutations and how different mutations affected Parkin protein levels, a Western blot analysis was performed. We analyzed Parkin protein abundance in primary skin fibroblasts from five PARK2 patients and five control subjects. As shown in Figure 6 Parkin protein was undetectable in fibroblasts derived from PARK2 patients, independent of the mutation type in all the samples analyzed.

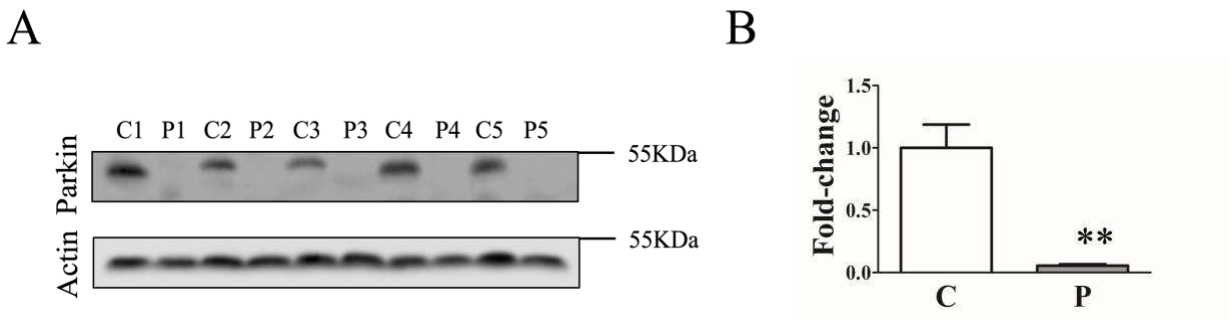

Figure 6. Parkin levels are reduced in PARK2 patients. (A) Representative Western blot image and (B) relative quantification of Parkin protein in primary skin fibroblasts of PARK2 patients (P1, P2, P3, P4 and P5) and control subjects (C1, C2, C3, C4 and C5). Data, expressed as mean ± SEM (three technical replicates), were analyzed by two-tailed, unpaired Student's t-test by comparison of PD patients and control subjects. ** $p < 0.001$.

4.2. Focus on mitochondrial function and dynamics

4.2.1. *PARK2* mutations induced a significant dissipation of mitochondrial membrane potential in PARK2 patients

In order to verify the impact of Parkin protein loss-of-function on mitochondrial function, living cells were stained with 100 nM Mitotracker Red CMXRos, which accumulates in mitochondria with an intact membrane potential. *PARK2* mutations induced a significant loss of mitochondrial membrane potential. In particular, $\Delta\Psi_m$ was reduced by 40% in PARK2 patients. Moreover, the mitochondrial fluorescence signal in *PARK2*-mutated fibroblasts was fainter compared to that of control subjects (Figure 7).

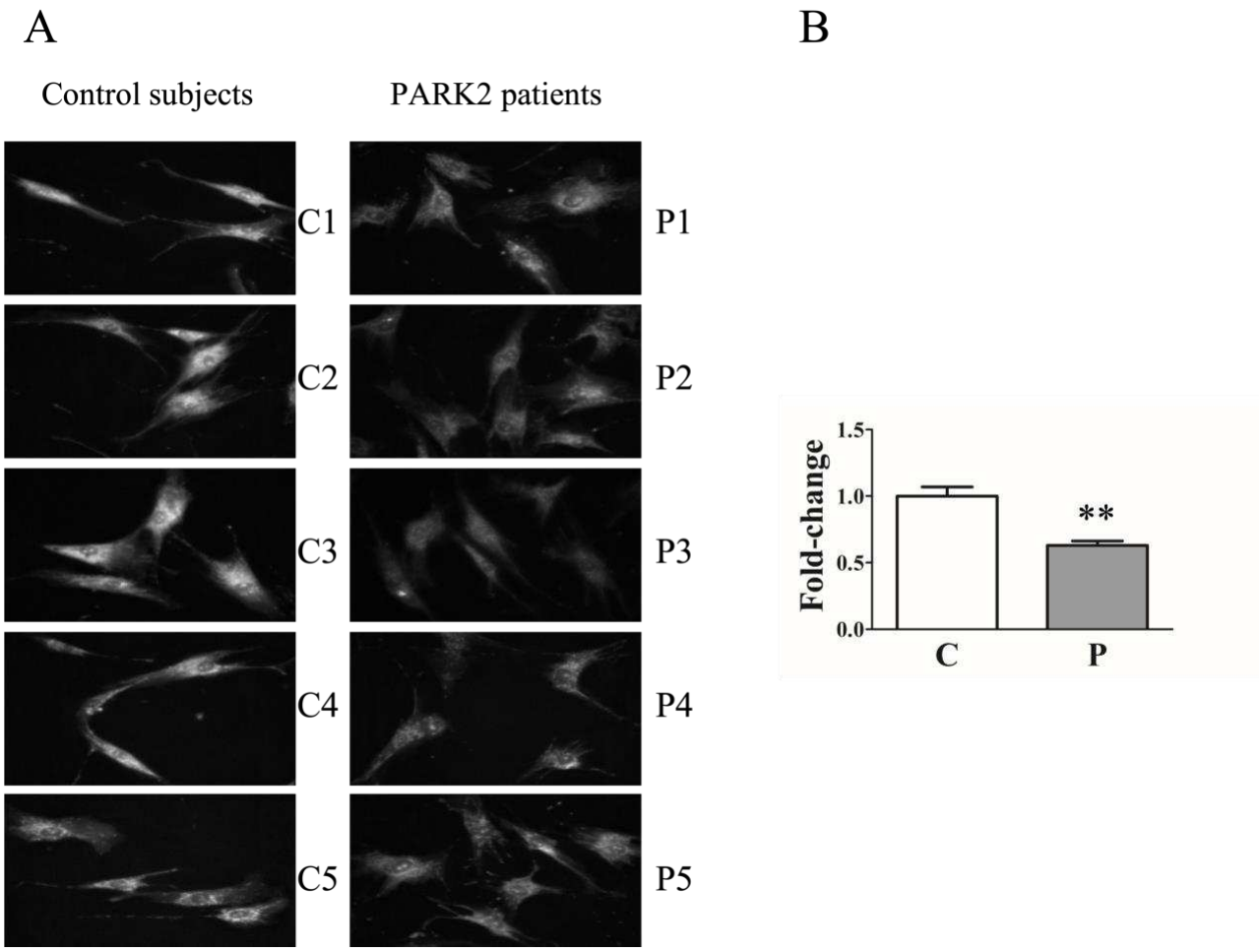

Figure 7. Mitochondria are depolarized in PARK2 patients. (A) Representative images of fibroblast cells from five control subjects (C1, C2, C3, C4 and C5) (left) and five PARK2 patients (P1, P2, P3, P4 and P5) (right) stained with 100 nM Mitotracker Red CMXRos. (B) Quantification of Mitotracker Red CMXRos fluorescence normalized to the number of cells. Data, expressed as mean ± SEM, were analyzed by two-tailed, unpaired Student's t-test. ** p = 0.0014.

4.2.2. Effect of *PARK2* mutations on PINK1 accumulation after CCCP exposure

To determine whether the mitochondrial depolarization induced the accumulation of PINK1 protein, we assessed the levels of this protein in whole cell extracts of fibroblasts from five PARK2 patients and five control subjects. Since PINK1 protein was slightly detectable at basal conditions, we decided to treat fibroblast cells with the protonophore CCCP that is able to induce the accumulation of PINK1 protein leading to the activation of PINK1/Parkin mitophagic pathway (Matsuda et al., 2010). Therefore, fibroblasts were treated with 60 μm CCCP for 24 hours in order to highlight possible differences in mitophagy induction. As expected, CCCP treatments determined the accumulation of PINK1 protein in control subjects, while it is completely undetectable in DMSO controls (Figure 8). On the other hand, PINK1 protein levels were

increased to a lesser extent by CCCP treatment in fibroblast cells from PARK2 patients (Figure 8).

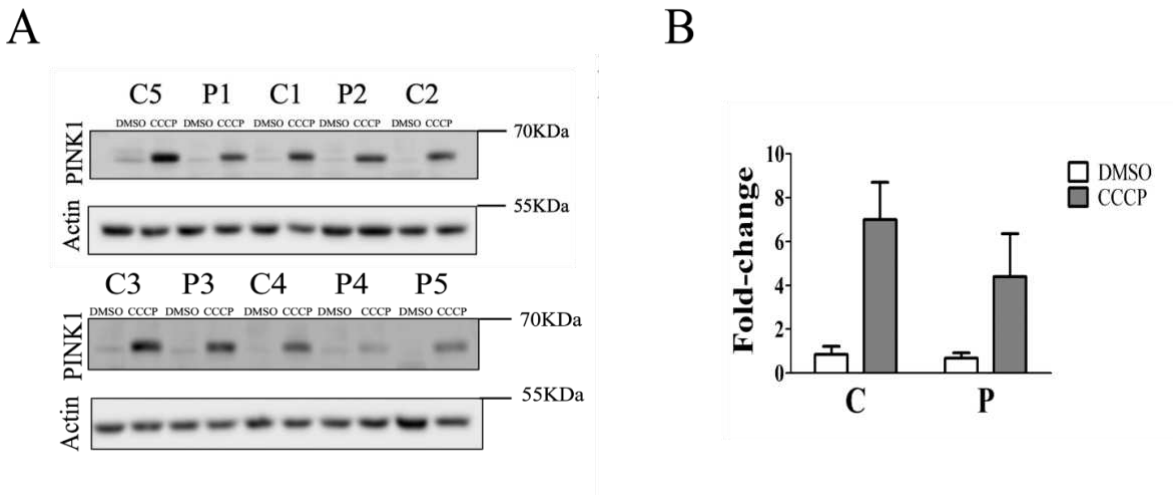

Figure 8. Mitophagy process is less activated after CCCP exposure in PARK2 patients respect to control subjects. (A) Representative Western blot image of PINK1 protein after DMSO (control) or CCCP treatment in primary skin fibroblasts of PARK2 patients (P) and control subjects (C). (B) Relative fold-change of PINK1 protein in both control subjects and PARK2 patients after CCCP treatment. Data were expressed as mean ± SEM (three technical replicates). Statistical analysis was performed by two-way ANOVA, to assess the effect of "mutation" (control subjects vs. PARK2 patients), "treatment" (DMSO vs. CCCP) and "interaction". "Mutation" ($p = 0.0001$; $F = 210.9$), "treatment" ($p = 0.0001$; $F = 16.92$) and "interaction" ($p = 0.0007$; $F = 12.75$) resulted to be significant sources of variation.

4.2.3. Morphological characterization of mitochondrial network

Immunofluorescence stain was performed on fibroblasts from five PARK2 patients and five control subjects in order to investigate whether *PARK2* mutations could affect mitochondrial network morphology. Fibroblast cells were labeled with ATP Synthase β and z-stacks of these cells were acquired using confocal microscopy (Figure 9). Images showed a filamentous mitochondrial network in both patients and control subjects, with mitochondria distributed all over the soma (Figure 9).

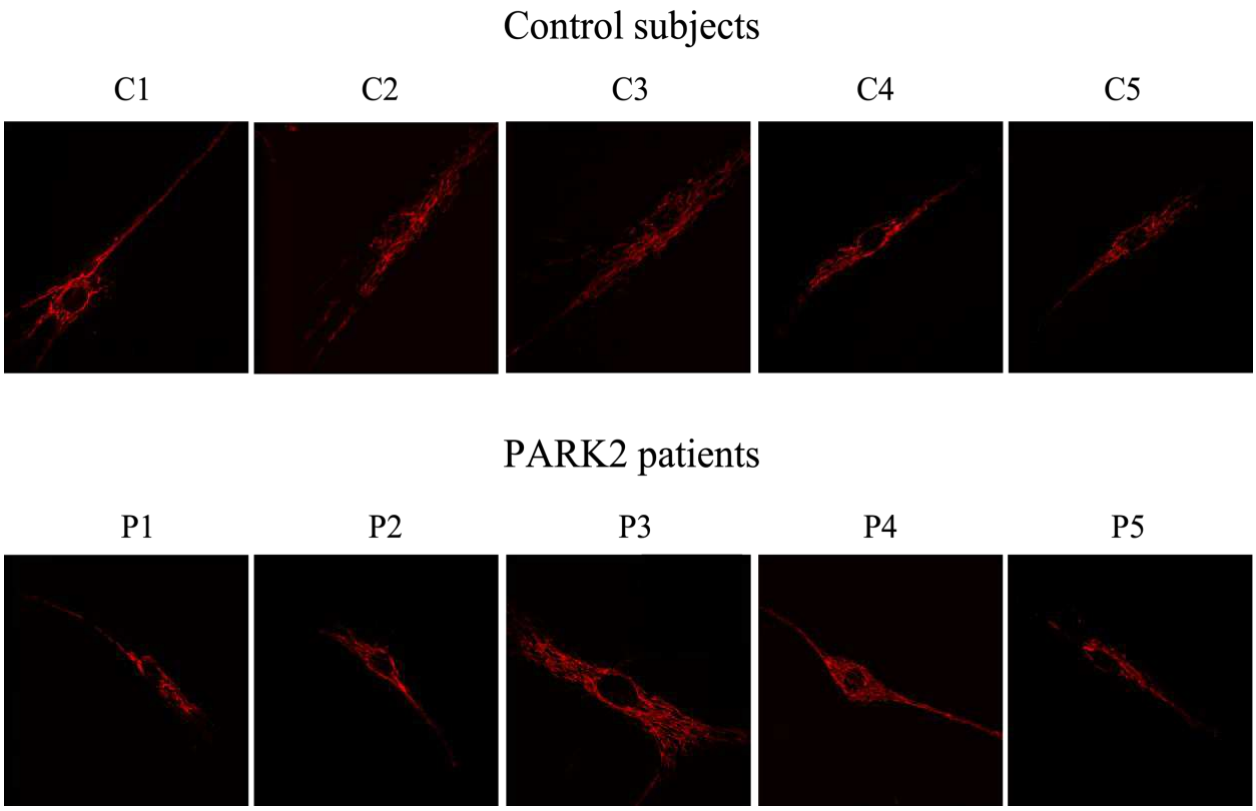

Figure 9. Immunofluorescence stain of mitochondrial network morphology. Representative immunofluorescence images of primary skin fibroblasts from five control subjects (C1, C2, C3, C4 and C5) (top panel) and five PARK2 patients (P1, P2, P3, P4 and P5) (bottom panel) stained for ATP synthase β.

To give a quantitative and statistical assessment of this qualitative evaluation, we focused on several shape descriptor parameters that best explain the morphology of these mitochondrial networks. Images were then analyzed using the "Analyze Particles" function of ImageJ software. Among all parameters analyzed (Appendix A), the distribution density of circularity, roundness and solidity are shown in Figure 10. Indeed, as previously described, these three parameters describe better than others the mitochondrial network dynamic alterations (Bondi et al., 2016).
No significant differences were observed between the distribution density of all parameters measured in PARK2 patients and control subjects.

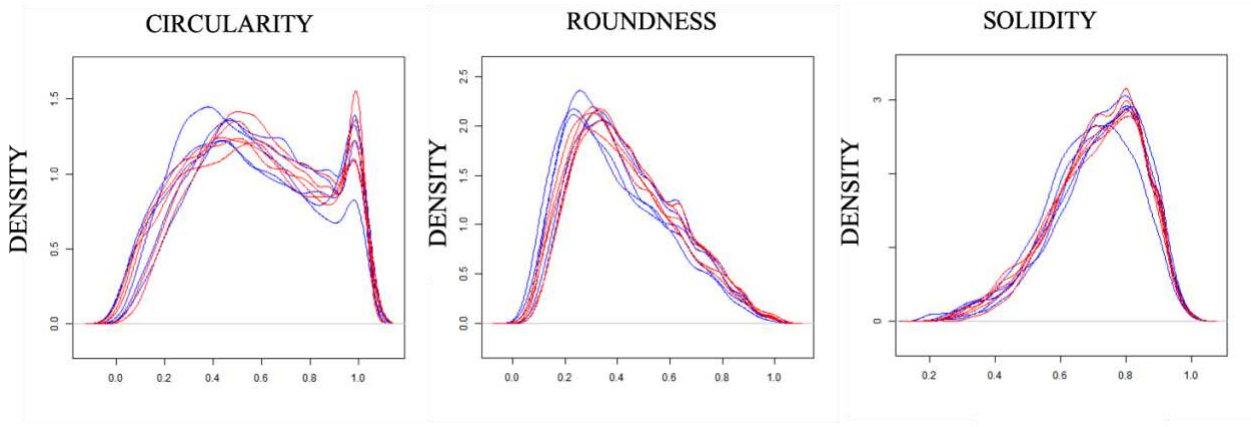

Figure 10. Analysis of mitochondrial network morphology using the "Analyze Particles" function. Example of the distribution density of circularity, roundness and solidity (for all particles analyzed in seven fields of view from each subject). Blue curves = control subjects; red curves = PARK2 patients.

To have a more fulfilling idea about the mitochondrial network morphology, we decided to use the "Analyze Skeleton" function of ImageJ (Valente et al., 2017). This tool gives more information about the shape of the network in terms of junctions and branches. Five parameters (*i.e.*, individuals, mean length, mean size, footprint and networks) were compared between PARK2 patients and control subjects (Figure 11). In addition, this analysis did not show any significant difference in the evaluated parameters, using the univariate non-parametric Wilcoxon test.

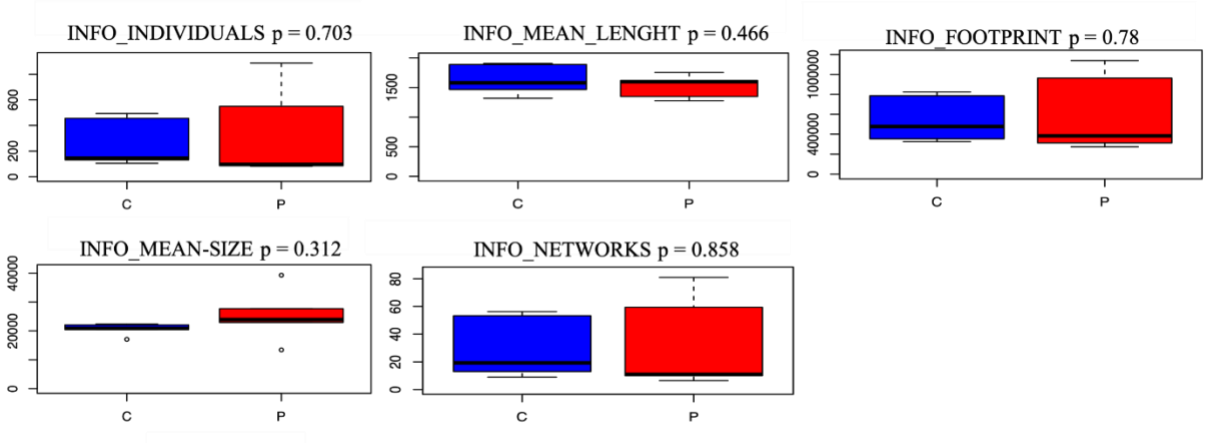

Figure 11. Analysis of mitochondrial network morphology using the "Analyze Skeleton" function. No statistical differences were observed between control subjects and PARK2 patients using the univariate non-parametric Wilcoxon test. C = control subjects; P = PARK2 patients.

These results suggest that *PARK2* mutations did not affect the morphology of the mitochondrial network (*i.e.*, fission and hyper-fusion processes), at least in fibroblasts.

4.3. Mitochondrial and total proteome analysis

4.3.1. Mitochondrial enrichment

Mass spectrometry quantitative analysis was performed on mitochondria1-enriched fractions. Mitochondria were isolated from control subjects and from PARK2 patients with a commercial kit based on surfactants. The effectiveness of the mitochondrial enrichment procedure was evaluated by Western blot. In particular, we verified the levels of VDAC1 and CS, markers of the OMM and IMM respectively, and of histone H3, a nuclear marker, both in the mitochondrial and in the nuclear fractions. Figure 12 shown that VDAC1 and CS were noticeably enriched in the mitochondrial fractions and almost undetectable in the nuclear fractions. While histone H3 was detected only in the nuclear fractions, thus indicating a good outcome of the mitochondria isolation procedure.

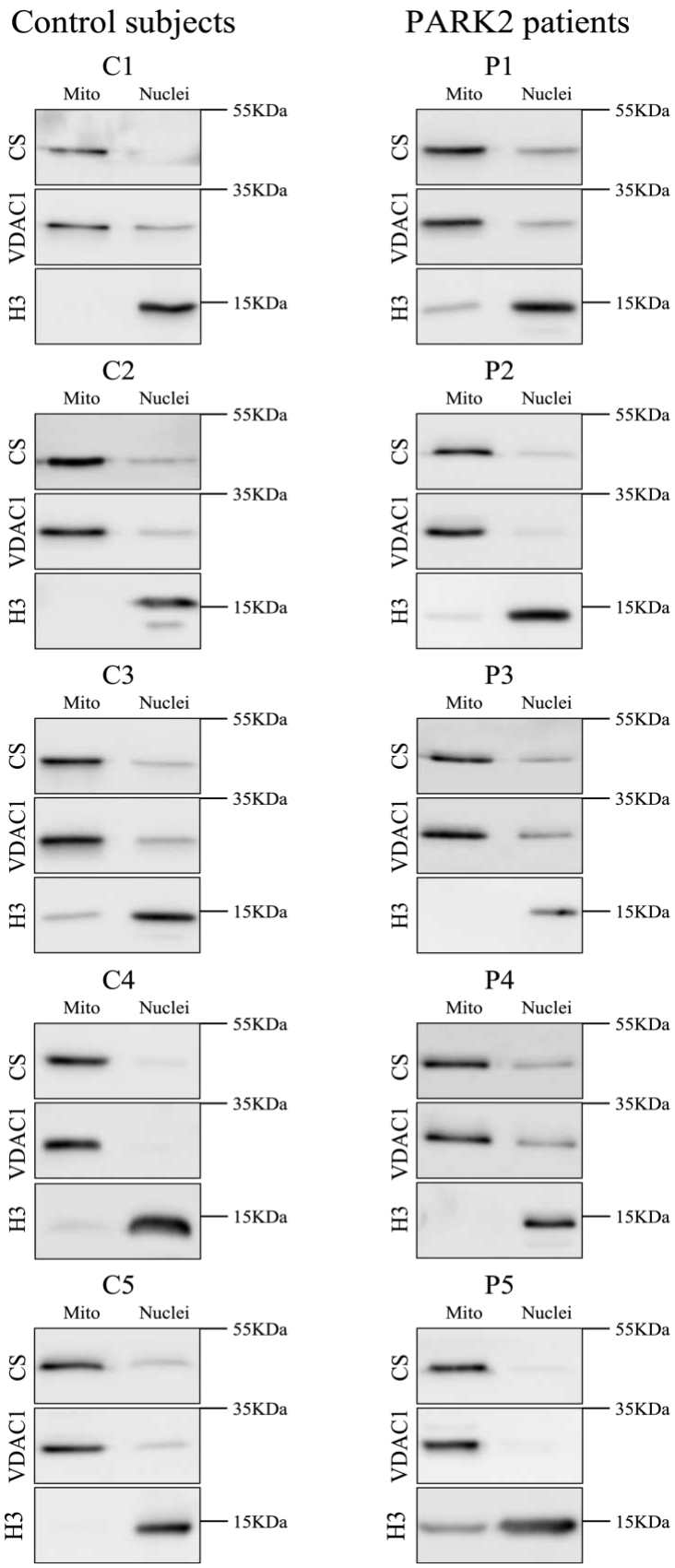

Figure 12. Mitochondrial enrichment procedure. Representative Western blot of VDAC1, CS and histone H3 proteins. PARK2 patients (Subjects P1, P2, P3, P4 and P5); control subjects (Subjects C1, C2, C3, C4 and C5). Mitochondrial markers (VDAC1 and CS) were enriched in the mitochondrial fractions, while the nuclear marker (histone H3) was detected only in the nuclear fractions.

4.3.2. Shotgun proteomics of mitochondrial and whole cell fractions

Mitochondrial-enriched and whole cell fractions were analyzed by quantitative shotgun proteomics. The differential analysis was performed using Synapt G2-Si Mass spectrometer (Waters), directly coupled to a nano-Ultra Performance Liquid Chromatography (nUPLC) system. Raw data are available in proteomeXchange with accession PXD015880. This analysis relies on the high reproducibility of retention time elution profiles. Moreover, since there was no isotopic labeling of samples, data complexity was reduced, and we can have a deeper view of the less abundant proteins.

To take into account the variability due to the experimental procedures, data from three replicate experiments for each sample were collected. Qualitative information about the LC-MS/MS procedure was evaluated by analyzing the analytical performances. The average distribution of the coefficient of variation (CV%) of peptide signal intensity was around 5%, while the CV% of retention time was centered on 1.5%. However, to keep a conservative approach, protein hits were filtered to a fold difference larger than 30%.

Moreover, quality assessment of data was further evaluated, and quantitative data were graphically represented with a Volcano plot (Figure 13), showing the selected thresholds for statistical significance and fold-change.

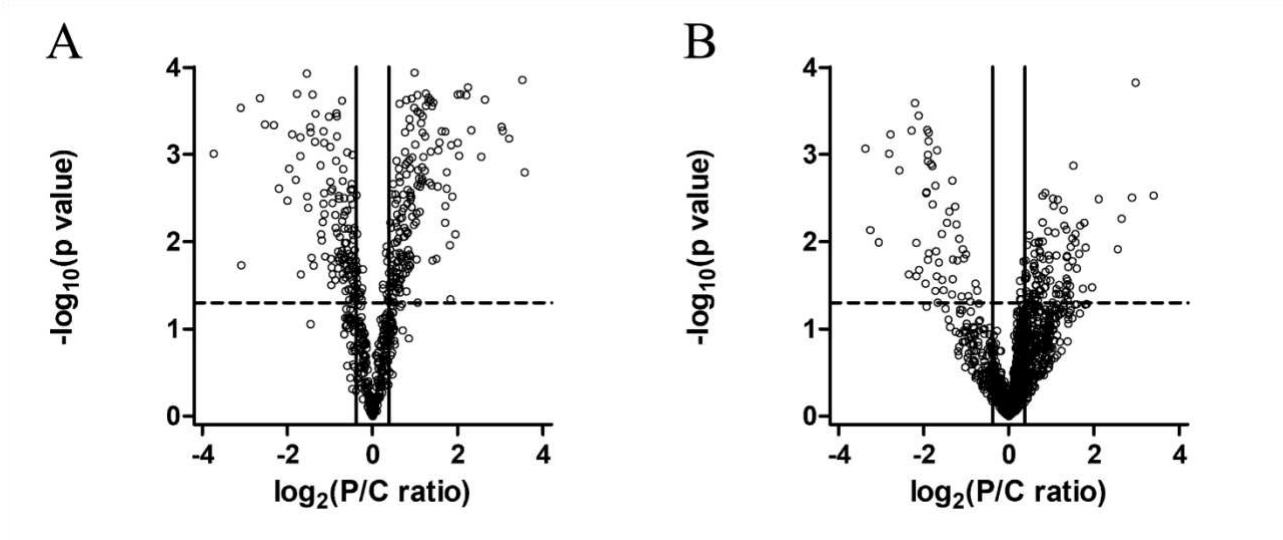

Figure 13. Volcano plot of proteins in the mitochondrial (A) and in the whole cell fractions (B). Dots represent proteins distributed by fold change along the axis and by p value along the y axis. Proteins with a statistically significant differential expression are located in the top right (up-regulated) and top left (down-regulated) quadrants.

A comparable number of up- and down- regulated proteins between the two conditions, both in the mitochondrial (Figure 13A) and in the whole cell fractions (Figure 13B) indicated the good

quality of the shotgun analysis. In particular, 649 proteins for the mitochondrial and 1 457 for the total fractions were identified by shotgun proteomics.

4.3.3. Bioinformatics analysis

4.3.3.1. Systems biology analysis

A comprehensive number of 227 proteins in the mitochondrial and 168 proteins in the total fractions, whose level was significantly altered in PARK2 patients, were identified using the protein expression analysis mode integrated in PLGS software. Filtered protein tables were generated to include proteins found at least in two out of three technical replicates and to exclude proteins showing less than 30% change (corresponding to a ratio of ± 0.38 in $\log_2$ scale) and those showing no statistical significance according to the PLGS software (Appendix B and C for mitochondrial and total fractions, respectively).

In order to interpret the results obtained by the proteomic approach and to understand which cellular pathways were mainly perturbed by Parkin loss-of-function, the proteins found to be altered in PARK2 patients were subjected to a network-based analysis, using STRING database as reference.

4.3.3.1.1. Molecular pathways altered in the mitochondrial proteome of PARK2 patients

A set of 227 mitochondrial proteins, up- or down- regulated or unique to one category, was filtered by considering only proteins present in the functional mitochondrial network (Monti et al., 2018). This network includes both mitochondrial and mitochondrial-associated proteins in the neXtProt and/or the Gene Ontology databases. Thus, 83 proteins were mapped on this reference network and a protein network was built by retrieving edge information in the STRING database, obtaining a protein-protein interaction (PPI) cluster made by 48 protein nodes (Figure 14). Among these nodes, only 21 proteins were strictly mitochondrial (round nodes) while 27 proteins were mitochondria-associated proteins (rectangular nodes).

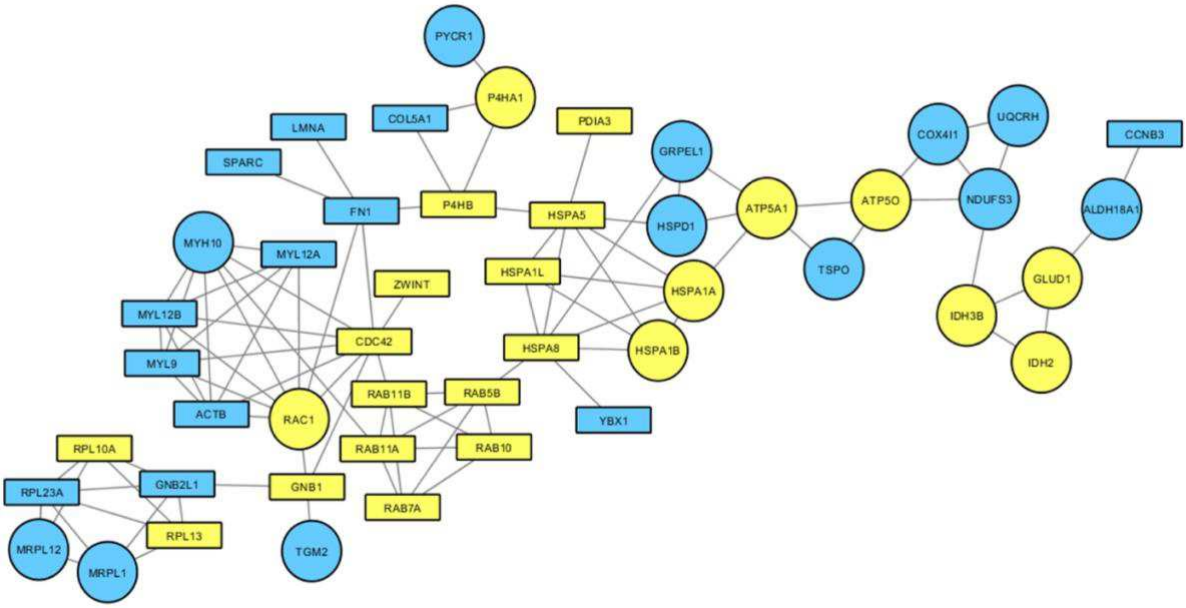

Figure 14. Mitochondrial pathways altered in PARK2 patients. PPI network was built considering both strictly mitochondrial and mitochondria-associated proteins. Round nodes = strictly mitochondrial proteins; rectangular nodes = mitochondria-associated proteins; yellow nodes = up- regulated proteins in PARK2 patients; blue nodes = down-regulated proteins in PARK2 patients.

The over-representation analysis was performed using BiNGO. The analysis revealed two main biological processes altered by *PARK2* mutations, the unfolded protein response and the small GTPases mediated signal transduction (Figure 15). Indeed, we found altered expression levels of several HSPs and Rab proteins.

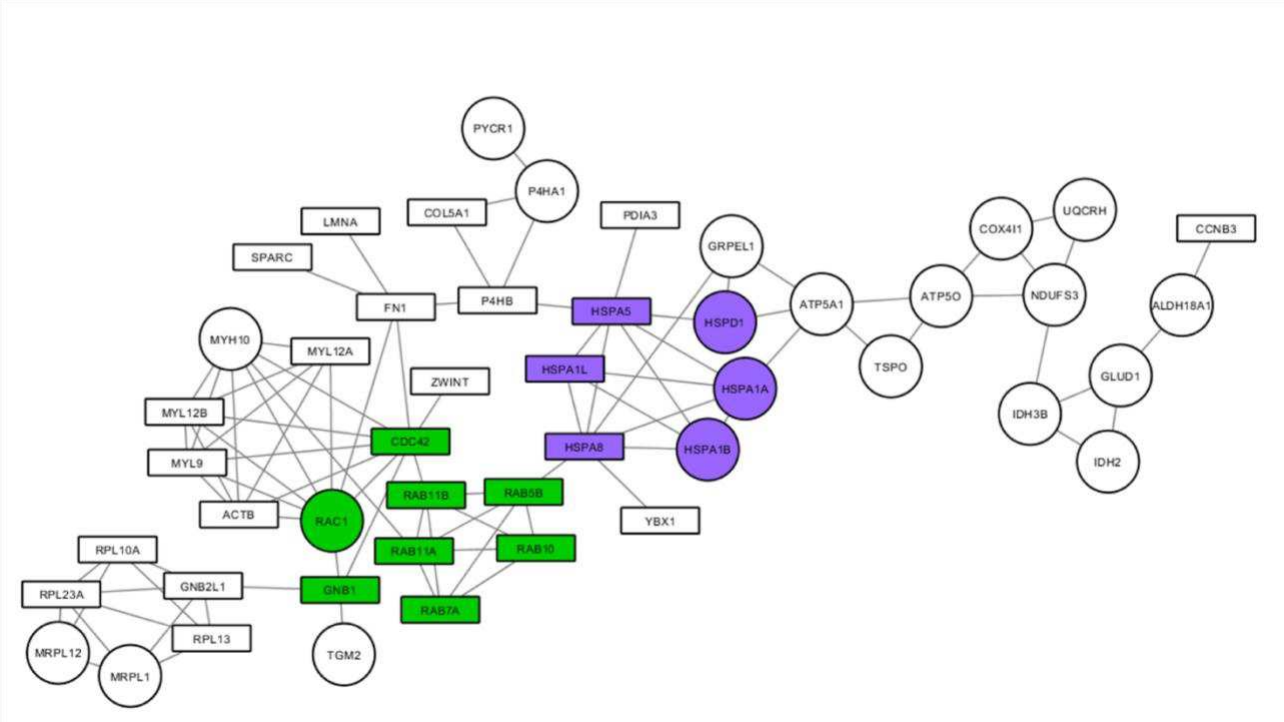

Figure 15. Over-represented pathways mapped on the PPI network. Green nodes = small GTPases mediated signal transduction pathway; purple nodes = unfolded protein response pathway.

4.3.3.1.2. Over-represented pathways altered in the whole cell fractions of *PARK2*-mutated samples

We then focused on the whole-cell proteome alterations. First of all, we created an input list of 168 proteins that changed in PARK2 patients, up- or down- regulated or unique to one category. This protein list was used to generate a PPI network including 100 proteins, using STRING database as reference (Figure 16).

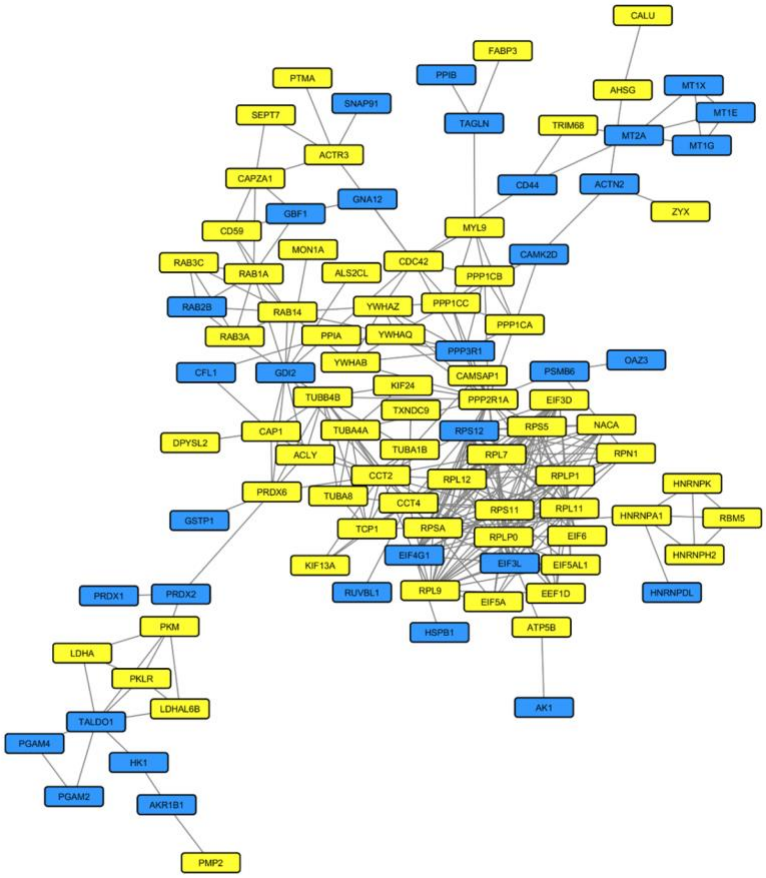

Figure 16. Molecular pathways altered in the whole cell proteome of PARK2 patients. The PPI network includes 100 nodes. Yellow nodes = up- regulated proteins in PARK2 patients; blue nodes = down- regulated proteins in PARK2 patients.

The network was divided in sub-clusters by the GLay algorithm and each cluster was analyzed by over-representation analysis. This allowed us to identify four molecular pathways altered by *PARK2* mutations: signal transmission and transduction, microtubule-based movement, translation and glucose and hexose catabolic pathways (Figure 17).

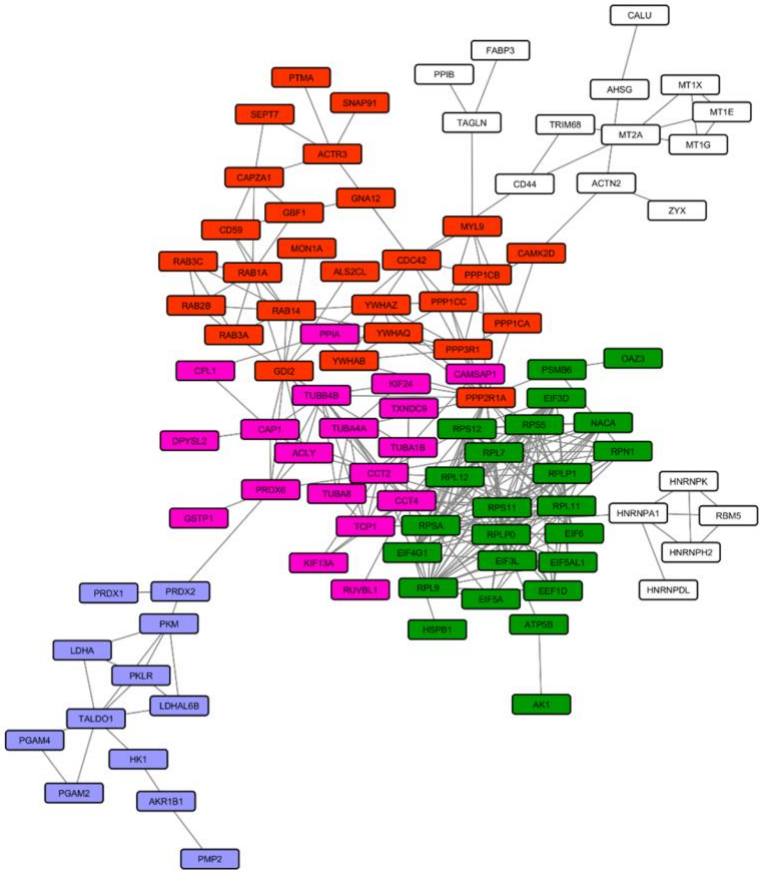

Figure 17. Over-represented pathways mapped on the PPI network. Pink nodes = microtubule-based movement; green nodes = translation; red nodes = signal transmission and transduction; purple nodes = glucose and hexose catabolic pathway.

4.3.3.2. Gene set enrichment analysis

To identify the over-represented classes of proteins, a GSEA both on the mitochondrial and on the whole cell fractions was performed. We considered 649 and 1 457 proteins for the mitochondrial and the whole cell fractions respectively. We plotted the significantly enriched pathways as graphs in order to visualize the results. In particular, the analysis revealed an enrichment of processes related to the RHO GTPases and the axon guidance for the mitochondrial fraction (Figure 18).

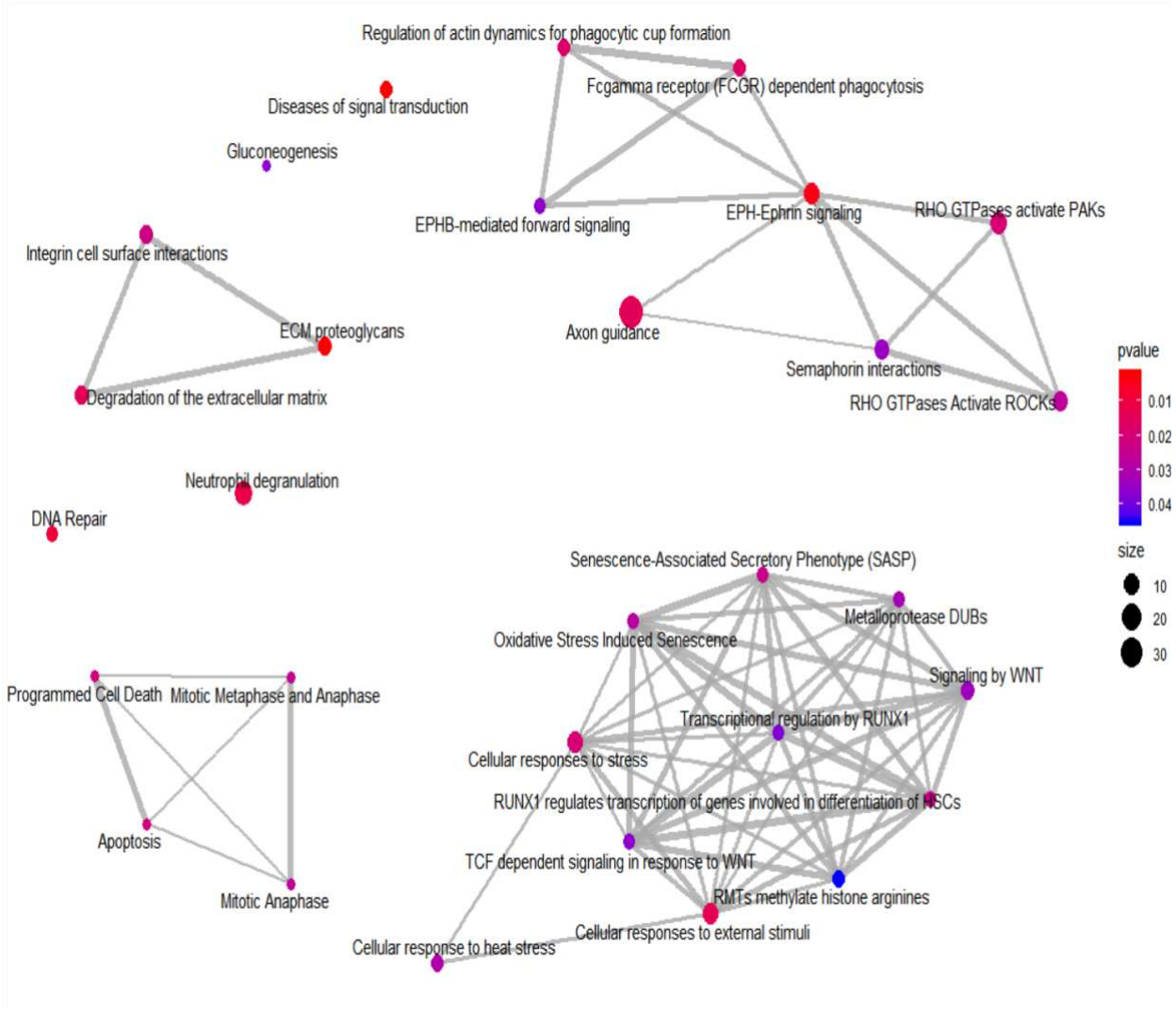

Figure 18. Enriched classes of proteins revealed using a GSEA approach. Enriched map of GSEA results for the mitochondrial fraction. Color coding represents significance of the gene set for the dataset. Node size corresponds to the number of genes from the reference set that are part of the gene set.

On the other hand, the analysis revealed an enrichment of the Rab GEFs exchange GTP for GDP on Rabs for the whole cell fraction (Figure 19).

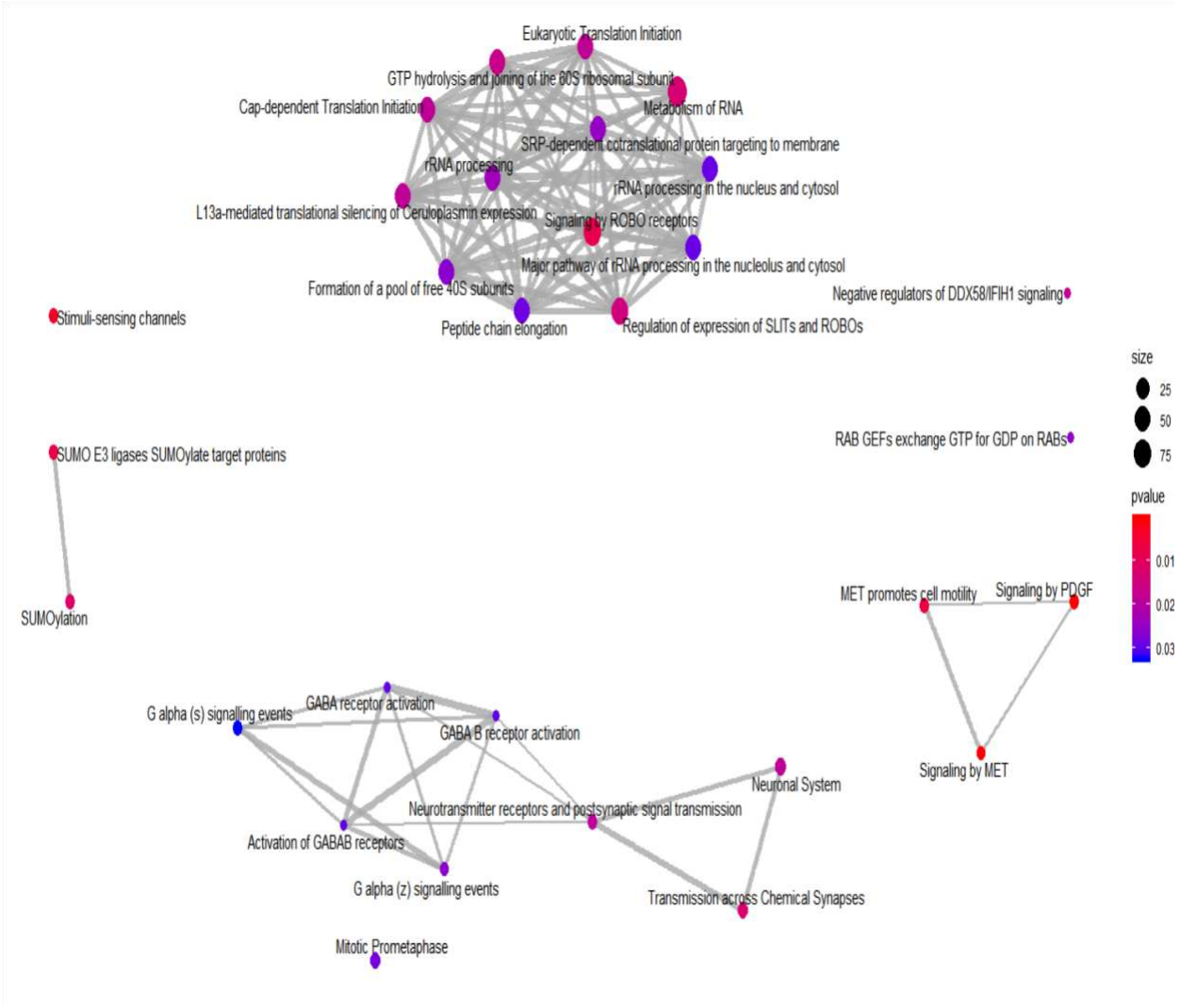

Figure 19. Enriched classes of proteins revealed using a GSEA approach. Enriched map of GSEA results for the whole cell fraction. Color coding represents significance of the gene set for the dataset. Node size corresponds to the number of genes from the reference set that are part of the gene set.

All identified enriched pathways both in the mitochondrial and in the total fractions are shown in Appendix D and F.

4.4. Rab7A did not localize to mitochondria after CCCP treatment

We decided to investigate the recruitment of Rab7A to mitochondria by immunofluorescence. To this end, both quantification and co-localization analysis, in terms of Manders' Overlap Coefficient, between ATP Synthase β and Rab7A protein were performed after CCCP treatment. As shown in Figure 20, we observed a significant increase of Rab7A at the mitochondrial level in PARK2 patients. On the other hand, a trigger of the mitophagy process did not amplify the observed increase. Nevertheless, the Manders' Overlap Coefficient did not show a positive co-localization.

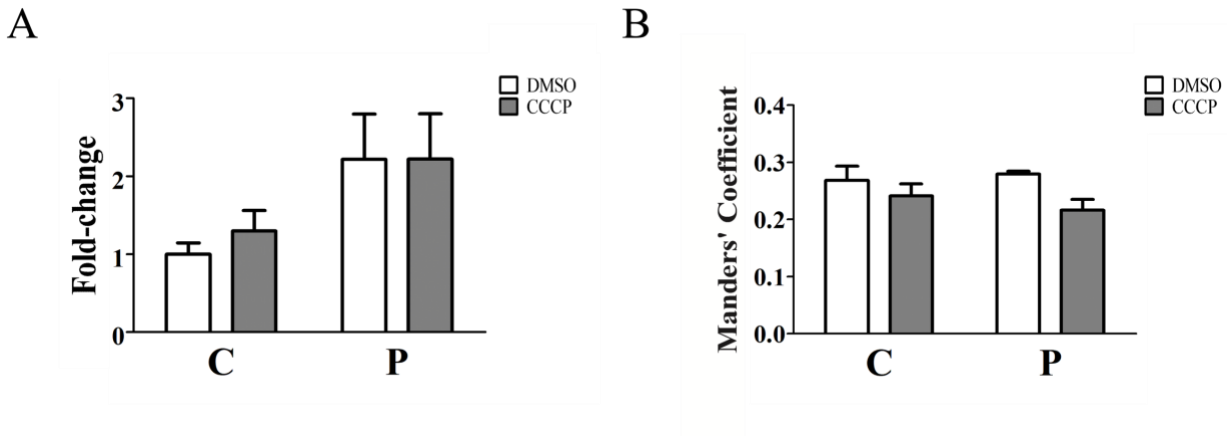

Figure 20. Effect of CCCP treatment and *PARK2* mutations on Rab7A mitochondrial localization. (A) Quantification of Rab7A signal per mitochondrial surface unit. Data were expressed as mean ± SEM. Statistical analysis was performed by two-way ANOVA, to assess the effect of "mutation" (control subjects vs. PARK2 patients), "treatment" (DMSO vs. CCCP) and "interaction". "Treatment" ($p = 0.74$; $F = 0.12$) and "interaction" ($p = 0.74$; $F = 0.11$) did not resulted to be significant sources of variation. "Mutation" ($p = 0.04$; $F = 5.97$) resulted to be a significant source of variation. (B) Manders' coefficient for the localization of Rab7A signal in ATP Synthase β positive pixels. Data were expressed as mean ± SEM. Statistical analysis was performed by two-way ANOVA, to assess the effect of "mutation" (control subjects vs. PARK2 patients), "treatment" (DMSO vs. CCCP) and "interaction". "Mutation" ($p = 0.73$; $F = 0.13$), and "interaction" ($p = 0.37$; $F = 0.89$) did not resulted to be significant sources of variation. "Treatment" ($p = 0.046$; $F = 5.55$) resulted to be a significant source of variation.

5. Discussion

PD is a complex and multifactorial neurodegenerative disease whose etiology has not been totally clarified yet. Strong evidences suggest that a complex interplay between environmental and genetic factors are involved in PD pathogenesis, underlining its multifactorial nature (Schapira and Jenner, 2011; Schapira and Tolosa, 2010). In this intricate scenario, many of the molecular pathways implicated in PD etiology converge on mitochondria, resulting in their dysfunction (Schapira and Jenner, 2011; Subramaniam and Chesselet, 2013). Since mitochondria are involved in a wide spectrum of cellular functions (calcium homeostasis, intracellular signaling and apoptosis), they play an essential role in the cell homeostasis. Indeed, the maintenance of a healthy mitochondria population is fundamental for cell survival. Mitochondrial dysfunctions and autophagy are strictly connected. Indeed, dysfunctional mitochondria are removed through the mitophagy process. Damaged mitochondria are isolated from mitochondrial network, sequestered in autophagosomes and delivered to lysosomes for degradation. The most characterized mitophagy mechanism is the PINK1/Parkin pathway (Youle and Narendra, 2011). Briefly, under basal conditions, when mitochondrial membrane is properly polarized, PINK1 is imported into the mitochondria, cleaved by several mitochondrial proteases, and rapidly removed through the proteasome. Upon mitochondrial depolarization, the mitochondrial import of PINK1 is inhibited, resulting in its accumulation into the OMM. This process triggers the recruitment of Parkin onto the mitochondrial surface, which, in turn, promotes the ubiquitination of different OMM proteins, thus initiating mitophagy. The improper disposal of mitochondria can cause an increment of ROS, a lower ATP production, and the apoptosis activation, thus oxidative stress is expected to occur (Alberio et al., 2012). In particular, mitophagy impairment seems to play a pivotal role in PD onset and progression (Fernandez-Moriano et al., 2015; Zilocchi et al., 2018). Noticeable, mutations in *PARK6* and *PARK2* genes, coding for PINK1 and Parkin respectively, are associated with autosomal recessive parkinsonism (Valente et al., 2004; Sun et al., 2006) and cause an impairment in the mitophagy process leading to an accumulation of damage mitochondria. Although PARK2 is a familiar and rare form of PD, it offers a unique opportunity to study how the impairment in Parkin functionality can cause the improper disposal of dysfunctional mitochondria. Nowadays, the molecular mechanisms underlying mitophagy impairment are not yet completely understood.
Taking these considerations into account, we decided to investigate the mitochondrial alterations that occur in *PARK2*-mutated skin fibroblasts.
In this intricate pathological landscape, it is particularly important the identification of experimental models that simplify the study of the pathogenetic mechanisms involved in the disease. For this reason, we used primary skin fibroblasts obtained from five PARK2 patients,

which were all characterized by the absence of Parkin protein, independent of the type of genetic mutation that affected these subjects.

Several studies have reported that skin fibroblasts from PD patients are a good cellular source for studying the disease phenotypes because they show some deficit associated with PD pathogenesis that are typical of the neuronal tissue (Connolly et al., 1998; Kilpatrick et al., 2016). Fibroblasts are an easily accessible source of proliferating cells that share the same genetic complexity of neurons, reflect the cumulative cell damage that occurs in patients, mirror the polygenic risk factors and mutations in *PARK* genes (Auburger et al., 2012). Fibroblasts obtained from skin biopsies from PARK2 patients show alterations in mitochondrial bioenergetics (lower membrane potential, lower complex I activity and lower ATP cellular levels) as described by Zanellati and colleagues (Zanellati et al., 2015). For these reasons, these proliferating cells can be used successfully to study the mitochondrial alterations that affect these patients. Despite all these features, the main concern is that fibroblasts do not represent the tissue directly affect by the disease. Therefore, iPSC-derived dopaminergic neurons can represent a good strategy to overcome this limit (Lang et al., 2019). However, fibroblasts constitute a unique opportunity to investigate molecular Parkin loss-of-function consequences in several patient-derived lines, with different genetic, epigenetic and environmental backgrounds.

First of all, we verified how *PARK2* mutations affected Parkin levels in different patients. Independently of the type of genetic mutation, we found that Parkin protein levels were drastically reduced in our group of patients. Disease-causing mutations include single base-pair substitutions, small and big (hundreds of thousands of nucleotides) deletions and splice site mutations. In all cases, mutations lead to a loss-of-function of Parkin protein, albeit through different mechanisms. This obviously occurs when deletions span several exons. Nonsense-mediated decay would destabilize any truncated transcripts, thus leading to the absence of protein expression. Indeed, there is little evidence that truncated Parkin proteins are expressed in patients with exon deletions. On the other hand, missense mutations appear to cause a loss-of-function of Parkin protein through decreased catalytic activity and/or aberrant ubiquitination. Point mutations might also cause the destabilization of Parkin, leading to insolubility or rapid proteasomal degradation of the mutant protein (Dawson and Dawson, 2010).

Then, we investigated the impact of Parkin loss-of-function on mitochondrial function and network morphology.

To determine if the loss-of-function of Parkin protein had an impact on mitochondrial function we decided to measure the mitochondrial membrane potential using Mitotracker Red CMXRos. As a result, we observed a reduction of the mitochondrial membrane potential in PARK2 patients, as

demonstrated by previous studies (Grunenwald et al, 2010; Zanellati et al., 2015). We also verified whether the mitochondrial depolarization, the main trigger for the activation of the PINK1/Parkin mitophagy pathway, could induce the accumulation of PINK1 protein (Matsuda et al., 2010; Narendra et al., 2010). Several studies on PINK1/Parkin-induced mitophagy used the protonophore CCCP as an established cellular model to induce the mitophagy process (Bondi et al., 2016; Gao et al., 2015; Gegg et al., 2010). The major critical issue is that this phenomenon occurs under pathophysiological stress conditions. Despite the lower mitochondrial polarization, PINK1 was undetectable both in fibroblasts derived from control subjects and PARK2 patients. This difference, not detectable at the baseline, can be revealed only by inducing a mitochondrial damage. For this reason, we assessed the accumulation of PINK1 after inducing the activation of this mitochondrial disposal pathway. As expected, CCCP treatment determined the accumulation of PINK1 in control subjects. On the other hand, PINK1 levels were drastically reduced in skin fibroblasts from PARK2 patients exposed to CCCP with respect to CCCP-exposed controls, thus suggesting that Parkin protein is necessary for the accumulation of PINK1 on the mitochondrial surface and that mitochondrial depolarization is not the only process that triggers the activation of the mitophagy process.

To have a more comprehensive view of the mitochondrial alterations due to *PARK2* mutations, we characterized the mitochondrial network morphology in order to understand the impact of Parkin loss-of-function on mitochondrial dynamics. To this purpose, we performed an immunofluorescence assay on skin fibroblasts from five PARK2 patients and five control subjects. Fibroblasts were stained with ATP Synthase β antibody (a mitochondrial marker) and images were analyzed through confocal microscopy. Images showed a filamentous mitochondrial network in both PARK2 patients and control subjects, with mitochondria distributed all over the cell. To give a statistical relevance to this qualitative assessment, we analyzed confocal microscopy images in terms of morphological descriptors using the "Analyze Particle" function of ImageJ software. This tool represents a method that can highlight the morphological alterations in the mitochondrial network (Bondi et al., 2016). The measurement of the distribution density of different morphological parameters, such as solidity, roundness and circularity showed no differences between PARK2 patients and control subjects. This suggests that *PARK2* mutations do not cause any significant morphological alteration in the mitochondrial network. This result is in agreement with the filamentous mitochondrial network visible in our confocal images and with previously published studies (Grunewald et al., 2010; Zanellati et al., 2015). To deepen and increase our knowledge about the network morphology, we used the "Analyze Skeleton" function of ImageJ (Valente et al., 2017). This option can give more informative notions about the shape of the

network, in particular regarding junctions and branches and can give a more fulfilling idea about the state of the network in the presence of *PARK2* mutations. Thus, some of the limitations of the "Analyze Particle" function should be overcome by implementing the results with the "Analyze Skeleton" function. Once again, no significant differences were observed in the evaluated parameters between PARK2 patients and control subjects. These results suggest a possible impairment of fission process and, more in general, of mitochondrial dynamics. Indeed, mitophagy and fission are strictly connected processes (Otera and Mihara, 2011). Nevertheless, PARK2 patients do not display skin problems. This can be a consequence that fibroblasts are not totally dependent on oxidative phosphorylation for their energetic demand, so they are less affected by mitochondrial failure than neurons. Moreover, unlike neurons, fibroblasts are not terminally differentiated cells. They undergo frequent cycles of cellular renewal that can somehow counteract the mitochondrial impairment.

To decipher the molecular pathways altered in PARK2 pathology, we used a global and unbiased proteomic approach to highlight the whole-cell and mitochondrial quantitative proteomic alterations that characterize these PD patients.

Given PD complexity, omics approaches, proteomics first, represent the most effective global strategies to unveil the pathogenetic mechanisms underlying PD pathogenesis. Proteomics is a powerful method that allows a global study of functional changes at the proteome level, without the restrictions of other techniques, such as antibody-based targeting of selected proteins, strictly connected to a hypothesis-driven approach. Moreover, proteomics has many advantages, it considers simultaneously several molecules, it is a technique highly standardized and easily automatized in order to process many biological samples (Hosp and Mann, 2017).

For these reasons, in order to investigate the mitochondrial and the total proteome alterations that characterize *PARK2* pathology, a label free quantitative proteomic approach was performed on the total and the mitochondrial-enriched fractions.

The mitochondrial-enriched fractions were obtained using a commercial kit based on surfactants. This kit has been demonstrated to be the best performing method for isolating mitochondria from fibroblast cells (compared to other techniques, such as differential centrifugation) by the mtHPP consortium, leading to an almost undetectable nuclear contamination in the mitochondrial fractions (Alberio et al., 2017). Previous to mass spectrometry we checked the quality of the mitochondrial isolation procedure by Western blot. The highest yield and the lowest nuclear contamination were obtained in our preparations. Indeed, VDAC1 and CS, two mitochondrial markers, were detected only in the mitochondrial-enriched fractions, while histone H3, a nuclear protein, was clearly detected only in the nuclear fractions.

The quantitative shotgun proteomics approach allowed us to detect and to quantify several hundreds of proteins, thus highlighting the protein expression level difference between PARK2 patients and control subjects. Quality assessment of the LC-MS data were evaluated, and we found a comparable number of up- and down- regulated proteins between the two conditions, both in the mitochondrial and in the total fractions indicated the good quality of shotgun analysis. The quantitative proteomics analysis performed on the mitochondrial-enriched fractions showed 227 proteins (among the 649 identified) whose levels were altered by *PARK2* mutations. On the other hand, the quantitative proteomic analysis performed on the whole cell fractions showed 168 proteins (among the 1 457 identified) whose levels were altered by *PARK2* mutations. These results highlighted a critical impact of Parkin loss-of-function on the mitochondrial proteome. Indeed, 35% of mitochondrial proteins identified in our study quantitatively changed in PARK2 patients, compared to 11% proteins in whole cell extracts. To highlight the molecular pathways altered by Parkin loss-of-function we performed a network-based analysis and a GSEA both on the mitochondrial and on the total fractions. The network enrichment is a powerful tool since several molecular factors could contribute to the effects observed. However, these factors could be not detected by the experiments due to the limits of the techniques. For this reason, the network enrichment adds nodes to the network and the over-representation analysis of the enriched network can reveal proteins that may previously be hidden. The network-based analysis performed on the mitochondrial fractions allowed us the visualization of PPI among the 227 mitochondrial proteins, while the over-representation analysis on the resulting network pointed-out several biochemical pathways altered by *PARK2* mutations. The unfolded protein response and the small GTPases mediated signal transduction were identified as the two main molecular pathways altered by the disease. HSPs consist of a heterogeneous group of highly conserved proteins that are fundamental in maintaining cellular homeostasis. Our analysis revealed the alteration of the expression levels of several HSPs. Interestingly, Parkin and HSP70 seem to be interconnected. First, Parkin is able to mono-ubiquitinate HSP70 at several sites (Moore et al., 2008). Second, Parkin, the C-terminus HSP70-interacting protein and HSP70 form a ternary complex that promotes the ubiquitination and the degradation of the Pael receptor, a protein whose accumulation has been linked to dopaminergic neuronal death (Imai et al., 2002). Moreover, a tight association between chaperone systems and PD pathology has been reported (Kalia et al., 2004). The second mitochondrial molecular pathway altered by *PARK2* mutations was the small GTPases mediated signal transduction. Rab proteins are a prerequisite for all the aspects of vesicular trafficking, such as trans/cis-Golgi transport, endosomal transport, lysosomal transport, and autophagy. Their role is essential for the spatiotemporal localization of proteins, which, in turn, determines their

intracellular functions and/or disposal (Gao et al., 2018). Rab proteins are small GTPases that cycle between a GTP-bound active state and a GDP-bound inactive state. The active GTPases can interact with different effector proteins and membranes, while the inactive form predominantly localizes in the cytosol. Some Rab proteins are highly expressed in brain (rather than in other tissues) and have a specific neuronal function (*e.g.*, neural development, neurite growth, axonal transport, and synaptic vesicles), thus pointing out how the impairment of these proteins may be involved in the neurodegenerative process (Gao et al., 2018).The role of Rab proteins in PD pathology has recently been proposed. The discovery of familial PD cases caused by mutations in Rab39B and Rab32 (Gao et al., 2018) suggested a new cellular pathway impairment that characterize this pathology. Recently, a tight relation between Rabs and mitophagy has been discovered (Yamano et al., 2014; Hammerling et al., 2017), suggesting that Parkin acts in the removal of damaged mitochondria not only by the canonical PINK1/Parkin pathway but also interacting with the Rab endosomal pathway. The hypothesis of Rabs involvement in mitochondrial quality control is conceived in light of the recent literature, which is revealing that these proteins are essential regulators of mitochondrial elimination both by mitophagy (Yamano et al., 2014) and by the endosomal pathway (Hammerling et al., 2017). The quantitative alteration of Rab proteins at the mitochondrial level, demonstrated by our proteomics data, strongly support the importance of these proteins in mitochondrial homeostasis and their involvement in PD pathology. The role of Rab alteration in PD pathology was further highlighted by the over-representation analysis and the GSEA conducted on the proteins with different levels in the total fractions. Then, we focused our attention on the characterization of the whole cell proteome alterations, since it is of great interest to find out differences that can be ignored by focusing only on the mitochondrial proteome. Indeed, many cellular pathways involved in PD pathogenesis are guided by mitochondria but involved cytosolic proteins. Thus, even if focus on mitochondria can reveal alterations otherwise masked, neglecting the analysis of the total proteome could lead to the loss of fundamental information. The quantitative proteomic investigation performed on the whole-cell lysates, coupled with a systems biology approach, allowed us to identify other molecular pathways altered by Parkin loss-of-function (*i.e.*, signal transmission and transduction, microtubule-based movement, translation, and glucose and hexose catabolic pathways). This analysis depicted a global impairment that affect cellular homeostasis at different level.

Eventually, given the fundamental role of Rab proteins in the mitophagy process, we decided to investigate the mitochondrial localization of Rab7A by immunofluorescence after triggering a mitochondrial damage. As a result, we found that Rab7A quantification displayed higher values in PARK2 patients, whereas no significant variations were reported to be associated with CCCP

treatment, nor with the interaction between the two factors. On the other hand, Mander's coefficient analysis displayed a very small significant variation associated with the mitochondrial triggering. Thus, the observed increase of Rab7A signal in mitochondrial area cannot be attributed to a change in mitochondrial localization and could better be associated to a general increase of Rab7A. This result is in line with our mitochondrial shotgun data. Indeed, we found an up-regulation of Rab7A in the mitochondrial fraction.

In conclusion, this thesis has contributed to a better understanding of the molecular mechanisms involved in PARK2 pathology, since *PARK2* mutations are the most frequent cause of early-onset PD. It is clear that a better understanding of the molecular actors involved in PARK2 pathogenesis will help to unravel possible biochemical pathways altered also in the sporadic form of the disease. Indeed, it is well known that in sporadic cases the genetic/epigenetic background and the environment lead to mitochondrial impairment and to the accumulation of damaged organelles. The loss-of-function of Parkin protein and the consequent mitophagy alteration that occurs in PARK2 patients lead to the specific neurodegeneration of the SNpc. For these reasons, it is essential to clarify the role of the mitophagy impairment in PD pathogenesis. Overall, the definition of a *PARK2*-related molecular signature will be crucial for providing new insights into the disease mechanisms and identifying new therapeutic targets for this pathology.

6. References

Abdallah C, Dumas-Gaudot E, Renaut J, Sergeant K. Gel-based and gel-free quantitative proteomics approaches at a glance. Int J Plant Genomics. 2012;2012:494572. doi: 10.1155/2012/494572. Epub 2012 Nov 20.

Alberio T, Bossi AM, Milli A, Parma E, Gariboldi MB, Tosi G, Lopiano L, Fasano M. Proteomic analysis of dopamine and α-synuclein interplay in a cellular model of Parkinson's disease pathogenesis. FEBS J. 2010 Dec;277(23):4909-19. doi: 10.1111/j.1742-4658.2010.07896.x.

Alberio T, Fasano M. Proteomics in Parkinson's disease: An unbiased approach towards peripheral biomarkers and new therapies. J Biotechnol. 2011 Dec 20;156(4):325-37. doi: 10.1016/j.jbiotec.2011.08.004. Epub 2011 Sep 2. Review.

Alberio T, Lopiano L, Fasano M. Cellular models to investigate biochemical pathways in Parkinson's disease. FEBS J. 2012 Apr;279(7):1146-55. doi: 10.1111/j.1742-4658.2012.08516.x. Epub 2012 Feb 28. Review.

Alberio T, Pieroni L, Ronci M, Banfi C, Bongarzone I, Bottoni P, Brioschi M, Caterino M, Chinello C, Cormio A, Cozzolino F, Cunsolo V, Fontana S, Garavaglia B, Giusti L, Greco V, Lucacchini A, Maffioli E, Magni F, Monteleone F, Monti M, Monti V, Musicco C, Petrosillo G, Porcelli V, Saletti R, Scatena R, Soggiu A, Tedeschi G, Zilocchi M, Roncada P, Urbani A, Fasano M. Toward the Standardization of Mitochondrial Proteomics: The Italian Mitochondrial Human Proteome Project Initiative. J Proteome Res. 2017 Dec 1;16(12):4319-4329. doi:10.1021/acs.jproteome.7b00350. Epub 2017 Sep 13.

Albrecht D, Kniemeyer O, Brakhage AA, Guthke R. Missing values in gel-based proteomics. Proteomics. 2010 Mar;10(6):1202-11. doi: 10.1002/pmic.200800576. Review.

Anderson S, Bankier AT, Barrell BG, de Bruijn MH, Coulson AR, Drouin J, Eperon IC, Nierlich DP, Roe BA, Sanger F, Schreier PH, Smith AJ, Staden R, Young IG. Sequence and organization of the human mitochondrial genome. Nature. 1981 Apr 9;290(5806):457-65.

Antony PM, Diederich NJ, Krüger R, Balling R. The hallmarks of Parkinson's disease. FEBS J. 2013 Dec;280(23):5981-93. doi: 10.1111/febs.12335. Epub 2013 Jun 10. Review.

Ashrafi G, Schwarz TL. The pathways of mitophagy for quality control and clearance of mitochondria. Cell Death Differ. 2013 Jan;20(1):31-42. doi: 10.1038/cdd.2012.81. Epub 2012 Jun 29. Review.

Auburger G, Klinkenberg M, Drost J, Marcus K, Morales-Gordo B, Kunz WS, Brandt U, Broccoli V, Reichmann H, Gispert S, Jendrach M. Primary skin fibroblasts as a model of Parkinson's disease. Mol Neurobiol. 2012 Aug;46(1):20-7. doi: 10.1007/s12035-012-8245-1. Epub 2012 Feb 19. Review.

Bantscheff M, Schirle M, Sweetman G, Rick J, Kuster B. Quantitative mass spectrometry in proteomics: a critical review. Anal Bioanal Chem. 2007 Oct;389(4):1017-31. Epub 2007 Aug 1. Review.

Beavan MS, Schapira AH. Glucocerebrosidase mutations and the pathogenesis of Parkinson disease. Ann Med. 2013 Dec;45(8):511-21. doi: 10.3109/07853890.2013.849003. Review.

Beevers JE, Caffrey TM, Wade-Martins R. Induced pluripotent stem cell (iPSC)-derived dopaminergic models of Parkinson's disease. Biochem Soc Trans. 2013 Dec;41(6):1503-8. doi: 10.1042/BST20130194. Review.

Bellot G, Garcia-Medina R, Gounon P, Chiche J, Roux D, Pouysségur J, Mazure NM. Hypoxia-induced autophagy is mediated through hypoxia-inducible factor induction of BNIP3 and BNIP3L via their BH3 domains. Mol Cell Biol. 2009 May;29(10):2570-81. doi: 10.1128/MCB.00166-09. Epub 2009 Mar 9.

Benard G, Rossignol R. Ultrastructure of the mitochondrion and its bearing on function and bioenergetics. Antioxid Redox Signal. 2008 Aug;10(8):1313-42. doi: 10.1089/ars.2007.2000. Review.

Berg D, Hochstrasser H, Schweitzer KJ, Riess O. Disturbance of iron metabolism in Parkinson's disease -- ultrasonography as a biomarker. Neurotox Res. 2006 Jan;9(1):1-13. Review.

Berman SB, Hastings TG. Dopamine oxidation alters mitochondrial respiration and induces permeability transition in brain mitochondria: implications for Parkinson's disease. J Neurochem. 1999 Sep;73(3):1127-37.

Boengler K, Heusch G, Schulz R. Nuclear-encoded mitochondrial proteins and their role in cardioprotection. Biochim Biophys Acta. 2011 Jul;1813(7):1286-94. doi: 10.1016/j.bbamcr.2011.01.009. Epub 2011 Jan 19. Review.

Bolte S, Cordelières FP. A guided tour into subcellular colocalization analysis in light microscopy. J Microsc. 2006 Dec;224(Pt 3):213-32.

Bondi H, Zilocchi M, Mare MG, D'Agostino G, Giovannardi S, Ambrosio S, Fasano M, Alberio T. Dopamine induces mitochondrial depolarization without activating PINK1-mediated mitophagy. J Neurochem. 2016 Mar;136(6):1219-1231. doi: 10.1111/jnc.13506. Epub 2016 Jan 13.

Bonifati V, Rizzu P, van Baren MJ, Schaap O, Breedveld GJ, Krieger E, Dekker MC, Squitieri F, Ibanez P, Joosse M, van Dongen JW, Vanacore N, van Swieten JC, Brice A, Meco G, van Duijn CM, Oostra BA, Heutink P. Mutations in the DJ-1 gene associated with autosomal recessive early-onset parkinsonism. Science. 2003 Jan 10;299(5604):256-9. Epub 2002 Nov 21.

Bose A, Beal MF. Mitochondrial dysfunction in Parkinson's disease. J Neurochem. 2016 Oct;139 Suppl 1:216-231. doi: 10.1111/jnc.13731. Epub 2016 Aug 21. Review.

Büeler H. Impaired mitochondrial dynamics and function in the pathogenesis of Parkinson's disease. Exp Neurol. 2009 Aug;218(2):235-46. doi: 10.1016/j.expneurol.2009.03.006. Epub 2009 Mar 18. Review.

Buhlman L, Damiano M, Bertolin G, Ferrando-Miguel R, Lombès A, Brice A, Corti O. Functional interplay between Parkin and Drp1 in mitochondrial fission and clearance. Biochim Biophys Acta. 2014 Sep;1843(9):2012-26. doi: 10.1016/j.bbamcr.2014.05.012. Epub 2014 May 27.

Carlson M, Ortutay C. UniProt.ws: R Interface to UniProt Web Services. Bioconductor version: Release (3.9). 2019. doi:10.18129/B9.bioc.UniProt.ws.

Caudle WM, Bammler TK, Lin Y, Pan S, Zhang J. Using 'omics' to define pathogenesis and biomarkers of Parkinson's disease. Expert Rev Neurother. 2010 Jun;10(6):925-42. doi: 10.1586/ern.10.54. Review.

Chan DC. Dissecting mitochondrial fusion. Dev Cell. 2006 Nov;11(5):592-4.

Charcot JM. Lectures on the diseases of the nervous system: delivered at la Salpêtrière. 1879

Chen H, Detmer SA, Ewald AJ, Griffin EE, Fraser SE, Chan DC. Mitofusins Mfn1 and Mfn2 coordinately regulate mitochondrial fusion and are essential for embryonic development. J Cell Biol. 2003 Jan 20;160(2):189-200. Epub 2003 Jan 13.

Chen H, Chan DC. Critical dependence of neurons on mitochondrial dynamics. Curr Opin Cell Biol. 2006 Aug;18(4):453-9. Epub 2006 Jun 14. Review.

Chen H, Chan DC. Mitochondrial dynamics--fusion, fission, movement, and mitophagy--in neurodegenerative diseases. Hum Mol Genet. 2009 Oct 15;18(R2):R169-76. doi: 10.1093/hmg/ddp326. Review.

Chipuk JE, Bouchier-Hayes L, Green DR. Mitochondrial outer membrane permeabilization during apoptosis: the innocent bystander scenario. Cell Death Differ. 2006 Aug;13(8):1396-402. Epub 2006 May 19. Review.

Chou AP, Li S, Fitzmaurice AG, Bronstein JM. Mechanisms of rotenone-induced proteasome inhibition. Neurotoxicology. 2010 Aug;31(4):367-72. doi: 10.1016/j.neuro.2010.04.006. Epub 2010 Apr 22.

Cipolat S, Martins de Brito O, Dal Zilio B, Scorrano L. OPA1 requires mitofusin 1 to promote mitochondrial fusion. Proc Natl Acad Sci U S A. 2004 Nov 9;101(45):15927-32. Epub 2004 Oct 27.

Cipolat S, Rudka T, Hartmann D, Costa V, Serneels L, Craessaerts K, Metzger K, Frezza C, Annaert W, D'Adamio L, Derks C, Dejaegere T, Pellegrini L, D'Hooge R, Scorrano L, De Strooper B. Mitochondrial rhomboid PARL regulates cytochrome c release during apoptosis via OPA1-dependent cristae remodeling. Cell. 2006 Jul 14;126(1):163-75.

Colinge J, Chiappe D, Lagache S, Moniatte M, Bougueleret L. Differential proteomics via probabilistic peptide identification scores. Anal Chem. 2005 Jan 15;77(2):596-606.

Connolly GP. Fibroblast models of neurological disorders: fluorescence measurement studies. Trends Pharmacol Sci. 1998 May;19(5):171-7. Review.

Conway KA, Rochet JC, Bieganski RM, Lansbury PT Jr. Kinetic stabilization of the alpha-synuclein protofibril by a dopamine-alpha-synuclein adduct. Science. 2001 Nov 9;294(5545):1346-9.

Cookson MR. The role of leucine-rich repeat kinase 2 (LRRK2) in Parkinson's disease. Nat Rev Neurosci. 2010 Dec;11(12):791-7. doi: 10.1038/nrn2935. Epub 2010 Nov 19. Review.

Corti O, Lesage S, Brice A. What genetics tells us about the causes and mechanisms of Parkinson's disease. Physiol Rev. 2011 Oct;91(4):1161-218. doi: 10.1152/physrev.00022.2010. Review.

Dauer W, Przedborski S. Parkinson's disease: mechanisms and models. Neuron. 2003 Sep 11;39(6):889-909. Review.

Dawson TM, Dawson VL. The role of parkin in familial and sporadic Parkinson's disease. Mov Disord. 2010;25 Suppl 1:S32-9. doi: 10.1002/mds.22798. Review.

de Brito OM, Scorrano L. Mitofusin 2 tethers endoplasmic reticulum to mitochondria. Nature. 2008 Dec 4;456(7222):605-10. doi: 10.1038/nature07534. Erratum in: Nature. 2014 Sep 11;513(7517):266.

Deng H, Wang P, Jankovic J. The genetics of Parkinson disease. Ageing Res Rev. 2018 Mar;42:72-85. doi: 10.1016/j.arr.2017.12.007. Epub 2017 Dec 26. Review.

Detmer SA, Chan DC. Complementation between mouse Mfn1 and Mfn2 protects mitochondrial fusion defects caused by CMT2A disease mutations. J Cell Biol. 2007 Feb 12;176(4):405-14.

Devine MJ, Ryten M, Vodicka P, Thomson AJ, Burdon T, Houlden H, Cavaleri F, Nagano M, Drummond NJ, Taanman JW, Schapira AH, Gwinn K, Hardy J, Lewis PA, Kunath T. Parkinson's disease induced pluripotent stem cells with triplication of the α-synuclein locus. Nat Commun. 2011 Aug 23;2:440. doi: 10.1038/ncomms1453.

Di Fonzo A, Rohé CF, Ferreira J, Chien HF, Vacca L, Stocchi F, Guedes L, Fabrizio E, Manfredi M, Vanacore N, Goldwurm S, Breedveld G, Sampaio C, Meco G, Barbosa E, Oostra BA, Bonifati V; Italian Parkinson Genetics Network. A frequent LRRK2 gene mutation associated with autosomal dominant Parkinson's disease. Lancet. 2005 Jan 29-Feb 4;365(9457):412-5.

Dimmer KS, Scorrano L. (De)constructing mitochondria: what for? Physiology (Bethesda). 2006 Aug;21:233-41. Review.

Distler U, Kuharev J, Navarro P, Tenzer S. Label-free quantification in ion mobility-enhanced data-independent acquisition proteomics. Nat Protoc. 2016 Apr;11(4):795-812. doi: 10.1038/nprot.2016.042. Epub 2016 Mar 24.

Eiyama A, Okamoto K. PINK1/Parkin-mediated mitophagy in mammalian cells. Curr Opin Cell Biol. 2015 Apr;33:95-101. doi: 10.1016/j.ceb.2015.01.002. Epub 2015 Feb 17. Review.

Fasano M, Giraudo S, Coha S, Bergamasco B, Lopiano L. Residual substantia nigra neuromelanin in Parkinson's disease is cross-linked to alpha-synuclein. Neurochem Int. 2003 Jun;42(7):603-6.

Fasano M, Bergamasco B, Lopiano L. Modifications of the iron-neuromelanin system in Parkinson's disease. J Neurochem. 2006 Feb;96(4):909-16. Epub 2006 Jan 17. Review.

Fasano M, Alberio T, Babu M, Lundberg E, Urbani A. Towards a functional definition of the mitochondrial human proteome. EuPA Open Proteom. 2016 Jan 7;10:24-27. doi: 10.1016/j.euprot.2016.01.004. eCollection 2016 Mar.

Fernández-Moriano C, González-Burgos E, Gómez-Serranillos MP. Mitochondria-Targeted Protective Compounds in Parkinson's and Alzheimer's Diseases. Oxid Med Cell Longev. 2015;2015:408927. doi: 10.1155/2015/408927. Epub 2015 Apr 29. Review.

Fimia GM, Stoykova A, Romagnoli A, Giunta L, Di Bartolomeo S, Nardacci R, Corazzari M, Fuoco C, Ucar A, Schwartz P, Gruss P, Piacentini M, Chowdhury K, Cecconi F. Ambra1 regulates autophagy and development of the nervous system. Nature. 2007 Jun 28;447(7148):1121-5. Epub 2007 Jun 24.

Frey TG, Mannella CA. The internal structure of mitochondria. Trends Biochem Sci. 2000 Jul;25(7):319-24. Review.

Gallagher DA, Lees AJ, Schrag A. What are the most important nonmotor symptoms in patients with Parkinson's disease and are we missing them? Mov Disord. 2010 Nov 15;25(15):2493-500. doi: 10.1002/mds.23394.

Gao F, Chen D, Si J, Hu Q, Qin Z, Fang M, Wang G. The mitochondrial protein BNIP3L is the substrate of PARK2 and mediates mitophagy in PINK1/PARK2 pathway. Hum Mol Genet. 2015 May 1;24(9):2528-38. doi: 10.1093/hmg/ddv017. Epub 2015 Jan 22.

Gao Y, Wilson GR, Stephenson SEM, Bozaoglu K, Farrer MJ, Lockhart PJ. The emerging role of Rab GTPases in the pathogenesis of Parkinson's disease. Mov Disord. 2018 Feb;33(2):196-207. doi: 10.1002/mds.27270. Epub 2018 Jan 9. Review.

Gasser T. Molecular pathogenesis of Parkinson disease: insights from genetic studies. Expert Rev Mol Med. 2009 Jul 27;11:e22. doi: 10.1017/S1462399409001148. Review.

Gegg ME, Cooper JM, Chau KY, Rojo M, Schapira AH, Taanman JW. Mitofusin 1 and mitofusin 2 are ubiquitinated in a PINK1/parkin-dependent manner upon induction of mitophagy. Hum Mol Genet. 2010 Dec 15;19(24):4861-70. doi: 10.1093/hmg/ddq419. Epub 2010 Sep 24. Erratum in: Hum Mol Genet. 2013 Apr 15;22(8):1697.

Geisler S, Holmström KM, Treis A, Skujat D, Weber SS, Fiesel FC, Kahle PJ, Springer W. The PINK1/Parkin-mediated mitophagy is compromised by PD-associated mutations. Autophagy. 2010 Oct;6(7):871-8. Epub 2010 Oct 3.

Gitler AD, Bevis BJ, Shorter J, Strathearn KE, Hamamichi S, Su LJ, Caldwell KA, Caldwell GA, Rochet JC, McCaffery JM, Barlowe C, Lindquist S. The Parkinson's disease protein alpha-synuclein disrupts cellular Rab homeostasis. Proc Natl Acad Sci U S A. 2008 Jan 8;105(1):145-50. Epub 2007 Dec 27.

Gleyzer N, Vercauteren K, Scarpulla RC. Control of mitochondrial transcription specificity factors (TFB1M and TFB2M) by nuclear respiratory factors (NRF-1 and NRF-2) and PGC-1 family coactivators. Mol Cell Biol. 2005 Feb;25(4):1354-66.

Golpich M, Amini E, Mohamed Z, Azman Ali R, Mohamed Ibrahim N, Ahmadiani A. Mitochondrial Dysfunction and Biogenesis in Neurodegenerative diseases: Pathogenesis and Treatment. CNS Neurosci Ther. 2017 Jan;23(1):5-22. doi: 10.1111/cns.12655. Epub 2016 Nov 22. Review.

Grünewald A, Gegg ME, Taanman JW, King RH, Kock N, Klein C, Schapira AH. Differential effects of PINK1 nonsense and missense mutations on mitochondrial function and morphology. Exp Neurol. 2009 Sep;219(1):266-73. doi: 10.1016/j.expneurol.2009.05.027. Epub 2009 Jun 3.

Grünewald A, Voges L, Rakovic A, Kasten M, Vandebona H, Hemmelmann C, Lohmann K, Orolicki S, Ramirez A, Schapira AH, Pramstaller PP, Sue CM, Klein C. Mutant Parkin impairs mitochondrial function and morphology in human fibroblasts. PLoS One. 2010 Sep 27;5(9):e12962. doi: 10.1371/journal.pone.0012962.

Hammerling BC, Najor RH, Cortez MQ, Shires SE, Leon LJ, Gonzalez ER, Boassa D, Phan S, Thor A, Jimenez RE, Li H, Kitsis RN, Dorn GW II, Sadoshima J, Ellisman MH, Gustafsson ÅB. A Rab5 endosomal pathway mediates Parkin-dependent mitochondrial clearance. Nat Commun. 2017 Jan 30;8:14050. doi: 10.1038/ncomms14050.

Hamon MP, Bulteau AL, Friguet B. Mitochondrial proteases and protein quality control in ageing and longevity. Ageing Res Rev. 2015 Sep;23(Pt A):56-66. doi: 10.1016/j.arr.2014.12.010. Epub 2015 Jan 8. Review.

Herrera A, Muñoz P, Steinbusch HWM, Segura-Aguilar J. Are Dopamine Oxidation Metabolites Involved in the Loss of Dopaminergic Neurons in the Nigrostriatal System in Parkinson's Disease? ACS Chem Neurosci. 2017 Apr 19;8(4):702-711. doi: 10.1021/acschemneuro.7b00034. Epub 2017 Mar 3. Review.

Herrmann JM, Riemer J. The intermembrane space of mitochondria. Antioxid Redox Signal. 2010 Nov 1;13(9):1341-58. doi: 10.1089/ars.2009.3063. Review.

Herzig S, Long F, Jhala US, Hedrick S, Quinn R, Bauer A, Rudolph D, Schutz G, Yoon C, Puigserver P, Spiegelman B, Montminy M. CREB regulates hepatic gluconeogenesis through the coactivator PGC-1. Nature. 2001 Sep 13;413(6852):179-83. Erratum in: Nature 2001 Oct 11;413(6856):652.

Hindle JV. Ageing, neurodegeneration and Parkinson's disease. Age Ageing. 2010 Mar;39(2):156-61. doi: 10.1093/ageing/afp223. Epub 2010 Jan 5. Review.

Hosp F, Mann M. A Primer on Concepts and Applications of Proteomics in Neuroscience. Neuron. 2017 Nov 1;96(3):558-571. doi: 10.1016/j.neuron.2017.09.025. Review.

Hoppins S, Lackner L, Nunnari J. The machines that divide and fuse mitochondria. Annu Rev Biochem. 2007;76:751-80. Review.

Hoppins S. The regulation of mitochondrial dynamics. Curr Opin Cell Biol. 2014 Aug;29:46-52. doi: 10.1016/j.ceb.2014.03.005. Epub 2014 Apr 17. Review. Erratum in: Curr Opin Cell Biol. 2014 Aug;29:143.

Imai Y, Soda M, Hatakeyama S, Akagi T, Hashikawa T, Nakayama KI, Takahashi R. CHIP is associated with Parkin, a gene responsible for familial Parkinson's disease, and enhances its ubiquitin ligase activity. Mol Cell. 2002 Jul;10(1):55-67.

Ishihara N, Eura Y, Mihara K. Mitofusin 1 and 2 play distinct roles in mitochondrial fusion reactions via GTPase activity. J Cell Sci. 2004 Dec 15;117(Pt 26):6535-46. Epub 2004 Nov 30.

Jin SM, Lazarou M, Wang C, Kane LA, Narendra DP, Youle RJ. Mitochondrial membrane potential regulates PINK1 import and proteolytic destabilization by PARL. J Cell Biol. 2010 Nov 29;191(5):933-42. doi: 10.1083/jcb.201008084.

Johnson ME, Bobrovskaya L. An update on the rotenone models of Parkinson's disease: their ability to reproduce the features of clinical disease and model gene-environment interactions. Neurotoxicology. 2015 Jan;46:101-16. doi: 10.1016/j.neuro.2014.12.002. Epub 2014 Dec 13. Review.

Jorrin-Novo JV, Komatsu S, Sanchez-Lucas R, Rodríguez de Francisco LE. Gel electrophoresis-based plant proteomics: Past, present, and future. Happy 10th anniversary Journal of Proteomics! J Proteomics. 2018 Aug 29. pii: S1874-3919(18)30326-9. doi: 10.1016/j.jprot.2018.08.016. Review.

Kalia SK, Lee S, Smith PD, Liu L, Crocker SJ, Thorarinsdottir TE, Glover JR, Fon EA, Park DS, Lozano AM. BAG5 inhibits parkin and enhances dopaminergic neuron degeneration. Neuron. 2004 Dec 16;44(6):931-45.

Kang Y, Fielden LF, Stojanovski D. Mitochondrial protein transport in health and disease. Semin Cell Dev Biol. 2018 Apr;76:142-153. doi:10.1016/j.semcdb.2017.07.028. Epub 2017 Jul 29. Review.

Kilpatrick BS, Magalhaes J, Beavan MS, McNeill A, Gegg ME, Cleeter MW, Bloor-Young D, Churchill GC, Duchen MR, Schapira AH, Patel S. Endoplasmic reticulum and lysosomal Ca^{2+} stores are remodelled in GBA1-linked Parkinson disease patient fibroblasts. Cell Calcium. 2016 Jan;59(1):12-20. doi: 10.1016/j.ceca.2015.11.002. Epub 2015 Nov 26.

Klinkenberg M, Thurow N, Gispert S, Ricciardi F, Eich F, Prehn JH, Auburger G, Kögel D. Enhanced vulnerability of PARK6 patient skin fibroblasts to apoptosis induced by proteasomal stress. Neuroscience. 2010 Mar 17;166(2):422-34. doi: 10.1016/j.neuroscience.2009.12.068. Epub 2010 Jan 4.

Kondapalli C, Kazlauskaite A, Zhang N, Woodroof HI, Campbell DG, Gourlay R, Burchell L, Walden H, Macartney TJ, Deak M, Knebel A, Alessi DR, Muqit MM. PINK1 is activated by mitochondrial membrane potential depolarization and stimulates Parkin E3 ligase activity by phosphorylating Serine 65. Open Biol. 2012 May;2(5):120080. doi: 10.1098/rsob.120080.

Koppen M, Langer T. Protein degradation within mitochondria: versatile activities of AAA proteases and other peptidases. Crit Rev Biochem Mol Biol. 2007 May-Jun;42(3):221-42. Review.

Kuznetsov AV, Hermann M, Saks V, Hengster P, Margreiter R. The cell-type specificity of mitochondrial dynamics. Int J Biochem Cell Biol. 2009 Oct;41(10):1928-39. doi: 10.1016/j.biocel.2009.03.007. Epub 2009 Mar 27. Review.

Lang C, Campbell KR, Ryan BJ, Carling P, Attar M, Vowles J, Perestenko OV, Bowden R, Baig F, Kasten M, Hu MT, Cowley SA, Webber C, Wade-Martins R. Single-Cell Sequencing of iPSC-Dopamine Neurons Reconstructs Disease Progression and Identifies HDAC4 as a Regulator of Parkinson Cell Phenotypes. Cell Stem Cell. 2019; 24(1):93-106.e6. doi: 10.1016/j.stem.2018.10.023.

Langston JW, Ballard PA Jr. Parkinson's disease in a chemist working with 1-methyl-4-phenyl-1,2,5,6-tetrahydropyridine. N Engl J Med. 1983 Aug 4;309(5):310.

Lee JY, Nagano Y, Taylor JP, Lim KL, Yao TP. Disease-causing mutations in parkin impair mitochondrial ubiquitination, aggregation, and HDAC6-dependent mitophagy. J Cell Biol. 2010 May 17;189(4):671-9. doi: 10.1083/jcb.201001039. Epub 2010 May 10.

Lee SJ. alpha-synuclein aggregation: a link between mitochondrial defects and Parkinson's disease? Antioxid Redox Signal. 2003 Jun;5(3):337-48. Review.

Lee VM, Trojanowski JQ. Mechanisms of Parkinson's disease linked to pathological alpha-synuclein: new targets for drug discovery. Neuron. 2006 Oct 5;52(1):33-8. Review.

Lee Y, Lee HY, Hanna RA, Gustafsson ÅB. Mitochondrial autophagy by Bnip3 involves Drp1-mediated mitochondrial fission and recruitment of Parkin in cardiac myocytes. Am J Physiol Heart Circ Physiol. 2011 Nov;301(5):H1924-31. doi: 10.1152/ajpheart.00368.2011. Epub 2011 Sep 2.

Lesage S, Brice A. Parkinson's disease: from monogenic forms to genetic susceptibility factors. Hum Mol Genet. 2009 Apr 15;18(R1):R48-59. doi: 10.1093/hmg/ddp012. Review.

Lesage S, Bras J, Cormier-Dequaire F, Condroyer C, Nicolas A, Darwent L, Guerreiro R, Majounie E, Federoff M, Heutink P, Wood NW, Gasser T, Hardy J, Tison F, Singleton A, Brice A; French Parkinson's Disease Genetics Study Group (PDG) and the International Parkinson's Disease Genomics Consortium (IPDGC). Loss-of-function mutations in RAB39B are associated with typical early-onset Parkinson disease. Neurol Genet. 2015 Jun 18;1(1):e9. doi: 10.1212/NXG.0000000000000009. eCollection 2015 Jun.

Lewy FH. Paralysis agitans. I. Pathologische anatomie. Handbuch der neurologie. 1912. 3(part 2), 920-933.

Li JQ, Tan L, Yu JT. The role of the LRRK2 gene in Parkinsonism. Mol Neurodegener. 2014 Nov 12;9:47. doi: 10.1186/1750-1326-9-47. Review.

Lill CM. Genetics of Parkinson's disease. Mol Cell Probes. 2016 Dec;30(6):386-396. doi: 10.1016/j.mcp.2016.11.001. Epub 2016 Nov 4. Review.

Lilley KS, Friedman DB. All about DIGE: quantification technology for differential-display 2D-gel proteomics. Expert Rev Proteomics. 2004 Dec;1(4):401-9.

Lippolis R, Siciliano RA, Pacelli C, Ferretta A, Mazzeo MF, Scacco S, Papa F, Gaballo A, Dell'Aquila C, De Mari M, Papa S, Cocco T. Altered protein expression pattern in skin fibroblasts from parkin-mutant early-onset Parkinson's disease patients. Biochim Biophys Acta. 2015 Sep;1852(9):1960-70. doi: 10.1016/j.bbadis.2015.06.015. Epub 2015 Jun 19.

Lotharius J, Brundin P. Impaired dopamine storage resulting from alpha-synuclein mutations may contribute to the pathogenesis of Parkinson's disease. Hum Mol Genet. 2002 Oct 1;11(20):2395-407. Review.

Maere S, Heymans K, Kuiper M. BiNGO: a Cytoscape plugin to assess overrepresentation of gene ontology categories in biological networks. Bioinformatics. 2005 Aug 15;21(16):3448-9. Epub 2005 Jun 21.

Manders EM, Stap J, Brakenhoff GJ, van Driel R, Aten JA. Dynamics of three-dimensional replication patterns during the S-phase, analysed by double labelling of DNA and confocal microscopy. J Cell Sci. 1992 Nov;103 (Pt 3):857-62.

Martin I, Kim JW, Dawson VL, Dawson TM. LRRK2 pathobiology in Parkinson's disease. J Neurochem. 2014 Dec;131(5):554-65. doi: 10.1111/jnc.12949. Epub 2014 Oct 10. Review.

Martin LJ, Pan Y, Price AC, Sterling W, Copeland NG, Jenkins NA, Price DL, Lee MK. Parkinson's disease alpha-synuclein transgenic mice develop neuronal mitochondrial degeneration and cell death. J Neurosci. 2006 Jan 4;26(1):41-50.

Matsuda N, Sato S, Shiba K, Okatsu K, Saisho K, Gautier CA, Sou YS, Saiki S, Kawajiri S, Sato F, Kimura M, Komatsu M, Hattori N, Tanaka K. PINK1 stabilized by mitochondrial depolarization recruits Parkin to damaged mitochondria and activates latent Parkin for mitophagy. J Cell Biol. 2010 Apr 19;189(2):211-21. doi: 10.1083/jcb.200910140.

McDonald WH, Yates JR 3rd. Shotgun proteomics and biomarker discovery. Dis Markers. 2002;18(2):99-105. Review.

Misko A, Jiang S, Wegorzewska I, Milbrandt J, Baloh RH. Mitofusin 2 is necessary for transport of axonal mitochondria and interacts with the Miro/Milton complex. J Neurosci. 2010 Mar 24;30(12):4232-40. doi: 10.1523/JNEUROSCI.6248-09.2010.

Moore DJ, West AB, Dikeman DA, Dawson VL, Dawson TM. Parkin mediates the degradation-independent ubiquitination of Hsp70. J Neurochem. 2008 Jun;105(5):1806-19. doi: 10.1111/j.1471-4159.2008.05261.x. Epub 2008 Feb 1.

Monti C, Zilocchi M, Colugnat I, Alberio T. Proteomics turns functional. J Proteomics. 2019 Apr 30;198:36-44. doi: 10.1016/j.jprot.2018.12.012. Epub 2018 Dec 13.

Monti C, Lane L, Fasano M, Alberio T. Update of the Functional Mitochondrial Human Proteome Network. J Proteome Res. 2018 Dec 7;17(12):4297-4306. doi: 10.1021/acs.jproteome.8b00447. Epub 2018 Oct 8.

Morais VA, Verstreken P, Roethig A, Smet J, Snellinx A, Vanbrabant M, Haddad D, Frezza C, Mandemakers W, Vogt-Weisenhorn D, Van Coster R, Wurst W, Scorrano L, De Strooper B. Parkinson's disease mutations in PINK1 result in decreased Complex I activity and deficient synaptic function. EMBO Mol Med. 2009 May;1(2):99-111. doi: 10.1002/emmm.200900006.

Mortiboys H, Thomas KJ, Koopman WJ, Klaffke S, Abou-Sleiman P, Olpin S, Wood NW, Willems PH, Smeitink JA, Cookson MR, Bandmann O. Mitochondrial function and morphology are impaired in parkin-mutant fibroblasts. Ann Neurol. 2008 Nov;64(5):555-65. doi: 10.1002/ana.21492.

Mortiboys H, Johansen KK, Aasly JO, Bandmann O. Mitochondrial impairment in patients with Parkinson disease with the G2019S mutation in LRRK2. Neurology. 2010 Nov 30;75(22):2017-20. doi: 10.1212/WNL.0b013e3181ff9685.

Mozdy AD, McCaffery JM, Shaw JM. Dnm1p GTPase-mediated mitochondrial fission is a multi-step process requiring the novel integral membrane component Fis1p. J Cell Biol. 2000 Oct 16;151(2):367-80.

Naghdi S, Hajnóczky G. VDAC2-specific cellular functions and the underlying structure. Biochim Biophys Acta. 2016 Oct;1863(10):2503-14. doi: 10.1016/j.bbamcr.2016.04.020. Epub 2016 Apr 23. Review.

Nandipati S, Litvan I. Environmental Exposures and Parkinson's Disease. Int J Environ Res Public Health. 2016 Sep 3;13(9). pii: E881. doi: 10.3390/ijerph13090881. Review.

Narendra DP, Jin SM, Tanaka A, Suen DF, Gautier CA, Shen J, Cookson MR, Youle RJ. PINK1 is selectively stabilized on impaired mitochondria to activate Parkin. PLoS Biol. 2010 Jan 26;8(1):e1000298. doi: 10.1371/journal.pbio.1000298.

Nisoli E, Falcone S, Tonello C, Cozzi V, Palomba L, Fiorani M, Pisconti A, Brunelli S, Cardile A, Francolini M, Cantoni O, Carruba MO, Moncada S, Clementi E. Mitochondrial biogenesis by NO yields functionally active mitochondria in mammals. Proc Natl Acad Sci U S A. 2004 Nov 23;101(47):16507-12. Epub 2004 Nov 15. Erratum in: Proc Natl Acad Sci U S A. 2005 Apr 12;102(15):5635.

Ong SE, Mann M. Mass spectrometry-based proteomics turns quantitative. Nat Chem Biol. 2005 Oct;1(5):252-62. Review.

Osellame LD, Duchen MR. Quality control gone wrong: mitochondria, lysosomal storage disorders and neurodegeneration. Br J Pharmacol. 2014 Apr;171(8):1958-72. doi: 10.1111/bph.12453. Review.

Otera H, Wang C, Cleland MM, Setoguchi K, Yokota S, Youle RJ, Mihara K. Mff is an essential factor for mitochondrial recruitment of Drp1 during mitochondrial fission in mammalian cells. J Cell Biol. 2010 Dec 13;191(6):1141-58. doi: 10.1083/jcb.201007152.

Otera H, Mihara K. Molecular mechanisms and physiologic functions of mitochondrial dynamics. J Biochem. 2011 Mar;149(3):241-51. doi: 10.1093/jb/mvr002. Epub 2011 Jan 13. Review.

Palikaras K, Tavernarakis N. Mitochondrial homeostasis: the interplay between mitophagy and mitochondrial biogenesis. Exp Gerontol. 2014 Aug;56:182-8. doi: 10.1016/j.exger.2014.01.021. Epub 2014 Jan 28. Review.

Palmer CS, Osellame LD, Laine D, Koutsopoulos OS, Frazier AE, Ryan MT. MiD49 and MiD51, new components of the mitochondrial fission machinery. EMBO Rep. 2011 Jun;12(6):565-73. doi: 10.1038/embor.2011.54. Epub 2011 Apr 21.

Paris I, Perez-Pastene C, Cardenas S, Iturriaga-Vasquez P, Muñoz P, Couve E, Caviedes P, Segura-Aguilar J. Aminochrome induces disruption of actin, alpha-, and beta-tubulin cytoskeleton networks in substantia-nigra-derived cell line. Neurotox Res. 2010 Jul;18(1):82-92. doi: 10.1007/s12640-009-9148-4. Epub 2010 Jan 20.

Parone PA, Da Cruz S, Tondera D, Mattenberger Y, James DI, Maechler P, Barja F, Martinou JC. Preventing mitochondrial fission impairs mitochondrial function and leads to loss of mitochondrial DNA. PLoS One. 2008 Sep 22;3(9):e3257. doi:10.1371/journal.pone.0003257.

Perier C, Vila M. Mitochondrial biology and Parkinson's disease. Cold Spring Harb Perspect Med. 2012 Feb;2(2):a009332. doi: 10.1101/cshperspect.a009332. Review.

Pickles S, Vigié P, Youle RJ. Mitophagy and Quality Control Mechanisms in Mitochondrial Maintenance. Curr Biol. 2018 Feb 19;28(4):R170-R185. doi: 10.1016/j.cub.2018.01.004. Review.

Pienaar IS, Daniels WM, Götz J. Neuroproteomics as a promising tool in Parkinson's disease research. J Neural Transm (Vienna). 2008 Oct;115(10):1413-30. doi: 10.1007/s00702-008-0070-3. Epub 2008 Jun 4. Review.

Polymeropoulos MH, Lavedan C, Leroy E, Ide SE, Dehejia A, Dutra A, Pike B, Root H, Rubenstein J, Boyer R, Stenroos ES, Chandrasekharappa S, Athanassiadou A, Papapetropoulos T, Johnson WG, Lazzarini AM, Duvoisin RC, Di Iorio G, Golbe LI, Nussbaum RL. Mutation in the alpha-synuclein gene identified in families with Parkinson's disease. Science. 1997 Jun 27;276(5321):2045-7.

Poole AC, Thomas RE, Andrews LA, McBride HM, Whitworth AJ, Pallanck LJ. The PINK1/Parkin pathway regulates mitochondrial morphology. Proc Natl Acad Sci U S A. 2008 Feb 5;105(5):1638-43. doi: 10.1073/pnas.0709336105. Epub 2008 Jan 29.

Ramonet D, Perier C, Recasens A, Dehay B, Bové J, Costa V, Scorrano L, Vila M. Optic atrophy 1 mediates mitochondria remodeling and dopaminergic neurodegeneration linked to complex I deficiency. Cell Death Differ. 2013 Jan;20(1):77-85. doi: 10.1038/cdd.2012.95. Epub 2012 Aug 3.

Ramsay RR, Salach JI, Dadgar J, Singer TP. Inhibition of mitochondrial NADH dehydrogenase by pyridine derivatives and its possible relation to experimental and idiopathic parkinsonism. Biochem Biophys Res Commun. 1986 Feb 26;135(1):269-75.

Ryan SD, Dolatabadi N, Chan SF, Zhang X, Akhtar MW, Parker J, Soldner F, Sunico CR, Nagar S, Talantova M, Lee B, Lopez K, Nutter A, Shan B, Molokanova E, Zhang Y, Han X, Nakamura T, Masliah E, Yates JR 3rd, Nakanishi N, Andreyev AY, Okamoto S, Jaenisch R, Ambasudhan R, Lipton SA. Isogenic human iPSC Parkinson's model shows nitrosative stress-induced dysfunction in MEF2-PGC1α transcription. Cell. 2013 Dec 5;155(6):1351-64. doi: 10.1016/j.cell.2013.11.009. Epub 2013 Nov 27.

Rugarli EI, Langer T. Mitochondrial quality control: a matter of life and death for neurons. EMBO J. 2012 Mar 21;31(6):1336-49. doi: 10.1038/emboj.2012.38. Epub 2012 Feb 21. Review.

Saez-Atienzar S, Bonet-Ponce L, Blesa JR, Romero FJ, Murphy MP, Jordan J, Galindo MF. The LRRK2 inhibitor GSK2578215A induces protective autophagy in SH-SY5Y cells: involvement of Drp-1-mediated mitochondrial fission and mitochondrial-derived ROS signaling. Cell Death Dis. 2014 Aug 14;5:e1368. doi: 10.1038/cddis.2014.320.

Samii A, Nutt JG, Ransom BR. Parkinson's disease. Lancet. 2004 May 29;363(9423):1783-93. Review.

Santos D, Cardoso SM. Mitochondrial dynamics and neuronal fate in Parkinson's disease. Mitochondrion. 2012 Jul;12(4):428-37. doi: 10.1016/j.mito.2012.05.002. Epub 2012 May 17. Review.

Scarpulla RC. Transcriptional paradigms in mammalian mitochondrial biogenesis and function. Physiol Rev. 2008 Apr;88(2):611-38. doi: 10.1152/physrev.00025.2007. Review.

Schapira AH. Mitochondria in the aetiology and pathogenesis of Parkinson's disease. Lancet Neurol. 2008 Jan;7(1):97-109. Review.

Schapira AH, Tolosa E. Molecular and clinical prodrome of Parkinson disease: implications for treatment. Nat Rev Neurol. 2010 Jun;6(6):309-17. doi: 10.1038/nrneurol.2010.52. Epub 2010 May 18. Review.

Schapira AH, Jenner P. Etiology and pathogenesis of Parkinson's disease. Mov Disord. 2011 May;26(6):1049-55. doi: 10.1002/mds.23732. Review.

Sherer TB, Betarbet R, Stout AK, Lund S, Baptista M, Panov AV, Cookson MR, Greenamyre JT. An in vitro model of Parkinson's disease: linking mitochondrial impairment to altered alpha-synuclein metabolism and oxidative damage. J Neurosci. 2002 Aug 15;22(16):7006-15.

Shimizu K, Ohtaki K, Matsubara K, Aoyama K, Uezono T, Saito O, Suno M, Ogawa K, Hayase N, Kimura K, Shiono H. Carrier-mediated processes in blood—brain barrier penetration and neural uptake of paraquat. Brain Res. 2001 Jul 6;906(1-2):135-42.

Shimura H, Hattori N, Kubo Si, Mizuno Y, Asakawa S, Minoshima S, Shimizu N, Iwai K, Chiba T, Tanaka K, Suzuki T. Familial Parkinson disease gene product, parkin, is a ubiquitin-protein ligase. Nat Genet. 2000 Jul;25(3):302-5.

Shin JH, Ko HS, Kang H, Lee Y, Lee YI, Pletinkova O, Troconso JC, Dawson VL, Dawson TM. PARIS (ZNF746) repression of PGC-1α contributes to neurodegeneration in Parkinson's disease. Cell. 2011 Mar 4;144(5):689-702. doi: 10.1016/j.cell.2011.02.010.

Shults CW. Lewy bodies. Proc Natl Acad Sci U S A. 2006 Feb 7;103(6):1661-8. Epub 2006 Jan 31.

Sidransky E, Nalls MA, Aasly JO, Aharon-Peretz J, Annesi G, Barbosa ER, Bar-Shira A, Berg D, Bras J, Brice A, Chen CM, Clark LN, Condroyer C, De Marco EV, Dürr A, Eblan MJ, Fahn S, Farrer MJ, Fung HC, Gan-Or Z, Gasser T, Gershoni-Baruch R, Giladi N, Griffith A, Gurevich T, Januario C, Kropp P, Lang AE, Lee-Chen GJ, Lesage S, Marder K, Mata IF, Mirelman A, Mitsui J, Mizuta I, Nicoletti G, Oliveira C, Ottman R, Orr-Urtreger A, Pereira LV, Quattrone A, Rogaeva E, Rolfs A, Rosenbaum H, Rozenberg R, Samii A, Samaddar T, Schulte C, Sharma M, Singleton A, Spitz M, Tan EK, Tayebi N, Toda T, Troiano AR, Tsuji S, Wittstock M, Wolfsberg TG, Wu YR, Zabetian CP, Zhao Y, Ziegler SG. Multicenter analysis of glucocerebrosidase mutations in Parkinson's disease. N Engl J Med. 2009 Oct 22;361(17):1651-61. doi: 10.1056/NEJMoa0901281.

Sim CH, Lio DS, Mok SS, Masters CL, Hill AF, Culvenor JG, Cheng HC. C-terminal truncation and Parkinson's disease-associated mutations down-regulate the protein serine/threonine kinase activity of PTEN-induced kinase-1. Hum Mol Genet. 2006 Nov 1;15(21):3251-62. Epub 2006 Sep 25.

Skulachev VP. Mitochondrial filaments and clusters as intracellular power-transmitting cables. Trends Biochem Sci. 2001 Jan;26(1):23-9. Review.

Smirnova E, Griparic L, Shurland DL, van der Bliek AM. Dynamin-related protein Drp1 is required for mitochondrial division in mammalian cells. Mol Biol Cell. 2001 Aug;12(8):2245-56.

Song Z, Ghochani M, McCaffery JM, Frey TG, Chan DC. Mitofusins and OPA1 mediate sequential steps in mitochondrial membrane fusion. Mol Biol Cell. 2009 Aug;20(15):3525-32. doi: 10.1091/mbc.E09-03-0252. Epub 2009 May 28.

Song S, Jang S, Park J, Bang S, Choi S, Kwon KY, Zhuang X, Kim E, Chung J. Characterization of PINK1 (PTEN-induced putative kinase 1) mutations associated with Parkinson disease in mammalian cells and Drosophila. J Biol Chem. 2013 Feb 22;288(8):5660-72. doi: 10.1074/jbc.M112.430801. Epub 2013 Jan 9.

Spillantini MG, Crowther RA, Jakes R, Hasegawa M, Goedert M. alpha-Synuclein in filamentous inclusions of Lewy bodies from Parkinson's disease and dementia with lewy bodies. Proc Natl Acad Sci U S A. 1998 May 26;95(11):6469-73.

Stefanis L. α-Synuclein in Parkinson's disease. Cold Spring Harb Perspect Med. 2012 Feb;2(2):a009399. doi: 10.1101/cshperspect.a009399. Review.

Stevens DA, Lee Y, Kang HC, Lee BD, Lee YI, Bower A, Jiang H, Kang SU, Andrabi SA, Dawson VL, Shin JH, Dawson TM. Parkin loss leads to PARIS-dependent declines in mitochondrial mass and respiration. Proc Natl Acad Sci U S A. 2015 Sep 15;112(37):11696-701. doi: 10.1073/pnas.1500624112. Epub 2015 Aug 31.

Strittmatter EF, Ferguson PL, Tang K, Smith RD. Proteome analyses using accurate mass and elution time peptide tags with capillary LC time-of-flight mass spectrometry. J Am Soc Mass Spectrom. 2003 Sep;14(9):980-91.

Su G, Kuchinsky A, Morris JH, States DJ, Meng F. GLay: community structure analysis of biological networks. Bioinformatics. 2010 Dec 15;26(24):3135-7. doi: 10.1093/bioinformatics/btq596.

Su T, Turnbull DM, Greaves LC. Roles of Mitochondrial DNA Mutations in Stem Cell Ageing. Genes (Basel). 2018 Mar 27;9(4). pii: E182. doi:10.3390/genes9040182. Review.

Subramaniam SR, Chesselet MF. Mitochondrial dysfunction and oxidative stress in Parkinson's disease. Prog Neurobiol. 2013 Jul-Aug;106-107:17-32. doi: 10.1016/j.pneurobio.2013.04.004. Epub 2013 Apr 30. Review.

Sun M, Latourelle JC, Wooten GF, Lew MF, Klein C, Shill HA, Golbe LI, Mark MH, Racette BA, Perlmutter JS, Parsian A, Guttman M, Nicholson G, Xu G, Wilk JB, Saint-Hilaire MH, DeStefano AL, Prakash R, Williamson S, Suchowersky O, Labelle N, Growdon JH, Singer C, Watts RL, Goldwurm S, Pezzoli G, Baker KB, Pramstaller PP, Burn DJ, Chinnery PF, Sherman S, Vieregge P, Litvan I, Gillis T, MacDonald ME, Myers RH, Gusella JF. Influence of heterozygosity for parkin mutation on onset age in familial Parkinson disease: the GenePD study. Arch Neurol. 2006 Jun;63(6):826-32.

Szklarczyk D, Morris JH, Cook H, Kuhn M, Wyder S, Simonovic M, Santos A, Doncheva NT, Roth A, Bork P, Jensen LJ, von Mering C. The STRING database in 2017: quality-controlled protein-protein association networks, made broadly accessible. Nucleic Acids Res. 2017 Jan 4;45(D1):D362-D368. doi: 10.1093/nar/gkw937. Epub 2016 Oct 18.

Takahashi K, Tanabe K, Ohnuki M, Narita M, Ichisaka T, Tomoda K, Yamanaka S. Induction of pluripotent stem cells from adult human fibroblasts by defined factors. Cell. 2007 Nov 30;131(5):861-72.

Tanaka A, Cleland MM, Xu S, Narendra DP, Suen DF, Karbowski M, Youle RJ. Proteasome and p97 mediate mitophagy and degradation of mitofusins induced by Parkin. J Cell Biol. 2010 Dec 27;191(7):1367-80. doi: 10.1083/jcb.201007013. Epub 2010 Dec 20.

Tanner CM, Kamel F, Ross GW, Hoppin JA, Goldman SM, Korell M, Marras C, Bhudhikanok GS, Kasten M, Chade AR, Comyns K, Richards MB, Meng C, Priestley B, Fernandez HH, Cambi F, Umbach DM, Blair A, Sandler DP, Langston JW. Rotenone, paraquat, and Parkinson's disease. Environ Health Perspect. 2011 Jun;119(6):866-72. doi: 10.1289/ehp.1002839. Epub 2011 Jan 26.

Tatsuta T. Protein quality control in mitochondria. J Biochem. 2009 Oct;146(4):455-61. doi: 10.1093/jb/mvp122. Epub 2009 Aug 7. Review.

Twig G, Elorza A, Molina AJ, Mohamed H, Wikstrom JD, Walzer G, Stiles L, Haigh SE, Katz S, Las G, Alroy J, Wu M, Py BF, Yuan J, Deeney JT, Corkey BE, Shirihai OS. Fission and selective fusion govern mitochondrial segregation and elimination by autophagy. EMBO J. 2008 Jan 23;27(2):433-46. doi: 10.1038/sj.emboj.7601963. Epub 2008 Jan 17.

Tysnes OB, Storstein A. Epidemiology of Parkinson's disease. J Neural Transm (Vienna). 2017 Aug;124(8):901-905. doi: 10.1007/s00702-017-1686-y. Epub 2017 Feb 1. Review.

Unlü M, Morgan ME, Minden JS. Difference gel electrophoresis: a single gel method for detecting changes in protein extracts. Electrophoresis. 1997 Oct;18(11):2071-7.

Vakifahmetoglu-Norberg H, Ouchida AT, Norberg E. The role of mitochondria in metabolism and cell death. Biochem Biophys Res Commun. 2017 Jan 15;482(3):426-431. doi: 10.1016/j.bbrc.2016.11.088. Epub 2017 Feb 3. Review.

Valente AJ, Maddalena LA, Robb EL, Moradi F, Stuart JA. A simple ImageJ macro tool for analyzing mitochondrial network morphology in mammalian cell culture. Acta Histochem. 2017 Apr;119(3):315-326. doi: 10.1016/j.acthis.2017.03.001. Epub 2017 Mar 15.

Valente EM, Abou-Sleiman PM, Caputo V, Muqit MM, Harvey K, Gispert S, Ali Z, Del Turco D, Bentivoglio AR, Healy DG, Albanese A, Nussbaum R, González-Maldonado R, Deller T, Salvi S, Cortelli P, Gilks WP, Latchman DS, Harvey RJ, Dallapiccola B, Auburger G, Wood NW. Hereditary early-onset Parkinson's disease caused by mutations in PINK1. Science. 2004 May 21;304(5674):1158-60. Epub 2004 Apr 15.

Van der Bliek AM, Shen Q, Kawajiri S. Mechanisms of mitochondrial fission and fusion. Cold Spring Harb Perspect Biol. 2013 Jun 1;5(6). pii: a011072. doi: 10.1101/cshperspect.a011072. Review.

Van Humbeeck C, Cornelissen T, Hofkens H, Mandemakers W, Gevaert K, De Strooper B, Vandenberghe W. Parkin interacts with Ambra1 to induce mitophagy. J Neurosci. 2011 Jul 13;31(28):10249-61. doi: 10.1523/JNEUROSCI.1917-11.2011.

Vande Walle L, Lamkanfi M, Vandenabeele P. The mitochondrial serine protease HtrA2/Omi: an overview. Cell Death Differ. 2008 Mar;15(3):453-60. doi: 10.1038/sj.cdd.4402291. Epub 2008 Jan 4. Review.

Vangipuram M, Ting D, Kim S, Diaz R, Schüle B. Skin punch biopsy explant culture for derivation of primary human fibroblasts. J Vis Exp. 2013 Jul 7;(77):e3779. doi: 10.3791/3779.

Villoslada P, Steinman L, Baranzini SE. Systems biology and its application to the understanding of neurological diseases. Ann Neurol. 2009 Feb;65(2):124-39. doi: 10.1002/ana.21634. Review.

Virbasius JV, Scarpulla RC. Activation of the human mitochondrial transcription factor A gene by nuclear respiratory factors: a potential regulatory link between nuclear and mitochondrial gene expression in organelle biogenesis. Proc Natl Acad Sci U S A. 1994 Feb 15;91(4):1309-13.

Walther TC, Mann M. Mass spectrometry-based proteomics in cell biology. J Cell Biol. 2010 Aug 23;190(4):491-500. doi: 10.1083/jcb.201004052. Review.

Wilhelmus MM, Nijland PG, Drukarch B, de Vries HE, van Horssen J. Involvement and interplay of Parkin, PINK1, and DJ1 in neurodegenerative and neuroinflammatory disorders. Free Radic Biol Med. 2012 Aug 15;53(4):983-92. doi: 10.1016/j.freeradbiomed.2012.05.040. Epub 2012 Jun 9. Review.

Wilkins MR, Sanchez JC, Gooley AA, Appel RD, Humphery-Smith I, Hochstrasser DF, Williams KL. Progress with proteome projects: why all proteins expressed by a genome should be identified and how to do it. Biotechnol Genet Eng Rev. 1996;13:19-50. Review.

Wilson GR, Sim JC, McLean C, Giannandrea M, Galea CA, Riseley JR, Stephenson SE, Fitzpatrick E, Haas SA, Pope K, Hogan KJ, Gregg RG, Bromhead CJ, Wargowski DS, Lawrence CH, James PA, Churchyard A, Gao Y, Phelan DG, Gillies G, Salce N, Stanford L, Marsh AP, Mignogna ML, Hayflick SJ, Leventer RJ, Delatycki MB, Mellick GD, Kalscheuer VM, D'Adamo P, Bahlo M, Amor DJ, Lockhart PJ. Mutations in RAB39B cause X-linked intellectual disability and early-onset Parkinson disease with α-synuclein pathology. Am J Hum Genet. 2014 Dec 4;95(6):729-35. doi: 10.1016/j.ajhg.2014.10.015. Epub 2014 Nov 26.

Winter DJ. rentrez: An R package for the NCBI eUtils API. 2017. doi:10.32614/RJ-2017-058.

Xilouri M, Brekk OR, Stefanis L. Autophagy and Alpha-Synuclein: Relevance to Parkinson's Disease and Related Synucleopathies. Mov Disord. 2016 Feb;31(2):178-92. doi: 10.1002/mds.26477. Epub 2016 Jan 27. Review.

Yamano K, Fogel AI, Wang C, van der Bliek AM, Youle RJ. Mitochondrial Rab GAPs govern autophagosome biogenesis during mitophagy. Elife. 2014 Feb 25;3:e01612. doi: 10.7554/eLife.01612.

Youle RJ, Narendra DP. Mechanisms of mitophagy. Nat Rev Mol Cell Biol. 2011 Jan;12(1):9-14. doi: 10.1038/nrm3028. Review.

Yu G, He QY. ReactomePA: an R/Bioconductor package for reactome pathway analysis and visualization. Mol Biosyst. 2016 Feb;12(2):477-9. doi: 10.1039/c5mb00663e.

Yu W, Sun Y, Guo S, Lu B. The PINK1/Parkin pathway regulates mitochondrial dynamics and function in mammalian hippocampal and dopaminergic neurons. Hum Mol Genet. 2011 Aug 15;20(16):3227-40. doi: 10.1093/hmg/ddr235. Epub 2011 May 25.

Yumino K, Kawakami I, Tamura M, Hayashi T, Nakamura M. Paraquat- and diquat-induced oxygen radical generation and lipid peroxidation in rat brain microsomes. J Biochem. 2002 Apr;131(4):565-70.

Zanellati MC, Monti V, Barzaghi C, Reale C, Nardocci N, Albanese A, Valente EM, Ghezzi D, Garavaglia B. Mitochondrial dysfunction in Parkinson disease: evidence in mutant PARK2 fibroblasts. Front Genet. 2015 Mar 11;6:78. doi: 10.3389/fgene.2015.00078. eCollection 2015.

Zeviani M, Di Donato S. Mitochondrial disorders. Brain. 2004 Oct;127(Pt 10):2153-72. Epub 2004 Sep 9. Review. Erratum in: Brain. 2004 Dec;127(Pt 12):2783.

Zhang A, Sun H, Wu G, Sun W, Yuan Y, Wang X. Proteomics analysis of hepatoprotective effects for scoparone using MALDI-TOF/TOF mass spectrometry with bioinformatics. OMICS. 2013 Apr;17(4):224-9. doi: 10.1089/omi.2012.0064. Epub 2013 Mar 20.

Zhang J, Xin L, Shan B, Chen W, Xie M, Yuen D, Zhang W, Zhang Z, Lajoie GA, Ma B. PEAKS DB: de novo sequencing assisted database search for sensitive and accurate peptide identification. Mol Cell Proteomics. 2012 Apr;11(4):M111.010587. doi: 10.1074/mcp.M111.010587. Epub 2011 Dec 20.

Zhang Y, Chan DC. New insights into mitochondrial fusion. FEBS Lett. 2007 May 22;581(11):2168-73. Epub 2007 Feb 20.

Zhou ZD, Lim TM. Dopamine (DA) induced irreversible proteasome inhibition via DA derived quinones. Free Radic Res. 2009 Apr;43(4):417-30. doi: 10.1080/10715760902801533. Epub 2009 Mar 17.

Zilocchi M, Finzi G, Lualdi M, Sessa F, Fasano M, Alberio T. Mitochondrial alterations in Parkinson's disease human samples and cellular models. Neurochem Int. 2018 Sep;118:61-72. doi: 10.1016/j.neuint.2018.04.013. Epub 2018 Apr 26.

7. Appendix

Appendix A

Analysis of mitochondrial network morphology.

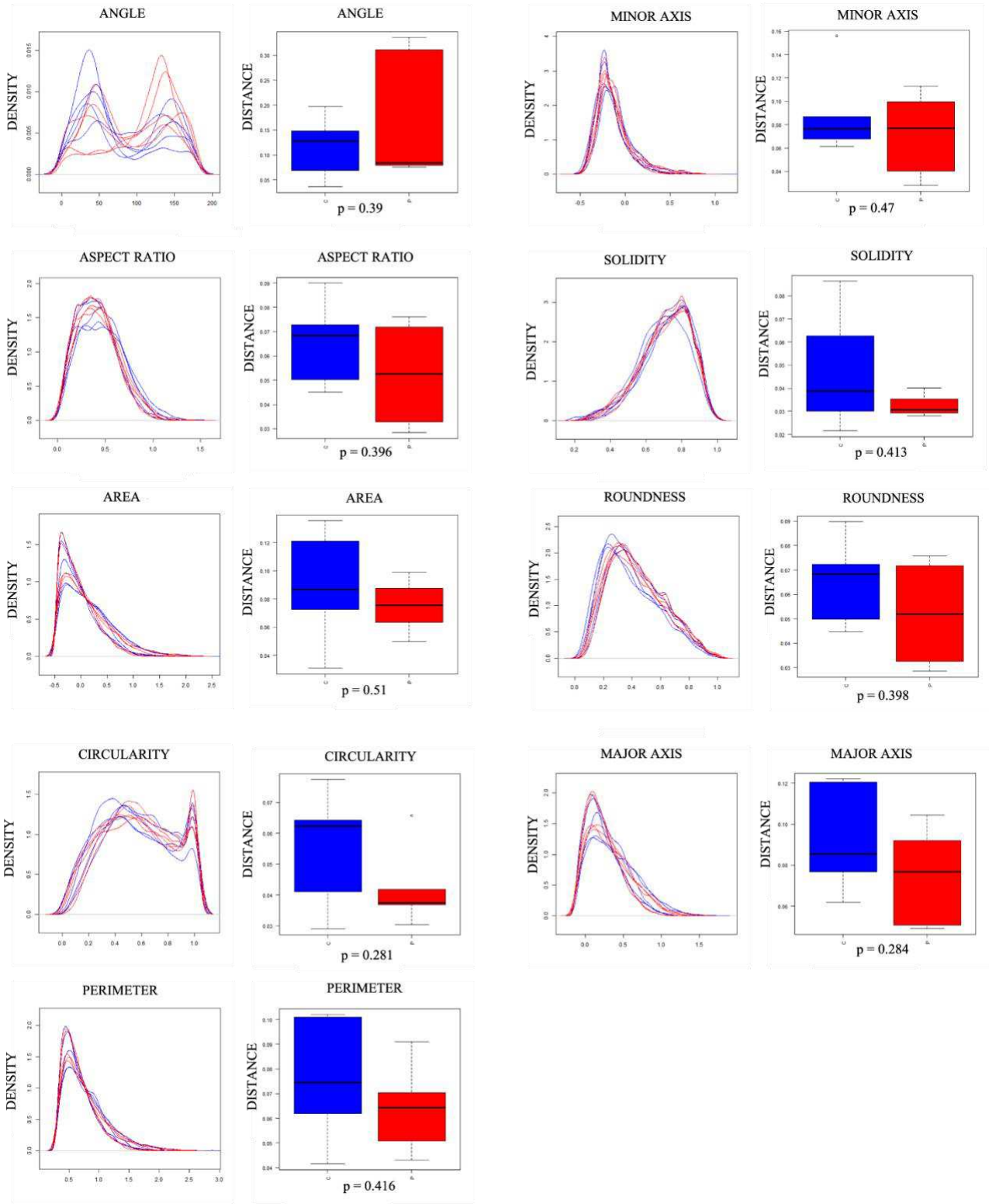

Appendix A. Morphological network parameters. Distribution density for all particles analyzed using the "Analyze Particles" tool in seven field of view from each subject and Kolmogorov-Smirnov distances of all parameters. C = control subjects; P = PARK2 patients.

Appendix B

Summary of proteins in the mitochondrial fractions significantly altered in PARK2 patients.

ID	Description	log 2 Ratio (P/C)	log 2 Variance (P/C)
B0I1T2	MYO1G Unconventional myosin-Ig Iso 1	Parkinson	Parkinson
O00410	IPO5 Importin-5 Iso 1	Parkinson	Parkinson
O14672	ADAM10 Disintegrin and metalloproteinase domain-containing protein 10 Iso 1	Parkinson	Parkinson
O15269	SPTLC1 Serine palmitoyltransferase 1 Iso 2	Parkinson	Parkinson
O15400	STX7 Syntaxin-7 Iso 1	Parkinson	Parkinson
O43837	IDH3B Isocitrate dehydrogenase [NAD] subunit beta_ mitochondrial B	Parkinson	Parkinson
O94832	MYO1D Unconventional myosin-Id Iso 1	Parkinson	Parkinson
O95229	ZWINT ZW10 interactor Iso 1	Parkinson	Parkinson
P04062	GBA Glucosylceramidase Iso 3	Parkinson	Parkinson
P09874	PARP1 Poly [ADP-ribose] polymerase 1 Iso 1	Parkinson	Parkinson
P0DMV8	HSPA1A Heat shock 70 kDa protein 1A Iso 1	Parkinson	Parkinson
P10314	HLA-A HLA class I histocompatibility antigen_ A-32 alpha chain Iso 1	Parkinson	Parkinson
P10620	MGST1 Microsomal glutathione S-transferase 1 Iso 1	Parkinson	Parkinson
P11279	LAMP1 Lysosome-associated membrane glycoprotein 1 Iso 2	Parkinson	Parkinson
P15153	RAC2 Ras-related C3 botulinum toxin substrate 2 Iso 1	Parkinson	Parkinson
P17081	RHOQ Rho-related GTP-binding protein RhoQ Iso 1	Parkinson	Parkinson
P18462	HLA-A HLA class I histocompatibility antigen_ A-25 alpha chain Iso 1	Parkinson	Parkinson
P20339	RAB5A Ras-related protein Rab-5A Iso 1	Parkinson	Parkinson
P27105	STOM Erythrocyte band 7 integral membrane protein Iso 1	Parkinson	Parkinson
P35613	BSG Basigin Iso 1	Parkinson	Parkinson
P48741	HSPA7 Putative heat shock 70 kDa protein 7 Iso 1	Parkinson	Parkinson
P51148	RAB5C Ras-related protein Rab-5C Iso 1	Parkinson	Parkinson
P60763	RAC3 Ras-related C3 botulinum toxin substrate 3 Iso 1	Parkinson	Parkinson
P60953	CDC42 Cell division control protein 42 homolog Iso 1	Parkinson	Parkinson
P61020	RAB5B Ras-related protein Rab-5B Iso 1	Parkinson	Parkinson
P62491	RAB11A Ras-related protein Rab-11A Iso 1	Parkinson	Parkinson
P62873	GNB1 Guanine nucleotide-binding protein G(I)/G(S)/G(T) subunit beta-1 Iso 1	Parkinson	Parkinson
P63000	RAC1 Ras-related C3 botulinum toxin substrate 1 A	Parkinson	Parkinson
Q13308	PTK7 Inactive tyrosine-protein kinase 7 Iso 1	Parkinson	Parkinson
Q13488	TCIRG1 V-type proton ATPase 116 kDa subunit a isoform 3 Long	Parkinson	Parkinson
Q15907	RAB11B Ras-related protein Rab-11B Iso 1	Parkinson	Parkinson
Q16270	IGFBP7 Insulin-like growth factor-binding protein 7 Iso 1	Parkinson	Parkinson
Q502W6	VWA3B von Willebrand factor A domain-containing protein 3B Iso 2	Parkinson	Parkinson
Q5T9A4	ATAD3B ATPase family AAA domain-containing protein 3B Iso 1	Parkinson	Parkinson
Q8TBY8	PMFBP1 Polyamine-modulated factor 1-binding protein 1 Iso 1	Parkinson	Parkinson
Q8WYA1	ARNTL2 Aryl hydrocarbon receptor nuclear translocator-like protein 2 Iso 1	Parkinson	Parkinson
Q96KQ7	EHMT2 Histone-lysine N-methyltransferase EHMT2 Iso 1	Parkinson	Parkinson
Q96PC5	MIA2 Melanoma inhibitory activity protein 2 Iso 1	Parkinson	Parkinson
Q99805	TM9SF2 Transmembrane 9 superfamily member 2 Iso 1	Parkinson	Parkinson
Q9H2F9	CCDC68 Coiled-coil domain-containing protein 68 Iso 1	Parkinson	Parkinson
Q9H4E5	RHOJ Rho-related GTP-binding protein RhoJ Iso 1	Parkinson	Parkinson
Q9NQC3	RTN4 Reticulon-4 Iso 3	Parkinson	Parkinson
Q9NX05	FAM120C Constitutive coactivator of PPAR-gamma-like protein 2 Iso 1	Parkinson	Parkinson
Q9P2D0	IBTK Inhibitor of Bruton tyrosine kinase Iso 1	Parkinson	Parkinson
Q9UBS4	DNAJB11 DnaJ homolog subfamily B member 11 Iso 1	Parkinson	Parkinson
Q9UBZ9	REV1 DNA repair protein REV1 Iso 1	Parkinson	Parkinson
Q9UDY6	TRIM10 Tripartite motif-containing protein 10 Alpha	Parkinson	Parkinson
Q9UFN0	NIPSNAP3A Protein NipSnap homolog 3A Iso 1	Parkinson	Parkinson
Q9Y2Q5	LAMTOR2 Ragulator complex protein LAMTOR2 Iso 1	Parkinson	Parkinson
Q9Y6A9	SPCS1 Signal peptidase complex subunit 1 Iso 1	Parkinson	Parkinson
Q93077	HIST1H2AC Histone H2A type 1-C Iso 1	-2.52	0.576
Q99715	COL12A1 Collagen alpha-1(XII) chain Iso 2	-2.3472	0.0576
Q9H9S3	SEC61A2 Protein transport protein Sec61 subunit alpha isoform 2 Iso 1	-1.8432	0.4608
P60709	ACTB Actin_ cytoplasmic 1 Iso 1	-1.5696	0.0432
P02545	LMNA Prelamin-A/C Iso 6	-1.5408	0.1224
P62805	HIST1H4A;HIST1H4B;HIST1H4C;HIST1H4D;HIST1H4E;HIST1H4F;HIST1H4H;HIST1H4I;HIST1H4J;HIST1H4K;HIST1H4L;HIST2H4A;HIST2H4B;HIST4H4 Histone H4 Iso 1	-1.4832	0.072
P61254	RPL26 60S ribosomal protein L26 Iso 1	-1.152	0.1296
P02452	COL1A1 Collagen alpha-1(I) chain Iso 1	-1.1376	0.0576
P32322	PYCR1 Pyrroline-5-carboxylate reductase 1_ mitochondrial Iso 3	-1.0224	0.0864
Q9Y2B0	CNPY2 Protein canopy homolog 2 Iso 2	-1.008	0.1296
P09486	SPARC SPARC Iso 1	-0.9936	0.1728
P30044	PRDX5 Peroxiredoxin-5_ mitochondrial Mitochondrial	-0.9648	0.1008
P16989	YBX3 Y-box-binding protein 3 Iso 3	-0.9504	0.0864
O60506	SYNCRIP Heterogeneous nuclear ribonucleoprotein Q Iso 1	-0.9504	0.0864
P35232	PHB Prohibitin Iso 1	-0.8568	0.1008
P08123	COL1A2 Collagen alpha-2(I) chain Iso 1	-0.8496	0.0576
P13804	ETFA Electron transfer flavoprotein subunit alpha_ mitochondrial Iso 2	-0.8496	0.144
P35580	MYH10 Myosin-10 Iso 2	-0.8352	0.072

P24844	MYL9 Myosin regulatory light polypeptide 9 Iso 2	-0.792	0.1296
P35749	MYH11 Myosin-11 Iso 1	-0.792	0.072
P30536	TSPO Translocator protein Iso 1	-0.792	0.288
P02751	FN1 Fibronectin Iso 4	-0.7488	0.0432
P35579	MYH9 Myosin-9 Iso 1	-0.72	0.036
P04181	OAT Ornithine aminotransferase_ mitochondrial Iso 2	-0.7128	0.144
P43307	SSR1 Translocon-associated protein subunit alpha Iso 1	-0.7056	0.1008
Q7Z406	MYH14 Myosin-14 Iso 5	-0.6912	0.072
P20908	COL5A1 Collagen alpha-1(V) chain Iso 1	-0.6912	0.3024
Q3SY69	ALDH1L2 Mitochondrial 10-formyltetrahydrofolate dehydrogenase Iso 3	-0.6768	0.144
P49748	ACADVL Very long-chain specific acyl-CoA dehydrogenase_ mitochondrial Iso 3	-0.6624	0.1152
Q9NYL4	FKBP11 Peptidyl-prolyl cis-trans isomerase FKBP11 Iso 2	-0.6624	0.0936
P61158	ACTR3 Actin-related protein 3 Iso 1	-0.648	0.1584
P61803	DAD1 Dolichyl-diphosphooligosaccharide--protein glycosyltransferase subunit DAD1 Iso 1	-0.6048	0.504
P32969	RPL9;RPL9P7;RPL9P8;RPL9P9 60S ribosomal protein L9 Iso 1	-0.5904	0.0432
P62424	RPL7A 60S ribosomal protein L7a Iso 1	-0.5904	0.144
P13073	COX4I1 Cytochrome c oxidase subunit 4 isoform 1_ mitochondrial Iso 1	-0.5904	0.0864
O15145	ARPC3 Actin-related protein 2/3 complex subunit 3 Iso 1	-0.5472	0.2592
P62829	RPL23 60S ribosomal protein L23 Iso 1	-0.5472	0.1296
P19338	NCL Nucleolin Iso 1	-0.5472	0.36
P84243	H3F3A;H3F3B Histone H3.3 Iso 1	-0.5472	0.1728
P63244	RACK1 Receptor of activated protein C kinase 1 Iso 1	-0.5184	0.0576
P18621	RPL17 60S ribosomal protein L17 Iso 3	-0.5184	0.0576
Q13283	G3BP1 Ras GTPase-activating protein-binding protein 1 Iso 1	-0.5184	0.3168
P07919	UQCRH Cytochrome b-c1 complex subunit 6_ mitochondrial Iso 1	-0.504	0.1152
P68431	HIST1H3A;HIST1H3B;HIST1H3C;HIST1H3D;HIST1H3E;HIST1H3F;HIST1H3G;HIST1H3H;HIST1H3I;HIST1H3J Histone H3.1 Iso 1	-0.504	0.1872
P08708	RPS17 40S ribosomal protein S17 Iso 1	-0.4896	0.1152
P63267	ACTG2 Actin_ gamma-enteric smooth muscle Iso 2	-0.4896	0.0432
P68133	ACTA1 Actin_ alpha skeletal muscle Iso 1	-0.4752	0.0432
Q9HAV7	GRPEL1 GrpE protein homolog 1_ mitochondrial Iso 1	-0.4752	0.1152
P62736	ACTA2 Actin_ aortic smooth muscle Iso 1	-0.4752	0.0288
P19105	MYL12A Myosin regulatory light chain 12A Iso 1	-0.4752	0.072
Q05682	CALD1 Caldesmon Iso 1	-0.4752	0.0432
P51571	SSR4 Translocon-associated protein subunit delta Iso 1	-0.4752	0.1008
Q9UNX3	RPL26L1 60S ribosomal protein L26-like 1 Iso 1	-0.4752	0.144
Q8NC51	SERBP1 Plasminogen activator inhibitor 1 RNA-binding protein Iso 3	-0.468	0.0936
P20020	ATP2B1 Plasma membrane calcium-transporting ATPase 1 K	-0.4608	0.1296
O14950	MYL12B Myosin regulatory light chain 12B Iso 1	-0.4608	0.072
P67809	YBX1 Nuclease-sensitive element-binding protein 1 Iso 1	-0.4464	0.072
P18124	RPL7 60S ribosomal protein L7 Iso 1	-0.432	0.0576
P61019	RAB2A Ras-related protein Rab-2A Iso 2	-0.432	0.1296
P10809	HSPD1 60 kDa heat shock protein_ mitochondrial Iso 2	-0.432	0.1152
P62277	RPS13 40S ribosomal protein S13 Iso 1	-0.432	0.144
P12111	COL6A3 Collagen alpha-3(VI) chain Iso 5	-0.2448	0.0864
Q15084	PDIA6 Protein disulfide-isomerase A6 Iso 4	-0.072	0.1224
P40926	MDH2 Malate dehydrogenase_ mitochondrial Iso 1	0.432	0.0288
Q8NHW5	RPLP0P6 60S acidic ribosomal protein P0-like Iso 1	0.432	0.0576
P18085	ARF4 ADP-ribosylation factor 4 Iso 1	0.432	0.3456
P61619	SEC61A1 Protein transport protein Sec61 subunit alpha isoform 1 Iso 1	0.432	0.072
P62899	RPL31 60S ribosomal protein L31 Iso 3	0.432	0.144
P25705	ATP5A1 ATP synthase subunit alpha_ mitochondrial Iso 2	0.4464	0.0288
P30040	ERP29 Endoplasmic reticulum resident protein 29 Iso 1	0.4608	0.5472
P68032	ACTC1 Actin_ alpha cardiac muscle 1 Iso 1	0.4608	0.0432
Q9Y224	C14orf166 UPF0568 protein C14orf166 Iso 1	0.4608	0.2736
P20393	NR1D1 Nuclear receptor subfamily 1 group D member 1 Iso 1	0.4752	0.1872
Q9Y2Q3	GSTK1 Glutathione S-transferase kappa 1 Iso 1	0.4752	0.1872
P46777	RPL5 60S ribosomal protein L5 Iso 1	0.4752	0.1152
Q96I99	SUCLG2 Succinate--CoA ligase [GDP-forming] subunit beta_ mitochondrial Iso 2	0.504	0.2016
P13674	P4HA1 Prolyl 4-hydroxylase subunit alpha-1 Iso 1	0.5328	0.0576
P09601	HMOX1 Heme oxygenase 1 Iso 1	0.5472	0.0864
P51149	RAB7A Ras-related protein Rab-7a Iso 1	0.5472	0.1584
P26373	RPL13 60S ribosomal protein L13 Iso 1	0.5472	0.1584
Q9UHD8	SEPT9 Septin-9 Iso 9	0.5688	0.1584
Q58FF3	HSP90B2P Putative endoplasmin-like protein Iso 1	0.576	0.072
Q9NVA2	SEPT11 Septin-11 Iso 1	0.6264	0.0648
P11021	HSPA5 78 kDa glucose-regulated protein Iso 1	0.6336	0.0288
Q07021	C1QBP Complement component 1 Q subcomponent-binding protein_ mitochondrial Iso 1	0.648	0.1152
P48735	IDH2 Isocitrate dehydrogenase [NADP]_ mitochondrial Iso 1	0.6624	0.072
P36957	DLST Dihydrolipoyllysine-residue succinyltransferase component of 2-oxoglutarate dehydrogenase complex_ mitochondrial Iso 1	0.6624	0.1008
P48047	ATP5O ATP synthase subunit O_ mitochondrial Iso 1	0.6768	0.2016
Q9UHA4	LAMTOR3 Ragulator complex protein LAMTOR3 Iso 1	0.72	0.3024
O95202	LETM1 Mitochondrial proton/calcium exchanger protein Iso 1	0.7488	0.1728
P40939	HADHA Trifunctional enzyme subunit alpha_ mitochondrial Iso 1	0.7632	0.0576
P12109	COL6A1 Collagen alpha-1(VI) chain Iso 1	0.7632	0.072

P13987	CD59 CD59 glycoprotein Iso 1	0.7776	0.0864
P14625	HSP90B1 Endoplasmin Iso 1	0.792	0.0432
Q6NUK1	SLC25A24 Calcium-binding mitochondrial carrier protein SCaMC-1 Iso 2	0.8064	0.2016
Q9NZM1	MYOF Myoferlin Iso 3	0.8208	0.0864
P61421	ATP6V0D1 V-type proton ATPase subunit d 1 Iso 1	0.8352	0.3744
Q9NQC3	RTN4 Reticulon-4 Iso 1	0.8352	0.1584
P56537	EIF6 Eukaryotic translation initiation factor 6 Iso 2	0.8496	0.3672
O43852	CALU Calumenin Iso 4	0.8784	0.0648
P27797	CALR Calreticulin Iso 1	0.8784	0.0288
P61026	RAB10 Ras-related protein Rab-10 Iso 1	0.8784	0.1584
A6NMY6	ANXA2P2 Putative annexin A2-like protein Iso 1	0.9216	0.0576
Q14697	GANAB Neutral alpha-glucosidase AB Iso 1	0.936	0.1152
P00338	LDHA L-lactate dehydrogenase A chain Iso 3	0.936	0.0864
P07355	ANXA2 Annexin A2 Iso 2	0.9936	0.0504
P04406	GAPDH Glyceraldehyde-3-phosphate dehydrogenase Iso 1	1.008	0.072
O75390	CS Citrate synthase_ mitochondrial Iso 1	1.0512	0.0864
P15144	ANPEP Aminopeptidase N Iso 1	1.0512	0.072
P49821	NDUFV1 NADH dehydrogenase [ubiquinone] flavoprotein 1_ mitochondrial Iso 2	1.0656	0.1872
P07237	P4HB Protein disulfide-isomerase Iso 1	1.0944	0.0432
P30101	PDIA3 Protein disulfide-isomerase A3 Iso 1	1.1088	0.0288
Q96D15	RCN3 Reticulocalbin-3 Iso 1	1.1376	0.1152
Q9UBI6	GNG12 Guanine nucleotide-binding protein G(I)/G(S)/G(O) subunit gamma-12 Iso 1	1.1808	0.1152
Q15758	SLC1A5 Neutral amino acid transporter B(0) Iso 1	1.1952	0.1008
P55145	MANF Mesencephalic astrocyte-derived neurotrophic factor Iso 1	1.2528	0.1152
Q6NZI2	CAVIN1 Caveolae-associated protein 1 Iso 1	1.2672	0.072
Q15293	RCN1 Reticulocalbin-1 Iso 2	1.2672	0.072
P13667	PDIA4 Protein disulfide-isomerase A4 Iso 1	1.3104	0.1152
P00367	GLUD1 Glutamate dehydrogenase 1_ mitochondrial Iso 3	1.3392	0.1296
P05091	ALDH2 Aldehyde dehydrogenase_ mitochondrial Iso 1	1.3392	0.144
Q14257	RCN2 Reticulocalbin-2 Iso 2	1.3824	0.4176
P62906	RPL10A 60S ribosomal protein L10a Iso 1	1.4256	0.144
O00469	PLOD2 Procollagen-lysine_2-oxoglutarate 5-dioxygenase 2 Iso 1	1.5768	0.2664
P11142	HSPA8 Heat shock cognate 71 kDa protein Iso 1	1.8576	0.144
P54652	HSPA2 Heat shock-related 70 kDa protein 2 Iso 1	2.016	0.144
P34931	HSPA1L Heat shock 70 kDa protein 1-like Iso 1	2.2032	0.3168
Q6FI13	HIST2H2AA3;HIST2H2AA4 Histone H2A type 2-A Iso 1	2.2752	0.216
Q96KK5	HIST1H2AH Histone H2A type 1-H Iso 1	2.2896	0.2304
P04908	HIST1H2AB;HIST1H2AE Histone H2A type 1-B/E Iso 1	2.2896	0.2016
Q9BTM1	H2AFJ Histone H2A.J Iso 1	2.2896	0.216
Q99878	HIST1H2AJ Histone H2A type 1-J Iso 1	2.2896	0.216
Q16777	HIST2H2AC Histone H2A type 2-C Iso 1	2.2896	0.1872
A5D8W1	CFAP69 Cilia- and flagella-associated protein 69 Iso 1	Control	Control
O14948	TFEC Transcription factor EC Iso 1	Control	Control
O43290	SART1 U4/U6.U5 tri-snRNP-associated protein 1 Iso 1	Control	Control
O75030	MITF Microphthalmia-associated transcription factor H1	Control	Control
O75064	DENND4B DENN domain-containing protein 4B Iso 1	Control	Control
O75489	NDUFS3 NADH dehydrogenase [ubiquinone] iron-sulfur protein 3_ mitochondrial Iso 2	Control	Control
O95886	DLGAP3 Disks large-associated protein 3 Iso 1	Control	Control
P14618	PKM Pyruvate kinase PKM M2	Control	Control
P21980	TGM2 Protein-glutamine gamma-glutamyltransferase 2 Iso 2	Control	Control
P52815	MRPL12 39S ribosomal protein L12_ mitochondrial Iso 1	Control	Control
P54259	ATN1 Atrophin-1 Iso 1	Control	Control
P54886	ALDH18A1 Delta-1-pyrroline-5-carboxylate synthase Long	Control	Control
P62750	RPL23A 60S ribosomal protein L23a Iso 1	Control	Control
P63241	EIF5A Eukaryotic translation initiation factor 5A-1 Iso 1	Control	Control
Q08257	CRYZ Quinone oxidoreductase Iso 1	Control	Control
Q12852	MAP3K12 Mitogen-activated protein kinase kinase kinase 12 Iso 1	Control	Control
Q12931	TRAP1 Heat shock protein 75 kDa_ mitochondrial Iso 1	Control	Control
Q14151	SAFB2 Scaffold attachment factor B2 Iso 2	Control	Control
Q14554	PDIA5 Protein disulfide-isomerase A5 Iso 2	Control	Control
Q15063	POSTN Periostin Iso 1	Control	Control
Q15424	SAFB Scaffold attachment factor B1 Iso 1	Control	Control
Q16527	CSRP2 Cysteine and glycine-rich protein 2 Iso 1	Control	Control
Q4VXU2	PABPC1L Polyadenylate-binding protein 1-like Iso 1	Control	Control
Q5VVM6	CCDC30 Coiled-coil domain-containing protein 30 Iso 2	Control	Control
Q7Z5J8	ANKAR Ankyrin and armadillo repeat-containing protein Iso 1	Control	Control
Q86WZ6	ZNF227 Zinc finger protein 227 Iso 1	Control	Control
Q8IUG5	MYO18B Unconventional myosin-XVIIIb Iso 2	Control	Control
Q8N1I0	DOCK4 Dedicator of cytokinesis protein 4 Iso 2	Control	Control
Q8N608	DPP10 Inactive dipeptidyl peptidase 10 Iso 2	Control	Control
Q8NB25	FAM184A Protein FAM184A Iso 1	Control	Control
Q8TE49	OTUD7A OTU domain-containing protein 7A Iso 1	Control	Control
Q8TF62	ATP8B4 Probable phospholipid-transporting ATPase IM Iso 1	Control	Control
Q8WWL7	CCNB3 G2/mitotic-specific cyclin-B3 Iso 1	Control	Control
Q92823	NRCAM Neuronal cell adhesion molecule Iso 1	Control	Control
Q969Q0	RPL36AL 60S ribosomal protein L36a-like Iso 1	Control	Control
Q9BQS8	FYCO1 FYVE and coiled-coil domain-containing protein 1 Iso 1	Control	Control

Q9BTM1	H2AFJ Histone H2A.J Iso 2	Control	Control
Q9BYD6	MRPL1 39S ribosomal protein L1_ mitochondrial Iso 1	Control	Control
Q9H173	SIL1 Nucleotide exchange factor SIL1 Iso 1	Control	Control
Q9NSY0	NRBP2 Nuclear receptor-binding protein 2 Iso 1	Control	Control
Q9NWH9	SLTM SAFB-like transcription modulator Iso 1	Control	Control
Q9NXG0	CNTLN Centlein Iso 1	Control	Control
Q9NZB2	FAM120A Constitutive coactivator of PPAR-gamma-like protein 1 B	Control	Control
Q9P219	CCDC88C Protein Daple Iso 1	Control	Control

Appendix B. Summary of 227 significantly up- and down- regulated and unique proteins in the mitochondrial fractions used for the enrichment analysis. P = PARK2 patients; C = control subjects; Parkinson = unique in PD patients; control = unique in control subjects.

Appendix C

Summary of proteins in the whole cell fractions significantly altered in PARK2 patients.

ID	Description	log 2 Ratio (P/C)	log 2 Variance (P/C)
A6NC98	CCDC88B Coiled-coil domain-containing protein 88B Iso 3	Parkinson	Parkinson
A8MW92	PHF20L1 PHD finger protein 20-like protein 1 Iso 1	Parkinson	Parkinson
O14530	TXNDC9 Thioredoxin domain-containing protein 9 Iso 1	Parkinson	Parkinson
O15371	EIF3D Eukaryotic translation initiation factor 3 subunit D Iso 2	Parkinson	Parkinson
O75344	FKBP6 Inactive peptidyl-prolyl cis-trans isomerase FKBP6 Iso 1	Parkinson	Parkinson
P02689	PMP2 Myelin P2 protein Iso 1	Parkinson	Parkinson
P05120	SERPINB2 Plasminogen activator inhibitor 2 Iso 1	Parkinson	Parkinson
P05413	FABP3 Fatty acid-binding protein_ heart Iso 1	Parkinson	Parkinson
P52756	RBM5 RNA-binding protein 5 Iso 1	Parkinson	Parkinson
Q12797	ASPH Aspartyl/asparaginyl beta-hydroxylase Iso 2	Parkinson	Parkinson
Q13126	MTAP S-methyl-5'-thioadenosine phosphorylase Iso 5	Parkinson	Parkinson
Q14CX7	NAA25 N-alpha-acetyltransferase 25_ NatB auxiliary subunit Iso 1	Parkinson	Parkinson
Q15274	QPRT Nicotinate-nucleotide pyrophosphorylase [carboxylating] Iso 1	Parkinson	Parkinson
Q5JR59	MTUS2 Microtubule-associated tumor suppressor candidate 2 Iso 2	Parkinson	Parkinson
Q5JRC9	FAM47A Protein FAM47A Iso 1	Parkinson	Parkinson
Q5T5Y3	CAMSAP1 Calmodulin-regulated spectrin-associated protein 1 Iso 1	Parkinson	Parkinson
Q5T7B8	KIF24 Kinesin-like protein KIF24 Iso 1	Parkinson	Parkinson
Q60I27	ALS2CL ALS2 C-terminal-like protein Iso 1	Parkinson	Parkinson
Q6AZZ1	TRIM68 E3 ubiquitin-protein ligase TRIM68 Iso 1	Parkinson	Parkinson
Q86VX9	MON1A Vacuolar fusion protein MON1 homolog A Iso 1	Parkinson	Parkinson
Q9H1H9	KIF13A Kinesin-like protein KIF13A Iso 1	Parkinson	Parkinson
Q9H4L7	SMARCAD1 SWI/SNF-related matrix-associated actin-dependent regulator of chromatin subfamily A containing DEAD/H box 1 Iso 1	Parkinson	Parkinson
Q9NUB1	ACSS1 Acetyl-coenzyme A synthetase 2-like_ mitochondrial Iso 1	Parkinson	Parkinson
Q9P035	HACD3 Very-long-chain (3R)-3-hydroxyacyl-CoA dehydratase 3 Iso 1	Parkinson	Parkinson
Q9UJV8	PURG Purine-rich element-binding protein gamma Iso 1	Parkinson	Parkinson
Q9Y483	MTF2 Metal-response element-binding transcription factor 2 Iso 1	Parkinson	Parkinson
P15559	NQO1 NAD(P)H dehydrogenase [quinone] 1 Iso 2	-1.6416	0.1728
Q96HC4	PDLIM5 PDZ and LIM domain protein 5 Iso 1	-0.9576	0.4032
P80297	MT1X Metallothionein-1X Iso 1	-1.4976	0.1728
P13640	MT1G Metallothionein-1G Iso 1	-1.4472	0.1728
P04732	MT1E Metallothionein-1E Iso 1	-1.4544	0.1872
Q8N339	MT1M Metallothionein-1M Iso 1	-0.8496	0.1296
Q9Y696	CLIC4 Chloride intracellular channel protein 4 Iso 1	-0.8208	0.0576
P32119	PRDX2 Peroxiredoxin-2 Iso 1	-0.8208	0.0576
P02795	MT2A Metallothionein-2 Iso 1	-0.8208	0.2016
P61077	UBE2D3 Ubiquitin-conjugating enzyme E2 D3 Iso 2	-0.792	0.1296
Q8IYT4	KATNAL2 Katanin p60 ATPase-containing subunit A-like 2 Iso 2	-0.7344	0.1872
Q01995	TAGLN Transgelin Iso 1	-0.7344	0.1296
P00568	AK1 Adenylate kinase isoenzyme 1 Iso 1	-0.72	0.432
P69891	HBG1 Hemoglobin subunit gamma-1 Iso 1	-0.7056	0.4896
P35609	ACTN2 Alpha-actinin-2 Iso 2	-0.648	0.0576
P02100	HBE1 Hemoglobin subunit epsilon Iso 1	-0.6336	0.3744
P23284	PPIB Peptidyl-prolyl cis-trans isomerase B Iso 1	-0.6336	0.0576
P15259	PGAM2 Phosphoglycerate mutase 2 Iso 1	-0.5904	0.144
P37837	TALDO1 Transaldolase Iso 1	-0.576	0.1296
Q13557	CAMK2D Calcium/calmodulin-dependent protein kinase type II subunit delta Delta 6	-0.576	0.5616
P09211	GSTP1 Glutathione S-transferase P Iso 1	-0.5472	0.0576
P23528	CFL1 Cofilin-1 Iso 1	-0.5472	0.0576
P04792	HSPB1 Heat shock protein beta-1 Iso 1	-0.5328	0.0432
Q06830	PRDX1 Peroxiredoxin-1 Iso 1	-0.5328	0.0288
P16070	CD44 CD44 antigen Iso 9	-0.4608	0.072
Q8N0Y7	PGAM4 Probable phosphoglycerate mutase 4 Iso 1	-0.504	0.1584

P27824	CANX Calnexin Iso 2	-0.4968	0.072
Q9Y617	PSAT1 Phosphoserine aminotransferase Iso 1	-0.4968	0.1296
O14979	HNRNPDL Heterogeneous nuclear ribonucleoprotein D-like Iso 1	-0.4608	0.1296
Q8WUD1	RAB2B Ras-related protein Rab-2B Iso 1	-0.4608	0.1152
P50395	GDI2 Rab GDP dissociation inhibitor beta Iso 1	-0.4608	0.072
Q9NSB2	KRT84 Keratin_ type II cuticular Hb4 Iso 1	-0.432	0.0864
P25398	RPS12 40S ribosomal protein S12 Iso 1	-0.432	0.0576
P14618	PKM Pyruvate kinase PKM Iso 3	0.432	0.0144
Q16555	DPYSL2 Dihydropyrimidinase-related protein 2 Iso 1	0.4392	0.0504
Q13501	SQSTM1 Sequestosome-1 Iso 1	0.4464	0.2304
Q01518	CAP1 Adenylyl cyclase-associated protein 1 Iso 2	0.4824	0.0576
P53396	ACLY ATP-citrate synthase Iso 3	0.4464	0.072
P00338	LDHA L-lactate dehydrogenase A chain Iso 5	0.5688	0.036
P62280	RPS11 40S ribosomal protein S11 Iso 1	0.4608	0.0576
Q58FF8	HSP90AB2P Putative heat shock protein HSP 90-beta 2 Iso 1	0.4608	0.0432
P30613	PKLR Pyruvate kinase PKLR L-type	0.4752	0.144
P17987	TCP1 T-complex protein 1 subunit alpha Iso 1	0.4752	0.0576
P56537	EIF6 Eukaryotic translation initiation factor 6 Iso 2	0.4824	0.108
P29692	EEF1D Elongation factor 1-delta Iso 2	0.4752	0.2016
Q58FF7	HSP90AB3P Putative heat shock protein HSP 90-beta-3 Iso 1	0.4752	0.0864
Q13642	FHL1 Four and a half LIM domains protein 1 Iso 2	0.7056	0.216
Q9BYZ2	LDHAL6B L-lactate dehydrogenase A-like 6B Iso 1	0.4896	0.1152
P27348	YWHAQ 14-3-3 protein theta Iso 1	0.4896	0.0432
P27816	MAP4 Microtubule-associated protein 4 Iso 1	0.5328	0.0864
P68363	TUBA1B Tubulin alpha-1B chain Iso 2	0.5184	0.0216
P55795	HNRNPH2 Heterogeneous nuclear ribonucleoprotein H2 Iso 1	0.5328	0.0864
P31946	YWHAB 14-3-3 protein beta/alpha Long	0.5832	0.0504
P24844	MYL9 Myosin regulatory light polypeptide 9 Iso 1	0.5328	0.1728
Q15942	ZYX Zyxin Iso 2	0.54	0.0864
O43852	CALU Calumenin Iso 5	0.7056	0.0864
P04843	RPN1 Dolichyl-diphosphooligosaccharide--protein glycosyltransferase subunit 1 Iso 1	0.5328	0.0576
Q9NY65	TUBA8 Tubulin alpha-8 chain Iso 2	0.5544	0.0288
P61978	HNRNPK Heterogeneous nuclear ribonucleoprotein K Iso 3	0.5904	0.0432
P68366	TUBA4A Tubulin alpha-4A chain Iso 2	0.5472	0.0288
P05388	RPLP0 60S acidic ribosomal protein P0 Iso 1	0.5616	0.072
P05386	RPLP1 60S acidic ribosomal protein P1 Iso 1	0.5616	0.0576
P15144	ANPEP Aminopeptidase N Iso 1	0.5616	0.0432
P62820	RAB1A Ras-related protein Rab-1A Iso 3	0.5904	0.0576
P62136	PPP1CA Serine/threonine-protein phosphatase PP1-alpha catalytic subunit Iso 3	0.6336	0.072
P07858	CTSB Cathepsin B Iso 1	0.6048	0.1296
P08865	RPSA 40S ribosomal protein SA Iso 1	0.6048	0.072
P06454	PTMA Prothymosin alpha Iso 2	0.6264	0.108
P30153	PPP2R1A Serine/threonine-protein phosphatase 2A 65 kDa regulatory subunit A alpha isoform Iso 1	0.6192	0.0864
P62140	PPP1CB Serine/threonine-protein phosphatase PP1-beta catalytic subunit Iso 1	0.6192	0.0864
Q14019	COTL1 Coactosin-like protein Iso 1	0.6336	0.0864
P50991	CCT4 T-complex protein 1 subunit delta Iso 2	0.6336	0.072
P52907	CAPZA1 F-actin-capping protein subunit alpha-1 Iso 1	0.6336	0.0576
P36873	PPP1CC Serine/threonine-protein phosphatase PP1-gamma catalytic subunit Gamma-1	0.6552	0.0792
Q96AG4	LRRC59 Leucine-rich repeat-containing protein 59 Iso 1	0.648	0.1008
O60664	PLIN3 Perilipin-3 Iso 2	0.6624	0.0576
P68371	TUBB4B Tubulin beta-4B chain Iso 1	0.6624	0.0288
P63104	YWHAZ 14-3-3 protein zeta/delta Iso 1	0.6912	0.036
P13987	CD59 CD59 glycoprotein Iso 1	0.6912	0.072
P18124	RPL7 60S ribosomal protein L7 Iso 1	0.72	0.0864
P30041	PRDX6 Peroxiredoxin-6 Iso 1	0.7344	0.1008
P17931	LGALS3 Galectin-3 Iso 1	0.7488	0.0864
P46782	RPS5 40S ribosomal protein S5 Iso 1	0.7632	0.0432
P20336	RAB3A Ras-related protein Rab-3A Iso 1	0.7632	0.072
Q12931	TRAP1 Heat shock protein 75 kDa_ mitochondrial Iso 1	0.7776	0.0432
Q96E17	RAB3C Ras-related protein Rab-3C Iso 1	0.7776	0.072
P04083	ANXA1 Annexin A1 Iso 1	0.7776	0.0288
P06576	ATP5B ATP synthase subunit beta_ mitochondrial Iso 1	0.7776	0.0576
P61106	RAB14 Ras-related protein Rab-14 Iso 1	0.792	0.0576
P08133	ANXA6 Annexin A6 Iso 1	0.8208	0.036
P63241	EIF5A Eukaryotic translation initiation factor 5A-1 Iso 2	0.8208	0.1368
P78371	CCT2 T-complex protein 1 subunit beta Iso 1	0.8424	0.0504
P09651	HNRNPA1 Heterogeneous nuclear ribonucleoprotein A1 A1-B	0.8496	0.1008
P62913	RPL11 60S ribosomal protein L11 Iso 2	0.8712	0.0432
P62937	PPIA Peptidyl-prolyl cis-trans isomerase A Iso 1	0.9288	0.0504
P02765	AHSG Alpha-2-HS-glycoprotein Iso 1	0.8784	0.1008
Q6IS14	EIF5AL1 Eukaryotic translation initiation factor 5A-1-like Iso 1	0.8928	0.1296
P29966	MARCKS Myristoylated alanine-rich C-kinase substrate Iso 1	0.8928	0.1008
P61158	ACTR3 Actin-related protein 3 Iso 1	0.8928	0.0864
P22314	UBA1 Ubiquitin-like modifier-activating enzyme 1 Iso 2	0.9072	0.072
P30050	RPL12 60S ribosomal protein L12 Iso 2	0.936	0.0864

P0DN26	PPIAL4F Peptidyl-prolyl cis-trans isomerase A-like 4F Iso 1	0.9504	0.072
F5H284	PPIAL4D Peptidyl-prolyl cis-trans isomerase A-like 4D Iso 1	0.9504	0.072
P0DN37	PPIAL4G Peptidyl-prolyl cis-trans isomerase A-like 4G Iso 1	0.9504	0.072
A0A0B4J2A2	PPIAL4C Peptidyl-prolyl cis-trans isomerase A-like 4C Iso 1	0.9504	0.0864
P60953	CDC42 Cell division control protein 42 homolog Iso 2	1.0224	0.0576
Q6NZI2	CAVIN1 Caveolae-associated protein 1 Iso 2	1.0368	0.0648
Q16851	UGP2 UTP--glucose-1-phosphate uridylyltransferase Iso 1	1.0512	0.0576
P32969	RPL9;RPL9P7;RPL9P8;RPL9P9 60S ribosomal protein L9 Iso 1	1.08	0.072
E9PAV3	NACA Nascent polypeptide-associated complex subunit alpha_ muscle-specific form Iso 2	1.1088	0.0864
Q13765	NACA Nascent polypeptide-associated complex subunit alpha Iso 1	1.1232	0.1152
Q58FG1	HSP90AA4P Putative heat shock protein HSP 90-alpha A4 Iso 1	1.2096	0.1296
Q16181	SEPT7 Septin-7 Iso 2	1.296	0.0864
Q69YH5	CDCA2 Cell division cycle-associated protein 2 Iso 1	1.512	1.1952
Q9NZU5	LMCD1 LIM and cysteine-rich domains protein 1 Iso 2	1.512	0.3024
Q58FG0	HSP90AA5P Putative heat shock protein HSP 90-alpha A5 Iso 1	1.8576	0.1008
O14772	FPGT Fucose-1-phosphate guanylyltransferase Iso 5	Control	Control
O60641	SNAP91 Clathrin coat assembly protein AP180 Iso 1	Control	Control
P15121	AKR1B1 Aldose reductase Iso 1	Control	Control
P19367	HK1 Hexokinase-1 Iso 1	Control	Control
P28072	PSMB6 Proteasome subunit beta type-6 Iso 1	Control	Control
P29279	CTGF Connective tissue growth factor Iso 1	Control	Control
P63098	PPP3R1 Calcineurin subunit B type 1 Iso 1	Control	Control
Q03113	GNA12 Guanine nucleotide-binding protein subunit alpha-12 Iso 2	Control	Control
Q04637	EIF4G1 Eukaryotic translation initiation factor 4 gamma 1 A	Control	Control
Q6P1J6	PLB1 Phospholipase B1_ membrane-associated Iso 1	Control	Control
Q6QNK2	ADGRD1 Adhesion G-protein coupled receptor D1 Iso 2	Control	Control
Q8TF72	SHROOM3 Protein Shroom3 Iso 2	Control	Control
Q92538	GBF1 Golgi-specific brefeldin A-resistance guanine nucleotide exchange factor 1 Iso 1	Control	Control
Q96K21	ZFYVE19 Abscission/NoCut checkpoint regulator Iso 2	Control	Control
Q9C0H9	SRCIN1 SRC kinase signaling inhibitor 1 Iso 1	Control	Control
Q9H582	ZNF644 Zinc finger protein 644 Iso 3	Control	Control
Q9NS61	KCNIP2 Kv channel-interacting protein 2 Iso 1	Control	Control
Q9NZC7	WWOX WW domain-containing oxidoreductase Iso 1	Control	Control
Q9NZU7	CABP1 Calcium-binding protein 1 L-CaBP1	Control	Control
Q9UBE0	SAE1 SUMO-activating enzyme subunit 1 Iso 2	Control	Control
Q9UBX0	HESX1 Homeobox expressed in ES cells 1 Iso 1	Control	Control
Q9UKY4	POMT2 Protein O-mannosyl-transferase 2 Iso 1	Control	Control
Q9UMX2	OAZ3 Ornithine decarboxylase antizyme 3 Iso 1	Control	Control
Q9Y224	C14orf166 UPF0568 protein C14orf166 Iso 1	Control	Control
Q9Y262	EIF3L Eukaryotic translation initiation factor 3 subunit L Iso 1	Control	Control
Q9Y265	RUVBL1 RuvB-like 1 Iso 2	Control	Control

Appendix C. Summary of 168 significantly up- and down- regulated proteins in the total fractions by shotgun proteomics used for the enrichment analysis. P = PARK2 patients; C = control subjects; parkinson = unique in PD patients; control = unique in control subjects.

Appendix D

Summary of all identified pathways in the mitochondrial fractions using GSEA approach.

ID	Description	setSize	ES	NES	p.adjust
R-HSA-5663202	Diseases of signal transduction	17	-0.679	-1.932	0.206
R-HSA-2682334	EPH-Ephrin signaling	19	-0.644	-1.880	0.206
R-HSA-3000178	ECM proteoglycans	11	-0.741	-1.873	0.206
R-HSA-73894	DNA Repair	12	-0.691	-1.788	0.206
R-HSA-6798695	Neutrophil degranulation	40	0.521	1.600	0.206
R-HSA-422475	Axon guidance	103	-0.328	-1.400	0.206
R-HSA-8953897	Cellular responses to external stimuli	45	0.497	1.561	0.206
R-HSA-1474228	Degradation of the extracellular matrix	11	-0.682	-1.724	0.206
R-HSA-2262752	Cellular responses to stress	41	0.496	1.533	0.206
R-HSA-109581	Apoptosis	16	-0.594	-1.668	0.206
R-HSA-5357801	Programmed Cell Death	16	-0.594	-1.668	0.206
R-HSA-2029480	Fcgamma receptor (FCGR) dependent phagocytosis	12	-0.654	-1.691	0.206
R-HSA-2029482	Regulation of actin dynamics for phagocytic cup formation	12	-0.654	-1.691	0.206
R-HSA-2559582	Senescence-Associated Secretory Phenotype (SASP)	16	0.625	1.581	0.206
R-HSA-8939236	RUNX1 regulates transcription of genes involved in differentiation of HSCs	16	0.625	1.581	0.206
R-HSA-216083	Integrin cell surface interactions	13	-0.634	-1.679	0.206
R-HSA-3371556	Cellular response to heat stress	11	0.679	1.567	0.206
R-HSA-2559580	Oxidative Stress Induced Senescence	17	0.608	1.562	0.206
R-HSA-5627117	RHO GTPases Activate ROCKs	12	-0.638	-1.652	0.206
R-HSA-195721	Signaling by WNT	25	0.549	1.536	0.206

R-HSA-5627123	RHO GTPases activate PAKs	11	-0.657	-1.661	0.206
R-HSA-5689901	Metalloprotease DUBs	15	0.625	1.557	0.206
R-HSA-201681	TCF dependent signaling in response to WNT	20	0.576	1.533	0.206
R-HSA-2555396	Mitotic Metaphase and Anaphase	11	-0.652	-1.647	0.206
R-HSA-68882	Mitotic Anaphase	11	-0.652	-1.647	0.206
R-HSA-70263	Gluconeogenesis	10	0.681	1.533	0.206
R-HSA-8878171	Transcriptional regulation by RUNX1	19	0.579	1.524	0.206
R-HSA-373755	Semaphorin interactions	14	-0.592	-1.607	0.206
R-HSA-2299718	Condensation of Prophase Chromosomes	13	0.627	1.510	0.206
R-HSA-912446	Meiotic recombination	13	0.627	1.510	0.206
R-HSA-201722	Formation of the beta-catenin:TCF transactivating complex	13	0.627	1.510	0.206
R-HSA-3214858	RMTs methylate histone arginines	17	0.585	1.503	0.206
R-HSA-2559583	Cellular Senescence	20	0.560	1.492	0.206
R-HSA-5617472	Activation of anterior HOX genes in hindbrain development during early embryogenesis	13	0.626	1.506	0.206
R-HSA-5619507	Activation of HOX genes during differentiation	13	0.626	1.506	0.206
R-HSA-3928662	EPHB-mediated forward signaling	10	-0.643	-1.583	0.206
R-HSA-8939211	ESR-mediated signaling	14	0.616	1.508	0.206
R-HSA-9018519	Estrogen-dependent gene expression	14	0.616	1.508	0.206
R-HSA-73886	Chromosome Maintenance	10	0.668	1.504	0.206
R-HSA-157579	Telomere Maintenance	10	0.668	1.504	0.206
R-HSA-171306	Packaging Of Telomere Ends	10	0.668	1.504	0.206
R-HSA-1474165	Reproduction	16	0.590	1.492	0.206
R-HSA-1500620	Meiosis	16	0.590	1.492	0.206
R-HSA-1221632	Meiotic synapsis	13	0.621	1.496	0.206
R-HSA-427413	NoRC negatively regulates rRNA expression	12	0.630	1.485	0.206
R-HSA-5250941	Negative epigenetic regulation of rRNA expression	12	0.630	1.485	0.206
R-HSA-73777	RNA Polymerase I Chain Elongation	12	0.630	1.485	0.206
R-HSA-73854	RNA Polymerase I Promoter Clearance	12	0.630	1.485	0.206
R-HSA-427359	SIRT1 negatively regulates rRNA expression	12	0.630	1.485	0.206
R-HSA-427389	ERCC6 (CSB) and EHMT2 (G9a) positively regulate rRNA expression	12	0.630	1.485	0.206
R-HSA-5334118	DNA methylation	12	0.630	1.485	0.206
R-HSA-5625886	Activated PKN1 stimulates transcription of AR (androgen receptor) regulated genes KLK2 and KLK3	12	0.630	1.485	0.206
R-HSA-73728	RNA Polymerase I Promoter Opening	12	0.630	1.485	0.206
R-HSA-212300	PRC2 methylates histones and DNA	13	0.616	1.484	0.206
R-HSA-211000	Gene Silencing by RNA	14	0.604	1.478	0.206
R-HSA-5578749	Transcriptional regulation by small RNAs	14	0.604	1.478	0.206
R-HSA-69620	Cell Cycle Checkpoints	17	-0.528	-1.504	0.206
R-HSA-71387	Metabolism of carbohydrates	22	0.533	1.447	0.217
R-HSA-8936459	RUNX1 regulates genes involved in megakaryocyte differentiation and platelet function	14	0.599	1.465	0.217
R-HSA-1474244	Extracellular matrix organization	28	-0.441	-1.420	0.225
R-HSA-2559586	DNA Damage/Telomere Stress Induced Senescence	12	0.614	1.448	0.235
R-HSA-3247509	Chromatin modifying enzymes	20	0.538	1.432	0.235
R-HSA-4839726	Chromatin organization	20	0.538	1.432	0.235
R-HSA-9006931	Signaling by Nuclear Receptors	18	0.552	1.434	0.238
R-HSA-2022090	Assembly of collagen fibrils and other multimeric structures	10	-0.608	-1.495	0.238
R-HSA-73864	RNA Polymerase I Transcription	13	0.598	1.440	0.238
R-HSA-5673001	RAF/MAP kinase cascade	12	-0.571	-1.476	0.238
R-HSA-5684996	MAPK1/MAPK3 signaling	12	-0.571	-1.476	0.238
R-HSA-977225	Amyloid fiber formation	15	0.571	1.422	0.245
R-HSA-400685	Sema4D in semaphorin signaling	11	-0.578	-1.462	0.245
R-HSA-416572	Sema4D induced cell migration and growth-cone collapse	11	-0.578	-1.462	0.245
R-HSA-382556	ABC-family proteins mediated transport	11	0.615	1.419	0.249
R-HSA-5625900	RHO GTPases activate CIT	11	-0.575	-1.453	0.249
R-HSA-68875	Mitotic Prophase	20	0.523	1.392	0.251
R-HSA-5250913	Positive epigenetic regulation of rRNA expression	13	0.576	1.388	0.292
R-HSA-5250924	B-WICH complex positively regulates rRNA expression	13	0.576	1.388	0.292
R-HSA-212165	Epigenetic regulation of gene expression	14	0.565	1.382	0.292
R-HSA-3214815	HDACs deacetylate histones	14	0.564	1.379	0.293
R-HSA-9006925	Intracellular signaling by second messengers	10	0.611	1.375	0.297
R-HSA-168928	DDX58/IFIH1-mediated induction of interferon-alpha/beta	10	-0.568	-1.399	0.301
R-HSA-71406	Pyruvate metabolism and Citric Acid (TCA) cycle	15	0.546	1.361	0.301
R-HSA-70326	Glucose metabolism	13	0.568	1.367	0.301
R-HSA-983169	Class I MHC mediated antigen processing & presentation	15	0.543	1.354	0.308
R-HSA-3214847	HATs acetylate histones	16	0.531	1.345	0.320
R-HSA-5689880	Ub-specific processing proteases	22	0.487	1.322	0.320
R-HSA-1266738	Developmental Biology	119	-0.269	-1.170	0.342
R-HSA-5683057	MAPK family signaling cascades	14	-0.492	-1.335	0.343
R-HSA-76002	Platelet activation, signaling and aggregation	22	-0.421	-1.284	0.352
R-HSA-112315	Transmission across Chemical Synapses	13	0.547	1.317	0.365
R-HSA-69481	G2/M Checkpoints	15	-0.474	-1.307	0.365
R-HSA-73857	RNA Polymerase II Transcription	47	0.391	1.238	0.380
R-HSA-5689603	UCH proteinases	17	0.501	1.286	0.381
R-HSA-5358351	Signaling by Hedgehog	10	-0.533	-1.311	0.383
R-HSA-1852241	Organelle biogenesis and maintenance	31	-0.374	-1.235	0.385

R-HSA-1236975	Antigen processing-Cross presentation	11	0.555	1.282	0.396
R-HSA-1640170	Cell Cycle	45	0.389	1.220	0.400
R-HSA-71403	Citric acid cycle (TCA cycle)	11	0.553	1.276	0.400
R-HSA-8873719	RAB geranylgeranylation	11	0.553	1.275	0.400
R-HSA-72312	rRNA processing	67	-0.299	-1.172	0.407
R-HSA-5625740	RHO GTPases activate PKNs	30	0.420	1.224	0.407
R-HSA-68886	M Phase	34	0.406	1.210	0.417
R-HSA-1799339	SRP-dependent cotranslational protein targeting to membrane	76	-0.287	-1.150	0.423
R-HSA-212436	Generic Transcription Pathway	45	0.382	1.198	0.423
R-HSA-5617833	Cilium Assembly	12	-0.479	-1.240	0.423
R-HSA-1650814	Collagen biosynthesis and modifying enzymes	20	-0.400	-1.188	0.423
R-HSA-156902	Peptide chain elongation	67	-0.291	-1.143	0.423
R-HSA-69473	G2/M DNA damage checkpoint	11	-0.487	-1.232	0.423
R-HSA-156827	L13a-mediated translational silencing of Ceruloplasmin expression	67	-0.290	-1.139	0.423
R-HSA-72613	Eukaryotic Translation Initiation	67	-0.290	-1.139	0.423
R-HSA-72737	Cap-dependent Translation Initiation	67	-0.290	-1.139	0.423
R-HSA-2565942	Regulation of PLK1 Activity at G2/M Transition	11	-0.483	-1.221	0.423
R-HSA-927802	Nonsense-Mediated Decay (NMD)	66	-0.290	-1.133	0.423
R-HSA-975956	Nonsense Mediated Decay (NMD) independent of the Exon Junction Complex (EJC)	66	-0.290	-1.133	0.423
R-HSA-975957	Nonsense Mediated Decay (NMD) enhanced by the Exon Junction Complex (EJC)	66	-0.290	-1.133	0.423
R-HSA-69278	Cell Cycle, Mitotic	37	0.389	1.178	0.423
R-HSA-6791226	Major pathway of rRNA processing in the nucleolus and cytosol	66	-0.289	-1.131	0.423
R-HSA-8868773	rRNA processing in the nucleus and cytosol	66	-0.289	-1.131	0.423
R-HSA-9010553	Regulation of expression of SLITs and ROBOs	68	-0.288	-1.133	0.425
R-HSA-168256	Immune System	105	0.317	1.136	0.425
R-HSA-1236974	ER-Phagosome pathway	10	0.540	1.214	0.427
R-HSA-376176	Signaling by ROBO receptors	71	-0.283	-1.123	0.427
R-HSA-114608	Platelet degranulation	12	-0.459	-1.188	0.428
R-HSA-76005	Response to elevated platelet cytosolic Ca2+	12	-0.459	-1.188	0.428
R-HSA-168249	Innate Immune System	66	0.340	1.142	0.437
R-HSA-195258	RHO GTPase Effectors	50	-0.304	-1.119	0.437
R-HSA-901042	Calnexin/calreticulin cycle	10	-0.483	-1.188	0.444
R-HSA-532668	N-glycan trimming in the ER and Calnexin/Calreticulin cycle	12	-0.450	-1.163	0.453
R-HSA-74160	Gene expression (Transcription)	51	0.352	1.133	0.453
R-HSA-72706	GTP hydrolysis and joining of the 60S ribosomal subunit	66	-0.281	-1.099	0.453
R-HSA-1474290	Collagen formation	21	-0.378	-1.135	0.453
R-HSA-72649	Translation initiation complex formation	31	-0.337	-1.114	0.456
R-HSA-72662	Activation of the mRNA upon binding of the cap-binding complex and eIFs, and subsequent binding to 43S	31	-0.337	-1.114	0.456
R-HSA-192823	Viral mRNA Translation	65	-0.278	-1.083	0.456
R-HSA-2408522	Selenoamino acid metabolism	65	-0.278	-1.083	0.456
R-HSA-2408557	Selenocysteine synthesis	65	-0.278	-1.083	0.456
R-HSA-72689	Formation of a pool of free 40S subunits	65	-0.278	-1.083	0.456
R-HSA-72764	Eukaryotic Translation Termination	65	-0.278	-1.083	0.456
R-HSA-381426	Regulation of Insulin-like Growth Factor (IGF) transport and uptake by Insulin-like Growth Factor Binding Proteins (IGFBPs)	13	0.473	1.139	0.474
R-HSA-8957275	Post-translational protein phosphorylation	13	0.473	1.139	0.474
R-HSA-72766	Translation	90	-0.259	-1.073	0.475

Appendix D. Summary of all identified enriched pathways in the mitochondrial fraction using the GSEA approach. ES = enrichment score; NES = normalized enrichment score.

Appendix F

Summary of all identified pathways in the whole cell fractions using GSEA approach.

ID	Description	setSize	ES	NES	p.adjust
R-HSA-186797	Signaling by PDGF	10	-0.857	-1.972	0.126
R-HSA-6806834	Signaling by MET	18	-0.707	-1.886	0.425
R-HSA-2672351	Stimuli-sensing channels	10	0.768	1.661	0.425
R-HSA-8875878	MET promotes cell motility	11	-0.771	-1.818	0.425
R-HSA-3108232	SUMO E3 ligases SUMOylate target proteins	11	-0.767	-1.810	0.425
R-HSA-376176	Signaling by ROBO receptors	117	0.411	1.480	0.425
R-HSA-8953854	Metabolism of RNA	165	0.373	1.404	0.425
R-HSA-2990846	SUMOylation	12	-0.724	-1.742	0.425
R-HSA-112315	Transmission across Chemical Synapses	32	-0.540	-1.646	0.425
R-HSA-9010553	Regulation of expression of SLITs and ROBOs	110	0.401	1.432	0.425
R-HSA-72706	GTP hydrolysis and joining of the 60S ribosomal subunit	92	0.418	1.457	0.425
R-HSA-156827	L13a-mediated translational silencing of Ceruloplasmin expression	93	0.415	1.448	0.425
R-HSA-72613	Eukaryotic Translation Initiation	93	0.415	1.448	0.425
R-HSA-72737	Cap-dependent Translation Initiation	93	0.415	1.448	0.425
R-HSA-112314	Neurotransmitter receptors and postsynaptic signal transmission	24	-0.572	-1.622	0.425

R-HSA-112316	Neuronal System	34	-0.512	-1.581	0.425
R-HSA-68877	Mitotic Prometaphase	43	-0.468	-1.520	0.425
R-HSA-72312	rRNA processing	84	0.419	1.442	0.425
R-HSA-72689	Formation of a pool of free 40S subunits	85	0.414	1.428	0.425
R-HSA-936440	Negative regulators of DDX58/IFIH1 signaling	11	0.693	1.535	0.425
R-HSA-8876198	RAB GEFs exchange GTP for GDP on RABs	24	0.568	1.530	0.425
R-HSA-418597	G alpha (z) signalling events	11	-0.701	-1.655	0.425
R-HSA-156902	Peptide chain elongation	83	0.414	1.421	0.425
R-HSA-977443	GABA receptor activation	10	-0.710	-1.634	0.425
R-HSA-977444	GABA B receptor activation	10	-0.710	-1.634	0.425
R-HSA-991365	Activation of GABAB receptors	10	-0.710	-1.634	0.425
R-HSA-1799339	SRP-dependent cotranslational protein targeting to membrane	93	0.404	1.412	0.425
R-HSA-6791226	Major pathway of rRNA processing in the nucleolus and cytosol	83	0.412	1.417	0.425
R-HSA-8868773	rRNA processing in the nucleus and cytosol	83	0.412	1.417	0.425
R-HSA-418555	G alpha (s) signalling events	12	-0.668	-1.608	0.444
R-HSA-381426	Regulation of Insulin-like Growth Factor (IGF) transport and uptake by Insulin-like Growth Factor Binding Proteins (IGFBPs)	13	-0.655	-1.607	0.444
R-HSA-8957275	Post-translational protein phosphorylation	13	-0.655	-1.607	0.444
R-HSA-192823	Viral mRNA Translation	81	0.410	1.402	0.444
R-HSA-2408557	Selenocysteine synthesis	82	0.408	1.398	0.444
R-HSA-156842	Eukaryotic Translation Elongation	87	0.400	1.384	0.459
R-HSA-1428517	The citric acid (TCA) cycle and respiratory electron transport	25	0.544	1.477	0.477
R-HSA-3371556	Cellular response to heat stress	27	-0.516	-1.508	0.488
R-HSA-927802	Nonsense-Mediated Decay (NMD)	87	0.395	1.368	0.488
R-HSA-975957	Nonsense Mediated Decay (NMD) enhanced by the Exon Junction Complex (EJC)	87	0.395	1.368	0.488
R-HSA-2408522	Selenoamino acid metabolism	91	0.390	1.358	0.492

Appendix F. Summary of all identified enriched pathways in the whole cell fraction using the GSEA approach. ES = enrichment score; NES = normalized enrichment score.

Publications

Zilocchi M, **Colugnat I**, Lualdi M, Meduri M, Marini F, Corasolla Carregari V, Moutaoufik MT, Phanse S, Pieroni L, Babu M, Garavaglia B, Fasano M, Alberio T. Exploring the impact of PARK2 mutations on the total and mitochondrial proteome of human skin fibroblasts. [Under review]

Monti C, Zilocchi M, **Colugnat I**, Alberio T. Proteomics turns functional. J Proteomics. 2019 Apr 30;198:36-44. doi: 10.1016/j.jprot.2018.12.012.

Monti C, **Colugnat I**, Lopiano L, Chiò A, Alberio T. Network Analysis Identifies Disease-Specific Pathways for Parkinson's Disease. Mol Neurobiol. 2018 Jan;55(1):370-381. doi: 10.1007/s12035-016-0326-0.

Posters

Abstract and Selected Oral Presentation ItPA XIII annual congress, Como, September 5-7, 2018. The impact of PARK2 mutations on the total and mitochondrial proteome. **Colugnat I,** Zilocchi M, Meduri M, Pieroni L, Marini F, Corasolla Carregari V, Garavaglia B, Fasano M, Alberio T.

Poster ItPA XII annual congress, Lecce, June 12-15, 2017. ProLyPALS: Proteomics of Lymphocytes from Parkinson's Disease and Amyotrophic Lateral Sclerosis patients. **Colugnat I**, Monti C, Sironi C, Lopiano L, Chiò A, Di Pierro A, Comi C, Fasano M, Alberio T.